UNIVERSITY OF CALIFORNIA
SANTA CRUZ

NATURE OF THE SPIN-GLASS PHASE IN MODELS WITH LONG-RANGE INTERACTIONS

A dissertation submitted in partial satisfaction of the
requirements for the degree of

DOCTOR OF PHILOSOPHY

in

PHYSICS

by

Matthew C. Wittmann

September 2015

The Dissertation of Matthew C. Wittmann
is approved:

Professor A. Peter Young, Chair

Professor B. Sriram Shastry

Professor Joshua M. Deutsch

Tyrus Miller
Vice Provost and Dean of Graduate Studies

Contents

Contents iii

List of Figures vi

List of Tables ix

Abstract x

Acknowledgments xiii

1 Introduction 1
- 1.1 Motivation . . . 1
- 1.2 Ising model of ferromagnetism . . . 3
  - 1.2.1 Mean-field theory . . . 5
  - 1.2.2 Landau theory . . . 10
- 1.3 Disorder and spin glasses . . . 15
  - 1.3.1 Edwards-Anderson model . . . 16
  - 1.3.2 Sherrington-Kirkpatrick mean-field model . . . 19
  - 1.3.3 Replica symmetry breaking . . . 21
  - 1.3.4 Theories of short-range spin glasses . . . 24
- 1.4 Organization of the dissertation . . . 27

2 Numerical methods 30
- 2.1 Importance sampling . . . 30
- 2.2 Markov Chain Monte Carlo . . . 31
  - 2.2.1 Constructing a Markov chain . . . 33
- 2.3 Algorithms for the Ising model . . . 34
  - 2.3.1 Single-spin flip dynamics . . . 35
  - 2.3.2 Cluster dynamics . . . 36
- 2.4 Convergence to equilibrium . . . 39
  - 2.4.1 Estimating the relaxation time . . . 42
  - 2.4.2 Equilibration test for Gaussian spin glasses . . . 43
- 2.5 Parallel tempering . . . 45
- 2.6 Finite-size scaling . . . 47

2.7 Statistical error analysis . . . 50
2.7.1 Manual error propagation . . . 52
2.7.2 Resampling methods . . . 54

3 Nonextensive spin glasses 58
3.1 Motivation . . . 58
3.1.1 Long-range interactions . . . 59
3.1.2 Nonextensive regime . . . 60
3.1.3 Spin glasses with long-range interactions . . . 62
3.2 Models . . . 63
3.3 Method . . . 66
3.4 Results . . . 70
3.5 Conclusions . . . 75

4 Statistics of the overlap distribution 77
4.1 Introduction . . . 77
4.2 Models . . . 79
4.2.1 Edwards-Anderson models on hypercubic lattices . . . 79
4.2.2 Sherrington-Kirkpatrick model . . . 80
4.2.3 One-dimensional diluted long-range model . . . 80
4.3 Methods . . . 81
4.4 Measured quantities . . . 84
4.5 Results . . . 88
4.5.1 Fraction of peaked samples, $\Delta(q_0, \kappa)$ . . . 88
4.5.2 Median $I^{\mathrm{med}}(q)$ and mean $I^{\mathrm{av}}(q)$ cumulative overlap distribution . . . 93
4.5.3 Typical overlap distribution, $P^{\mathrm{typ}}(q)$ . . . 95
4.6 Summary and conclusions . . . 96

5 Connection between dynamics and statics in spin glasses 99
5.1 Introduction . . . 99
5.2 Model . . . 105
5.3 Method . . . 107
5.4 Results . . . 107
5.5 Conclusion . . . 110

6 Finite-size scaling above the upper critical dimension 112
6.1 Introduction . . . 112
6.1.1 Periodic boundary conditions . . . 114
6.1.2 Free boundary conditions . . . 115
6.2 Model . . . 119
6.3 Quotient method . . . 121
6.4 Results: periodic boundary conditions . . . 124

6.4.1 $k = 0$ fluctuations 124
6.4.2 $k \neq 0$ fluctuations 126
6.5 Results: free boundary conditions 127
6.5.1 $k = 0$ fluctuations 127
6.5.2 $k \neq 0$ fluctuations 135
6.6 Conclusions 136

Bibliography **138**

List of Figures

1.1 Plots of the mean-field self-consistency condition and the mean-field free energy for the Ising model. 10
1.2 Examples of frustrated Ising systems. 18
1.3 Sketches of the overlap distribution for a single sample and the sample average, according to replica symmetry breaking (RSB) theory. . . . 23
1.4 Comparison of disorder-averaged overlap distributions in the thermodynamic limit for the droplet picture and the RSB picture. 26

2.1 Comparison of the Metropolis and heat-bath transition probabilities as a function of the probability ratio of two states in the target distribution. 33
2.2 Example equilibration plots for a spin glass model with Gaussian couplings. 45
2.3 Replicas at different temperatures exploring a non-convex energy landscape. 46
2.4 Overlap of energy distributions of replicas of a system at nearby temperatures. 48

3.1 Schematic phase diagram of the one-dimensional Ising spin glass with power-law interactions. 64
3.2 Representation of the one-dimensional long-range Ising spin glass with periodic boundary conditions. 65
3.3 Data for the Binder ratio for the one-dimensional undiluted spin glass. 71
3.4 Data for the Binder ratio and the scaled spin-glass susceptibility for the one-dimensional undiluted spin glass with $\sigma = 0$ and $\sigma = 0.25$. . 71
3.5 Results for the intersection temperatures for the one-dimensional undilted model with $\sigma = 0$ (SK model) and $\sigma = 0.25$. 73
3.6 Data for the Binder ratio for the one-dimensional undiluted spin glass. 73
3.7 Data for the Binder ratio and the scaled spin-glass susceptibility for the one-dimensional diluted spin glass with $\sigma = 0$ and $\sigma = 0.25$. . . . 74
3.8 Results for the intersection temperatures for the one-dimensional diluted model with $\sigma = 0$ (VB model) and $\sigma = 0.25$. 74

3.9 Results for the intersection temperatures for the diluted model with $\sigma = 0.375$. 75

4.1 Example equilibration plots for the three-dimensional Edwards-Anderson model and the one-dimensional long-range model. 84
4.2 Plots of various statistics of the spin overlap distribution as a function of Monte Carlo time, indicating that the quantities have reached a steady state. 85
4.3 Plots of the overlap distribution $P_{\mathcal{J}}(q)$ for individual disorder samples. 87
4.4 Peak-counting statistic $\Delta(q_0, \kappa)$ for one-dimensional long-range spin glasses and the Sherrington-Kirckpatrick model. 89
4.5 Peak-counting statistic $\Delta(q_0, \kappa)$ for the three- and four-dimensional Edwards-Anderson models and the Sherrington-Kirkpatrick model. . 90
4.6 Mean and median over samples of the cumulative overlap distribution for one-dimensional long-range and Sherrington-Kirkpatrick spin-glass models. 93
4.7 Mean and median over samples of the cumulative overlap distribution for three- and four-dimensional Edwards-Anderson spin-glass models. 94
4.8 "Typical" overlap distribution for the Sherrington-Kirkpatrick spin glass for various zero-replacement values ϵ/k. 96

5.1 The spin-glass metastate as defined by C. M. Newman and Stein (1997) and by Aizenman and Wehr (1990). 103
5.2 Data for the correlation function averaged between $t = 2^{13}$ and 2^{14} for different sizes of the one-dimensional long-range diluted spin glass with $\sigma = 5/8$ at $T = 0.4T_c$. 108
5.3 Data for the correlation function at different times of the one-dimensional long-range diluted spin glass with $\sigma = 5/8$ at $T = 0.4T_c$. 110
5.4 Scaling plot of data for the dynamical correlation function $C_4(r, t)$ at different times for the one-dimensional long-range diluted spin glass with $\sigma = 0.74$ at $T = 0.4T_c$. 111

6.1 Data for the Binder ratio g for the five-dimensional Ising model with periodic boundary conditions. 125
6.2 Data for the Binder ratio g at the transition temperature T_c for the five-dimensional Ising model with periodic boundary conditions. . . 125
6.3 Wavevector-dependent susceptibility $\chi(\boldsymbol{k})$ for $\boldsymbol{k}L/(2\pi) = (1, 0, 0, 0, 0)$ for the five-dimensional Ising model with periodic boundary conditions. 126
6.4 Scaling plots of the susceptibility of the $d = 5$ periodic Ising model for two nonzero wavevectors. 127
6.5 Values of $\chi(\boldsymbol{k})/L^2$ at T_c for periodic boundary conditions. 128
6.6 Data for the Binder ratio g and the susceptibility χ for the five-dimensional Ising model with free boundary conditions. 128

6.7 Quotient estimation of the shift exponent λ for the five-dimensional Ising model with free boundary conditions. 129
6.8 Quotient estimation of the width exponent y_t^* for $k = 0$ modes of the five-dimensional Ising model with free boundary conditions. 131
6.9 Quotients for the value of the susceptibility χ at the finite-size pseudocritical temperature for the five-dimensional Ising model with free boundary conditions. 131
6.10 Quotient estimation of the width exponent y_t for $\boldsymbol{k} \neq \mathbf{0}$ modes of the five-dimensional Ising model with free boundary conditions. 132
6.11 Scaling plot of the susceptibility χ for the five-dimensional Ising model with free boundary conditions. 133
6.12 Wavevector-dependent susceptibility $\chi(\boldsymbol{k})$ for $(L+1)\boldsymbol{k}/\pi = (2, 1, 1, 1, 1)$ for the five-dimensional Ising model with free boundary conditions. . 136
6.13 Quotient estimates of the rounding exponent y_t for $\boldsymbol{k} \neq \mathbf{0}$ modes of the five-dimensional Ising model with free boundary conditions. . . . 137

List of Tables

3.1 Simulation parameters for one-dimensional long-range models with undiluted bonds. 67
3.2 Simulation parameters for one-dimensional long-range models with diluted bonds. 68

4.1 Simulation parameters for one-dimensional long-range spin-glass models with diluted bonds. 82
4.2 Simulation parameters for the three-dimensional Edwards-Anderson spin glass. 82
4.3 Simulation parameters for the four-dimensional Edwards-Anderson spin glass. 83
4.4 Simulation parameters for the Sherrington-Kirkpatrick spin glass. . . 83

Abstract

Nature of the spin-glass phase in models with long-range interactions

by

Matthew C. Wittmann

Despite decades of effort, our understanding of low-temperature phase of spin glass models with short-range interactions remains incomplete. Replica symmetry breaking (RSB) theory, based on the solution of the Sherrington-Kirkpatrick mean-field model, predicts many pure states; meanwhile, competing theories of short-range systems, such as the droplet picture, predict a single pair of pure states related by time-reversal symmetry, analogously to the ferromagnet. Since RSB certainly holds for the mean-field (infinite-range) model, it is interesting to study short-range models in high dimensions to observe whether RSB also holds here; however, computer simulations of short-range models in high dimensions are difficult because the number of spins to equilibrate grows so rapidly with the linear size of the system.

A relatively recent idea which has been fruitful is to instead study one-dimensional models with long-range (power-law) interactions, which are argued to have the same critical behavior as corresponding short-range models in high dimensions, but for which simulations for a range of sizes (crucial for finite-size scaling analysis) are feasible. For these one-dimensional long-range (1DLR) models, we fill in a previously unexplored region of parameter space where the interactions become sufficiently long-range that they must be rescaled with the system size to maintain the thermodynamic limit. We find strong evidence that detailed behavior of the 1DLR models everywhere in this "nonextensive regime" is identical to that of the Sherrington-Kirkpatrick model, lending support to a recent conjecture.

In an attempt to distinguish the RSB and droplet pictures, we study recently-proposed observables based on the statistics of individual disorder samples, rather than simply averaging over the disorder as is most frequently done in previous studies. We compare Monte Carlo results for 1DLR models which are proxies for short-range models in 3, 4, and 10 dimensions with previously-obtained data for the 3D and 4D short-range models and the SK model. For one statistic, which is expected to sharply distinguish between the two pictures in the thermodynamic limit, we find that larger system sizes than those currently feasible to simulate are needed to obtain an unambiguous result. We also find that two other recently-proposed statistics, the median of the cumulative overlap distribution and the "typical" overlap distribution, are not particularly helpful in distinguishing between the RSB and droplet pictures.

If there are many pure states in the spin-glass phase, we need to carry out some sort of statistical average over them to obtain the thermodynamics. One such prescription for doing this is called the "metastate." Motivated by similarities between the average over pure states specified by the metastate theory and that presumably generated by the nonequilibrium dynamics, we study a 1DLR model which is a proxy for a short-range model in $d = 8$ dimensions and measure the evolution of dynamical correlations. We find that the spatial decay of the correlations at distances less than the dynamical correlation length $\xi(t)$ agrees quantitatively with the predictions of the metastate theory, evaluated according to the RSB picture. We also compute the dynamic exponent defined by $\xi(t) \propto t^{1/z(T)}$ and find that it is compatible with the mean-field value of the critical dynamical exponent for short-range spin glasses.

Finally, we present a unified view of finite-size scaling (FSS) in dimensions d above the upper critical dimension d_u, for both free and periodic boundary con-

ditions. For $d > d_u$, a dangerous irrelevant variable is responsible for both the violation of hyperscaling and the violation of "standard" FSS. We find that the modified hyperscaling proposed to allow for this applies only to $\boldsymbol{k} = \mathbf{0}$ fluctuations, while standard FSS applies to $\boldsymbol{k} \neq \mathbf{0}$ fluctuations. Hence the exponent η describing the power-law decay of correlations at criticality is unambiguously $\eta = 0$. With free boundary conditions, the finite-size "shift" is greater than the rounding. Nonetheless, using $T - T_L$, where T_L is the finite-size pseudocritical temperature, as the scaling variable, the data do collapse onto a scaling form that includes the behavior both at T_L, where the susceptibility χ diverges like $L^{d/2}$, and the bulk T_c, where it diverges like L^2. We support these claims with data from large-scale simulations of the five-dimensional Ising model.

Acknowledgments

First and foremost I would like to thank my advisor, Peter Young, for his patience, support, and for his dedication to presenting and explaining ideas clearly in teaching and writing, which has been an inspiration to me. I would also like to thank him for the many opportunities he has provided me to enrich my education, including summer courses in Germany and France and a stay at the Max Planck Institute in Dresden. Additionally I would like to thank the remaining members of the reading committee, Sriram Shastry and Josh Deutsch, for their guidance and useful discussions both inside and outside the classroom.

I have benfitted immensely from the mentorship of Itay Hen, who taught me much of what I know about the topics of quantum Monte Carlo and quantum adiabatic algorithms, and has advised me on several research projects in the latter, all while juggling his own many responsibilities.

I have had the opportunity to collaborate with several excellent researchers; I would like to thank Helmut Katzgraber, Jonathan Machta, and Burcu Yucesoy for many useful discussions and for their contributions to the work which is reprinted in Chapter 4. Helmut deserves special thanks for donating a large chunk of his computer time for the simulations.

A big thanks goes out to my fellow graduate students and friends in the department who have made my time in Santa Cruz enjoyable and unforgettable. A special thanks goes to the musicians, backpackers, and cyclists with whom I have shared many adventures.

Finally, I would like to thank my best friend and partner Tia Plautz for her moral support and encouragement during the preparation of this thesis, and all of the unforgettable memories made during our time in Santa Cruz and abroad. I'm looking forward to seeing the world with you.

The text of this dissertation includes reprints of the following material, previously published or submitted for publication:

- Matthew Wittmann and A. P. Young. "Spin glasses in the nonextensive regime". In: *Phys. Rev. E* 85 (4 Apr. 2012), p. 041104. DOI: 10.1103/PhysRevE.85.041104

- Matthew Wittmann and A. P. Young. "Finite-size scaling above the upper critical dimension". In: *Phys. Rev. E* 90 (6 Dec. 2014), p. 062137. DOI: 10.1103/PhysRevE.90.062137

- Matthew Wittmann and A. P. Young. "The connection between statics and dynamics of spin glasses". Submitted. July 9, 2015

The co-author listed in these publications directed and supervised the research which forms the basis for the dissertation. The text of this dissertation also includes excerpts from the following collaboration,

- Matthew Wittmann, Burcu Yucesoy, et al. "Low-temperature behavior of the statistics of the overlap distribution in Ising spin-glass models". In: *Phys. Rev. B* 90 (13 Oct. 2014), p. 134419. DOI: 10.1103/PhysRevB.90.134419,

where I contributed simulation data for the one-dimensional long-range models, analysis of the data for all models, and wrote some of the text.

To my parents,

for their endless love and support.

Chapter 1

Introduction

> The behavior of large and complex aggregates of elementary particles, it turns out, is not to be understood in terms of a simple extrapolation of the properties of a few particles.
>
> Philip W. Anderson
> *More is Different* (1972)

1.1 Motivation

With the widespread adoption and rapid advancement of the digital computer in the mid-20th century have come new, powerful approaches to modeling systems using numerical simulations. Before the advent of computers, models of physical systems were restricted to those that could be solved analytically, or at least those for which a suitable approximation, or expansion in some small parameter, can be made while retaining the essential physics. Numerical simulations expand the space of practical models significantly, while simultaneously bringing a different set of challenges and limitations. With the present technology numerical simula-

tions of *classical* systems are limited to sizes many orders of magnitude below the macroscopic scale. For *quantum* systems the situation is much more difficult, as the computational resources required expand exponentially in the size of the system; furthermore, simulations of fermionic systems suffer from the "sign problem" in evaluating oscillatory integrals which also induces an exponential penalty in the size of the system. Nevertheless, numerical simulations have become a crucial complement to traditional theory and experiment as computing technology has advanced, allowing the simulation of progressively larger systems, and techniques such as finite-size scaling analysis (described in Section 2.6) have been developed to extrapolate results for finite systems into the thermodynamic (infinite-size) limit. It is hoped that an eventual practical *quantum computer* could efficiently simulate quantum systems.

Numerical simulations have been especially useful in the study of "complex systems," systems consisting of a large number of *strongly-interacting* parts whose aggregate behavior is strongly nonlinear, meaning (roughly) that the overall behavior cannot be approximated simply as the sum of its parts. Examples of such systems in science are numerous, including models of high-temperature superconductivity in many-body physics, the behavior of ant colonies and the interaction of cells in the immune system in biology, and neural networks in neuroscience and machine learning. In this thesis we focus on models of magnetism in statistical physics, which are among the simplest examples of complex systems to study from an analytical and numerical perspective.

1.2 Ising model of ferromagnetism

In the early 1920s, William Lenz gave his student Ernst Ising a simple mathematical model of ferromagnetism, now known as the *Ising model*, which was to be the topic of Ising's dissertation. The model consists of discrete variables, "spins," which can take one of two values, $+1$ or -1, and are arranged on a regular lattice with pairwise nearest-neighbor interactions. In addition to the nearest-neighbor interactions, the spins also interact with an externally-applied field H_i, which in general can be nonuniform. The Hamiltonian is given by

$$\mathcal{H} = -\frac{1}{2}\sum_{ij} J_{ij} S_i S_j - \sum_i H_i S_i, \tag{1.1}$$

where the first sum is over all pairs of spins, and $J_{ij} = J$, a positive constant, if i and j are nearest neighbors on the lattice and 0 otherwise.

As the temperature is decreased through the Curie temperature T_c, a ferromagnet in zero external field undergoes a continuous phase transition from the *paramagnetic* phase, in which the magnetization is zero, to the *ferromagnetic* phase, in which the magnetization is finite and can be either positive or negative. This is an example of spontaneous symmetry breaking, where a symmetry, in this case time-reversal symmetry $S_i \to -S_i$, is "broken" as the system undergoes a transition into a phase with lower symmetry. In his 1924 dissertation, Ising solved the one-dimensional version of the model that now bears his name and showed that it did *not* have a ferromagnetic phase at any positive temperature. From this he (incorrectly) concluded that the model does not admit a finite-temperature phase transition in any number of dimensions, and thus was not a suitable model of ferromagnetism (Ising 1925).

This assumption was proven incorrect by Peierls (1936), who gave an argument based on the free energy of *domain walls* (the boundaries separating regions of

positive and negative magnetization) showing that phase transitions *do* occur in the model for dimensions greater than two. The argument goes as follow. In one dimension, the energy cost of a domain wall is $2J$ since the energy of a pair of spins has magnitude J and changes sign when one of them is flipped. But the entropy added by the domain wall goes like the logarithm of the number of spins L, since there are L places[1] where it could go. Thus, in one dimension, the *free energy cost* of a domain wall is negative for any positive temperature in the infinite-size limit, so the system will form domain walls on all scales, destroying the ferromagnetic order. However, in two dimensions, the energy cost of a domain wall is $2Jn$, where n is the number of spins on the boundary. An upper bound on the number of ways to form a closed loop is $(z-1)^n$, where z is the coordination number of the lattice. This is an upper bound because it allows for self-intersections, which are not possible for a real domain wall. The free-energy cost ΔF_n to form a domain wall of length n is then bounded from below as

$$\Delta F_n > \left[2J - T\log(z-1)\right] n. \tag{1.2}$$

Thus, for small positive T the formation of domain walls of any size is suppressed, and the system will develop ferromagnetic order. This also gives a lower bound on the transition temperature T_c at which the system transitions to ferromagnetic order, $T_c > 2J/\log(z-1) \approx 1.82J$ in two dimensions. A similar argument can be made for all dimensions $d \geq 2$.

It turns out that it is a general feature of phase transitions in diverse systems that there is a number of dimensions d_l, called the *lower critical dimension*, below which a transition does not occur at finite temperature, so the above result can be stated as $d_l = 2$ for the Ising model. In fact, this result holds for all systems in the

[1] assuming periodic boundary conditions

Ising universality class, which includes systems with a scalar order parameter near a continuous phase transition, including (*e.g.*) magnetic systems and liquids. We will motivate the phenomenon of universality in the discussion of Landau theory in Section 1.2.2; it is now understood within the framework of the *renormalization group*.

Two decades after the introduction of the Ising model, in a remarkable mathematical achievement, Onsager (1944) gave an analytic solution of the two-dimensional Ising model in zero field. The exact transition temperature is given by

$$T_c = \frac{2J}{\log(1+\sqrt{2})} \approx 2.269J. \tag{1.3}$$

Onsager's solution is very complicated and the techniques do not generalize well. Subsequent attempts at an analytical solution in two dimensions with a field or in three and higher dimensions have been unsuccessful, and in fact recently arguments have been made from computational complexity theory that these problems are intractable.[2]

The Ising model is ubiquitous in the literature of statistical mechanics because it is a relatively uncomplicated model which, thanks to the phenomemon of *universality*, exhibits critical behavior *identical* to other systems in the same number of dimensions and with *scalar* order parameters, and thus provides a convenient setting for the study of phase transitions in a wide variety of systems.

1.2.1 Mean-field theory

Despite the apparent simplicity of Ising model, exact solutions do not appear to be possible in dimensions $d > 2$. The source of the difficulty is the spin-spin interactions, which preclude a solution by factorizing the partition function as a

[2]Istrail (2000) shows that computing the partition function for $d = 2$ with a field or for $d > 2$ belongs to the class of NP-complete problems, which are unlikely to have closed-form solutions.

product of single-site factors. This is a general problem in many-body statistical physics; as a result, exact analytical solutions are few and far between.

Mean-field theory (MFT) is the simplest possible approximation of an interacting system aside from ignoring the interactions altogether. The resulting model is usually straightforward to solve analytically, although there are exceptions (for example, the Sherrington-Kirkpatrick model discussed in Section 1.3.2.) There are many equivalent ways to generate a mean-field theory for a given system, but all are based on the same essential approximation of ignoring the interaction of *fluctuations*.

For example, following Cardy (1996), we can generate a mean-field theory of the Ising ferromagnet as follows. We write for the interacting part of the Hamiltonian

$$\begin{aligned}
\mathcal{H}_{\text{int}} &\equiv -\frac{1}{2}\sum_{ij} J_{ij} S_i S_j \\
&= -\frac{1}{2}\sum_{ij} J_{ij}\left[M + (S_i - M)\right]\left[M + (S_j - M)\right] \\
&\approx -\frac{1}{2}\sum_{ij} J_{ij}\left[-M^2 + M(S_i + S_j)\right] \\
&= \frac{1}{2} NzJM^2 - zJM\sum_i S_i,
\end{aligned}$$

where $M \equiv \langle S \rangle$ is the magnetization and $zJ = \sum_j J_{ij}$. The mean-field approximation comes in third step, where we have discarded the term which is quadratic in the fluctuations, *i.e.* $(S_i - M)(S_j - M)$. Thus we have decoupled the spin degrees of freedom and can solve the problem by factorizing the partition function,

$$\begin{aligned}
Z &= \mathrm{Tr}\exp\left[-\frac{1}{2}\beta NzJM^2 - \beta(H + zJM)\sum_i S_i\right] \\
&= e^{-\frac{1}{2}\beta NzJM^2}\left[2\cosh\beta(H + zJM)\right]^N.
\end{aligned}$$

The free energy per spin is then

$$f = \frac{1}{2} zJM^2 - \beta^{-1} \log \cosh \beta(H + zJM), \tag{1.4}$$

dropping the constant which vanishes in the thermodynamic limit. This expression depends on the magnetization M, which we have not yet specified. But since $M = -\partial f / \partial H$, we have the following *self-consistency condition*

$$M = \tanh \beta(H + zJM). \tag{1.5}$$

Note that this has the same form as the Curie law, which we would expect to obtain had we set the spin-spin couplings $J_{ij} = 0$, but with the external field H replaced by $H + zJM$. The additional term zJM has the simple interpretation as the "molecular field" generated by a spin's neighbors, neglecting fluctuations about the mean M. Note that for $H = 0$ and high temperature (small β), Eq. (1.5) has only a single solution at $M = 0$, corresponding to the paramagnetic state, while at low temperatures two additional solutions appear at $M = \pm M_0$ corresponding to the two pure states of the paramagnetic phase. Thus the mean field model demonstrates a continuous phase transition with spontaneous symmetry breaking. The (mean-field) transition temperature T_c^{MF} is given by the limit $M \to 0^+$ in Eq. (1.5), from which we obtain $M \equiv zJM/T_c^{\mathrm{MF}}$, or

$$T_c^{\mathrm{MF}} \equiv zJ \equiv \sum_j J_{ij}. \tag{1.6}$$

For a hypercubic lattice $z = 2d$ and thus the corresponding result for the two-dimensional Ising model is $T_c^{\mathrm{MF}} = 4J$, an overestimate of the exact transition temperature [see Eq. (1.3)]. Mean-field theories give an upper bound on the transition temperature because they neglect the effect of fluctuations, which drive the transition at lower temperatures. Hence, from the Peierls argument described

above and mean-field theory, we have (correctly) bounded the transition temperature for the two-dimensional Ising model as $1.82 \lessapprox T_c/J < 4$. Mean-field theory becomes more accurate as the dimensionality of a system is increased. An intuitive explanation for this is that in higher dimensions, each spin couples to more neighbors and thus fluctuations are averaged out to a greater degree. For example, in Chapter 6 we will find that $T_c \approx 8.78J$ for the five-dimensional Ising model, whereas the mean-field prediction is $T_c^{\mathrm{MF}} = 10J$, a relatively small error.

To understand the nature of the broken symmetry it is helpful to consider the behavior of the mean-field free energy near the transition. In zero field, Eq. (1.4) has the expansion

$$f = \frac{1}{2} zJ(1 - \beta zJ)M^2 + \mathcal{O}(M^4), \tag{1.7}$$

where the coefficient of the M^4 term is positive. As shown in Fig. 1.1b, for temperatures above T_c the coefficient of the quadratic term is positive and there is a single minimum at $M = 0$, corresponding to the paramagnetic state. As the temperature is lowered through T_c, the $M = 0$ solution of the minimum equation becomes unstable and is replaced by two new minima at $\pm M_0(t)$ which shift continuously from $M = 0$ as the temperature is lowered. The system will choose one of these minima, which correspond to the "up" and "down" pure states of the ferromagnetic phase. This situation describes a continuous phase transition with spontaneous symmetry breaking. Now consider what happens when a nonzero external field H is applied. For $T < T_c$, as H passes through zero from negative to positive, the global minimum of the free energy shifts discontinuously from $-M_0$ to M_0. This exemplifies a first-order phase transition.

Phase transitions are characterized by a set of *critical exponents*, which describe how various quantities vary asymptotically near the critical point. For

example, in magnetic systems, the critical exponent β is defined as

$$M \propto (T_c - T)^{\beta} \tag{1.8}$$

in the limit $T \to T_c^-$. We can estimate this exponent from the mean-field theory developed above. Expanding Eq. (1.4) in M, we find the form

$$f \propto atM^2 + \frac{1}{2}bM^4 - HM, \tag{1.9}$$

where a, b, and c are constants which depend only weakly on the reduced temperature $t = (T - T_c)/T_c$ (Cardy 1996). Minimizing with respect to M we find that, near T_c, $M^2 = (a/2b)t$, from which we read off the mean-field value of the critical exponent $\beta = 1/2$. This is not all that accurate compared with values measured in experiment, $\beta \approx 0.32$, but this is not surprising given the seemingly crude approximation that led to this result.

What *is* surprising is that the determination of the critical exponents from mean-field theory seems not to rely on any details of the model, *e.g.* the coefficients in Eq. (1.9), but only on the form of the expansion. In fact, Landau showed that such a form follows for systems with a scalar order parameter undergoing a continuous phase transition, from only simple symmetry arguments and assumptions of analyticity. Thus the disagreement between the critical exponents predicted by Landau theory and those observed in experiment was at first considered paradoxical, seemingly a violation of dimensional analysis (Goldenfeld 1992). The existence of so-called "anomalous dimensions," the differences between critical exponents observed in experiment and those predicted by Landau theory, was to be explained by the renormalization group. In the next section we will give a brief review of Landau theory and discuss how it breaks down near a critical point.

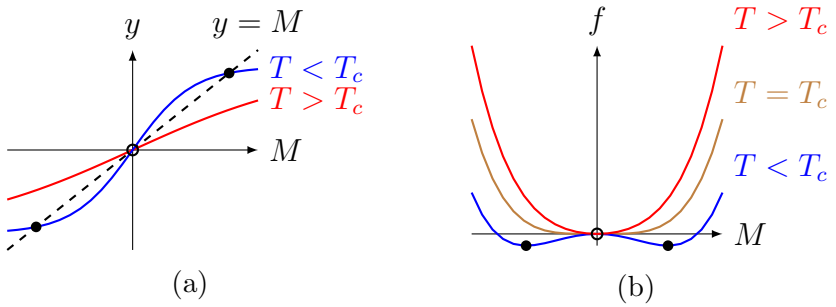

Figure 1.1: Panel (a) shows the right-hand side of the self-consistency condition, Eq. (1.5), as a function of the magnetization M for $H = 0$. Above the critical temperature T_c there is a single self-consistent solution corresponding to zero magnetization, while below T_c there are two solutions with nonvanishing magnetization $M = \pm M_0$ in addition to the solution at $M = 0$. Panel (b) shows the free energy as a function of M, showing that for $T < T_c$, the solution with $M = 0$ is *unstable*.

Finally, we emphasize that there are many ways to generate equivalent mean-field theories for a given system. For example, we could have arrived at Eq. (1.5) by supposing that each spin behaves as an isolated spin in an external field equal to $H + zJM$, where, ignoring fluctuations, we approximate the contribution of the neighbors as zJM. Note that this is *equivalent* to an (infinite-size) model where *every* pair of spins is coupled by an interaction J/N, because the thermal average M is equivalent to the average over an infinite number of neighbors in the latter case.

1.2.2 Landau theory

The Landau theory of phase transitions is a phenomenological theory based on a few simple assumptions about the behavior of the relevant order parameter η in the vicinity of a phase transition. We define a function $\mathcal{L}(\eta)$, called the Landau free energy, whose global minimum is supposed to give the equilibrium state of the system, and postulate that

1. The order parameter $\eta = 0$ in the disordered phase; η is small and nonzero in the ordered phase close to the transition.

2. $\mathcal{L}$ respects the symmetries of the underlying Hamiltonian.

3. $\mathcal{L}$ is an analytic function of both η and the set of couplings $\{K\}$ describing the interactions; thus it can be expanded as a power series in η near the critical point.

4. $\mathcal{L}$ is a local function of η, *i.e.* it only involves derivatives to a finite order.

For the Ising model an appropriate choice of order parameter is $\eta = M$, the magnetization. Because of the time-reversal ($S_i \to -S_i$) symmetry of the Hamiltonian, we require that the Landau free energy $\mathcal{L}(\eta)$ be symmetric about $\eta = 0$ in the absence of an external field. Expanding $\mathcal{L}(\eta)$ in powers of η near the critical point, we obtain the form

$$\mathcal{L} = at\eta^2 + \frac{1}{2}b\eta^4 - H\eta, \tag{1.10}$$

where the last term is the leading-order contribution to the energy in a field H and, as can be seen from Item 1, a and b are independent of the reduced temperature t to leading order. Note that this is the same form as Eq. (1.9), which we derived before by solving a mean-field model of Ising model Hamiltonian. Here, we arrive at the same form using only the postulates of Landau theory. The only details of the Ising model that were relevant to the derivation are the fact that the order parameter is a scalar, and that the Hamiltonian obeys time-reversal symmetry in zero field.

To calculate correlation functions in Landau theory, we allow η to vary in space. We may define a spatially-varying order parameter for the Ising model by using a coarse-graining procedure whereby $\eta(\boldsymbol{r})$ is defined to be the average of the spins

in a block of size Λ^{-1} centered at $\boldsymbol{r}$. Choosing $\Lambda^{-1} \sim \xi$, the correlation length, ensures that spins within a given block have similar values. The coarse-grained Landau free energy is then defined as the sum of the Landau free energies of the individual blocks, plus interaction terms that act to penalize differences in $\eta(\boldsymbol{r})$ between adjacent blocks. The latter are what give rise to spatial correlations. In the spirit of Landau theory we consider only the lowest-order (quadratic) term in the expansion of the interactions, and thus obtain for the coarse-grained Landau free energy

$$L_\Lambda[\eta] = \sum_{\boldsymbol{r}} \left[\sum_{\boldsymbol{\delta}} \frac{\gamma'}{2} \left(\frac{\eta(\boldsymbol{r}) - \eta(\boldsymbol{r}+\boldsymbol{\delta})}{\Lambda^{-1}} \right)^2 + at\eta^2 + \frac{1}{2} b\eta^4 - H(\boldsymbol{r})\eta(\boldsymbol{r}) \right], \quad (1.11)$$

where the second sum is over adjacent blocks with centers at $\boldsymbol{r}+\boldsymbol{\delta}, |\boldsymbol{\delta}| = \Lambda^{-1}$, and γ' is a coupling constant. Near a critical point, the correlation length ξ is much larger than the lattice spacing a; in this limit $\eta(\boldsymbol{r})$ is a continuous, slowly-varying function of position, and we obtain the *Ginzburg-Landau free energy*,

$$L_\Lambda[\eta] = \int \mathrm{d}^d \boldsymbol{r} \left\{ \frac{\gamma}{2} (\nabla\eta)^2 + at\eta^2 + \frac{1}{2} b\eta^4 - H\eta \right\}. \quad (1.12)$$

Note that $\eta(\boldsymbol{r})$ and $L_\Lambda[\eta(\boldsymbol{r})]$ both depend on the length scale Λ^{-1} over which the coarse graining is performed. To make a connection between the Ginzburg-Landau free energy and the *thermodynamic* free energy, we note that

$$e^{-\beta L_\Lambda[\eta(\boldsymbol{r})]} = \mathrm{Tr}'\, e^{-\beta H\{S_i\}}, \quad (1.13)$$

where Tr' indicates that the trace is to be taken over only those microscopic configurations which are compatible with the coarse-grained order parameter $\eta(\boldsymbol{r})$. Then the partition function is obtained by averaging over all configurations of the coarse-grained order parameter, *i.e.* by the functional integral

$$Z = \int \mathcal{D}\eta\, e^{-\beta L_\Lambda[\eta(\boldsymbol{r})]}, \quad (1.14)$$

called the Ginzburg-Landau-Wilson (GLW) functional. If we drop the quartic term in Eq. (1.12), then Eq. (1.14) reduces to a (functional) Gaussian integral which can be evaluated straightforwardly. The resulting *Gaussian approximation* corresponds to the assumption that the fluctuations of the order parameter are distributed as Gaussian random variables. From the resulting approximation of the free energy we obtain critical exponents characterizing the phase transition, which we refer to hereafter as the *mean-field exponents*.

In principle we should be able to improve on the Gaussian approximation by perturbatively including the quartic term in Eq. (1.12). First, we need to find a small, dimensionless parameter in which to expand. From Eq. (1.12) we define the *Ginzburg-Landau-Wilson effective Hamiltonian*,

$$\mathcal{H}_{\text{eff}}\left[\phi\right] \equiv \beta L_{\Lambda} = \int \mathrm{d}^{d}\boldsymbol{r}\left[\frac{1}{2}(\nabla\phi)^{2} + \frac{1}{2}r_{0}\phi^{2} + \frac{1}{4}u_{0}\phi^{4}\right], \tag{1.15}$$

where we have rescaled the order parameter $\phi \equiv (\beta\gamma)^{1/2}\eta$ so that the coefficient of the derivative term is just $1/2$, and $r_0/2 \equiv at/\gamma$, $u_0/4 \equiv b/(2\beta\gamma^2)$ (Goldenfeld 1992). Because $\mathcal{H}_{\text{eff}}$ is dimensionless, we find from the first term in Eq. (1.15) that ϕ must have dimensions $L^{1-d/2}$, where L is a unit of length. Hence we find that r_0 has dimensions of L^{-2} and u_0 has dimensions of L^{d-4}. To write this in terms of dimensionless variables we use as a length scale $L \equiv r_0^{-1/2}$, which is proportional to the correlation length in the Gaussian approximation since $\xi \propto t^{-1/2}$. Thus,

$$\mathcal{H}_{\text{eff}}\left[\varphi\right] = \int \mathrm{d}^{d}\boldsymbol{x}\left[\frac{1}{2}(\nabla\varphi)^{2} + \frac{1}{2}\varphi^{2} + \frac{1}{4}\overline{u}_{0}\varphi^{4}\right] \tag{1.16}$$

where

$$\boldsymbol{x} \equiv \boldsymbol{r}/L \qquad \varphi = \phi/L^{1-d/2} \qquad \overline{u}_{0} = u_{0}/L^{d-4}. \tag{1.17}$$

Now, to perturbatively include the quartic term, we define

$$\mathcal{H}_0 \equiv \int \mathrm{d}^d\boldsymbol{r} \left[\frac{1}{2}(\nabla\varphi)^2 + \frac{1}{2}\varphi^2\right] \tag{1.18}$$

$$\mathcal{H}_{\text{int}} \equiv \int \mathrm{d}^d\boldsymbol{r} \left[\frac{1}{4}\overline{u}_0\varphi^4\right], \tag{1.19}$$

where $\mathcal{H}_0$ is corresponds to the Gaussian approximation, and expand the partition function in powers of $\mathcal{H}_{\text{int}}$,

$$\begin{aligned} Z &= \int \mathcal{D}\phi\, e^{-\mathcal{H}_{\text{eff}}} \\ &= \int \mathcal{D}\phi\, e^{-\mathcal{H}_0} e^{-\mathcal{H}_{\text{int}}} \\ &= \int \mathcal{D}\phi\, e^{-\mathcal{H}_0}\left(1 - \mathcal{H}_{\text{int}} + \frac{1}{2}\mathcal{H}_{\text{int}}^2 - \cdots\right). \end{aligned}$$

Such an expansion is reasonable when the coefficient of the quartic term, $\overline{u}_0$, is small. However, using dimensional analysis, we have shown that $\overline{u}_0 \propto t^{(d-4)/2}$. This means that, in dimensions $d < 4$, the "perturbation" actually diverges as we approach the critical point; consequently, while keeping additional terms in the perturbation series may improve the accuracy of the theory away from the critical point, mean-field theory, the Gaussian approximation, and *any* theory based on keeping a finite number of terms in the perturbation series will fail to accurately describe the critical phenomena. On the other hand, for $d > 4$, the perturbation vanishes in the limit $t \to 0$, and hence including additional terms in the perturbation series has no effect on the asymptotic form of the solution. The conclusion is that the mean-field critical exponents are *exact* in dimensions $d > 4$ for systems described by the same Landau theory as the Ising model (*i.e.*, the Ising universality class). For a given universality class, we define the *upper critical dimension* d_u to be the dimension above which the mean-field critical exponents are exact. Hence this result corresponds to $d_u = 4$ for the Ising universality class.

1.3 Disorder and spin glasses

Historically, much progress has been made in the theory of condensed matter physics by studying idealized models in which atoms lie on a regular crystal lattice. For example, the theory of electronic band structures, which successfully explains many physical properties of solids, arises from Bloch waves in a periodic potential.

However, real crystals have some degree of *disorder* in the form of distortions, impurities, and, at finite temperature, thermal fluctuations of the atoms about their mean positions. One manifestation of this which is observed in experiment is a small positive correction to the resistivity of metals and semiconductors relative to the prediction of band theory. However, the effect of disorder can be drastic in some cases. In a seminal paper, Anderson (1958) demonstrated the phenomenon now known as *Anderson localization*, in which the diffusion of electrons is *entirely* suppressed in three-dimensional (and higher) systems when the amount of disorder exceeds a certain threshold. Furthermore, in one and two dimensions, diffusion is suppressed for *any* amount of disorder. The realization that the presence of disorder may result not just in quantitative corrections to an idealized theory, but in entirely new qualitative behavior, motivates the study of disordered systems.

In the early 1970s, experimental studies of magnetic ordering in a class of materials called "dilute magnetic alloys" found surprising results. The materials in question consist of a nonmagnetic "host" metal (*e.g.* Au, Ag, Cu, Pt) with a low concentration of magnetic impurities (*e.g.* Fe or Mn) occupying random sites. One historically-important result concerns the behavior of such a material at low temperature subjected to an oscillating magnetic field. Measuring the (ac) susceptibilty, defined as the time average of $\chi = \partial M/\partial H$, Cannella and Mydosh (1972) found that a cusp occured at a specific temperature which depended strongly on

the concentration of impurities. Below the cusp they found no evidence of ferromagnetic order, excluding the possibility of a ferromagnetic transition. Neither was this consistent with emergence of *anti*ferromagnetic order, where we would expect a peak in the susceptibility at the transition temperature, but this temperature should not to depend strongly on the concentration of impurities.

A unique feature of the "classical spin glasses" described above is the RKKY-type[3] interaction between the dilute magnetic impurities, mediated by conduction electrons. Thus, the effective exchange coupling $J(r)$ between two impurity atoms separated by a distance r has the form

$$J(r) \sim \frac{\cos(2k_F r)}{r^3}, \tag{1.20}$$

where k_F is the Fermi wavenumber of the host metal (Binder and A. P. Young 1986). The important feature here is the oscillation of the *sign* of the interaction with distance which, when combined with the spatial disorder of the impurity atoms, leads to interactions between each pair of impurity atoms which are randomly ferromagnetic or antiferromagnetic. In a seminal paper which initiated the modern theory of spin glasses, Edwards and Anderson (1975) identified this competition between ferromagnetic and antiferromagnetic interactions as the essential physics responsible for the surprising behavior of spin glasses.

1.3.1 Edwards-Anderson model

Edwards and Anderson (1975) proposed the following simple-looking model of a spin glass, whose Hamiltonian has the same form as that of the Ising model,

$$\mathcal{H} = -\frac{1}{2}\sum_{ij} J_{ij} S_i S_j - \sum_i H_i S_i, \tag{1.21}$$

[3]named for Ruderman, Kittel, Kasuya, and Yosida

but where the nearest-neighbor couplings J_{ij} are independent, Gaussian random variables with mean zero and variance σ^2, which is usually taken to be unity. As for the Ising model, the spins take values ± 1 and are arranged on a hypercubic lattice in d dimensions.

The Edwards-Anderson (EA) model captures the two essential features of spin glasses, *frustration* and *quenched disorder*. Frustration means that there is no configuration of the system which *simultaneously* minimizes all terms in the energy. A simple example of this is an Ising antiferromagnet (*i.e.* the Ising model with coupling $J < 0$) defined on a lattice with odd cycle lengths, for example on a hexagonal lattice as shown in Fig. 1.2a. Quenched disorder means that the interactions are random and expected to be independent of time, at least on experimental time scales. Figure 1.2b shows how the random interactions in EA model lead to frustration.

Within the framework of the EA model, we now return to the mystery of the apparent spin-glass phase transition observed in experiment. In (anti)ferromagnetism, the broken symmetry is characterized by a scalar order parameter, the (staggered) magnetization, but this is identically zero in the EA model. It is not at all obvious what is the nature of the broken symmetry in the spin glass phase and what is an appropriate order parameter to describe it. Edwards and Anderson (1975) proposed to use the sum of the squared thermal averages of the spins,

$$q_{\mathrm{EA}} = \frac{1}{N} \sum_{i=1}^{N} \langle S_i \rangle^2 \,, \tag{1.22}$$

which vanishes at high temperature, where the behavior is paramagnetic, but is certainly finite at zero temperature, where the spin settle into some (not necessarily unique) energy-minimizing configuration. It is now known that, in dimensions $d > 2$, there is a finite-temperature transition to a "spin-glass phase" accompanied

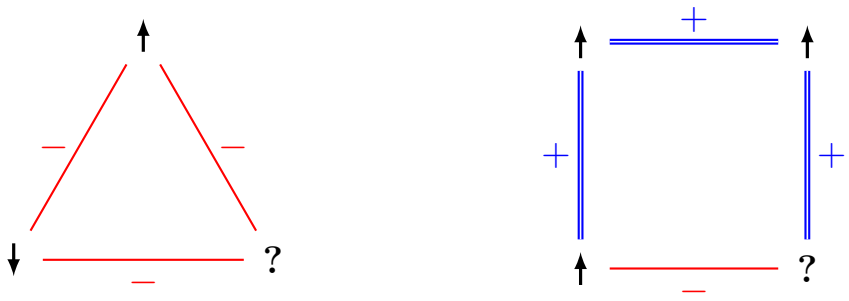

(a) frustration

(b) frustration and disorder

Figure 1.2: Examples of frustrated Ising systems. On the left (a) is an antiferromagnet on a lattice with odd cycles. On the right (b) is the EA model on a lattice which does not necessarily have odd cycles, but will in general have cycles with an odd number of antiferromagnetic bonds. In each example there is no assignment of "?" which simultaneously minimizes all terms of the Hamiltonian.

by a finite value of q_{EA}.

It is important to note that it is still unsettled issue whether this *scalar* order parameter fully characterizes the broken symmetry of the spin-glass phase. In fact, there are several competing theories which make quite different predictions as to the nature of the broken symmetry. For example, "replica symmetry breaking" (RSB) theory predicts that there are infinitely many "pure" states,[4] unrelated by any symmetry, and thus an infinite number of order parameters are necessary to describe the broken symmetry. In contrast, the "droplet picture" predicts that there is only a single pair of pure states, as for the ferromagnet, and thus a scalar order parameter is sufficient to describe the broken symmetry. These two theories will be discussed in more detail in Section 1.3.4.

As alluded to above, despite its apparent simplicity and decades of study, the EA model remains poorly understood. In contrast to the Ising ferromagnet, which is found to have a (finite-temperature) phase transition in dimensions $d \geq 2$, the

[4]That is, states analogous to the "up" or "down" states observed in an Ising ferromagnet below the transition temperature. See Section 5.1 for a discussion of this idea.

EA model has a finite-temperature transition only for $d > 2$.[5] But computing spin glass partition function, and even finding the ground state, for $d > 2$ appears to be intractable; in fact, both problems have been shown to be NP-hard by Barahona (1982), suggesting that an eventual closed-form solution is unlikely. This is unsurprising because the presence of frustration and disorder means that finding the ground state is a nontrivial optimization problem.

Even defining a mean-field theory for spin glasses in the way discussed previously does not seem at first straightforward, since it is not clear how to deal with the quenched disorder. Sherrington and Kirkpatrick (1975) made an important contribution to the theory of spin glasses by proposing a solvable mean-field model of a spin glass. The solution they provided successfully explained some features observed in experiment, such as the susceptibility cusp, but opened new important questions and deepened the mystery in some ways.

1.3.2 Sherrington-Kirkpatrick mean-field model

As noted above, one way to generate a mean-field theory is to extend interactions to be infinite-range, so that every degree of freedom interacts equally with all others, while rescaling the interactions with the inverse system size to preserve a sensible thermodynamic limit. In this way the model of Sherrington and Kirkpatrick (1975) is the mean-field counterpart of the EA model. That is, the Sherrington-Kirkpatrick (SK) model differs from the EA model in that all pairs of spins interact, with the variance of the couplings given by $\sigma^2 \propto 1/N$ regardless of distance (by convention the constant of proportionality is taken to be one).

While the analogous mean-field model has a straightforward solution for the

[5] In fact, evidence suggests that the lower critical dimension is between 2 and 3 for short-range models (Hartmann and A. P. Young 2001). Models with long-range interactions correspond to short-range models with non-integral effective dimension.

case of the ferromagnet, the introduction of disorder makes the solution of the SK model much more difficult. The difficulty arises in carrying out the average over the quenched disorder to obtain a result which does not depend on the particular realization of the random couplings. To obtain the disorder-averaged free energy, formally

$$[F] \equiv \int \mathcal{D}\mathcal{J}\, P(\mathcal{J}) F(\mathcal{J}) \tag{1.23}$$

(where $[\cdots]$ indicates a disorder average and $\mathcal{J} \equiv \{J_{ij}\}$ denotes a set of couplings), we need to carry out a disorder average of the logarithm of the partition function. Sherrington and Kirkpatrick (1975) did this in clever way, using the so-called "replica trick," which is based on the identity

$$\log Z = \lim_{n \to 0} \frac{Z^n - 1}{n}. \tag{1.24}$$

Using this to write

$$-\beta\,[F] = [\log Z] = \lim_{n \to 0} \frac{[Z^n] - 1}{n}, \tag{1.25}$$

we have reduced the problem to computing

$$\begin{aligned}
[Z^n] &= \left[\prod_{\alpha=1}^{n} \mathrm{Tr}_{S^\alpha}\, e^{-\beta \mathcal{H}\left(\{S^\alpha\}, \mathcal{J}\right)} \right] \\
&= \left[\mathrm{Tr}_{S^1} \cdots \mathrm{Tr}_{S^n}\, e^{-\beta \sum_{\alpha=1}^{n} \mathcal{H}\left(\{S^\alpha\}, \mathcal{J}\right)} \right] \\
&= \mathrm{Tr}_{S^1} \cdots \mathrm{Tr}_{S^n} \left[e^{-\beta \sum_{\alpha=1}^{n} \mathcal{H}\left(\{S^\alpha\}, \mathcal{J}\right)} \right],
\end{aligned}$$

for which the disorder average can be computed analytically. Finally, we take the limit $n \to 0$ to obtain the disorder-averaged free energy. The replica trick gets its name because the disorder average is done over a compound system of n replicas, all with the same realization of the disorder $\mathcal{J}$, described by the partition function Z^n. Interestingly, the effective Hamiltonian of the n-replica system $\mathcal{H}_n$, defined by

$$e^{-\beta \mathcal{H}_n} = \left[e^{-\beta \sum_{\alpha=1}^{n} \mathcal{H}\left(\{S^\alpha\}, \mathcal{J}\right)} \right], \tag{1.26}$$

is not just the sum of the Hamiltonians of the individual replicas; therefore, the disorder average *couples* the replicas. Because the effective Hamiltonian is symmetric under the permutation of replicas (after all the "replicas" were only introduced as a mathematical trick), the solution of Sherrington and Kirkpatrick makes the (reasonable) assumption that replicas may be treated on equal footing; theirs is a *replica-symmetric* solution.

The solution given by Sherrington and Kirkpatrick predicts a transition temperature

$$T_c^{\mathrm{MF}} = \sum_j \left[J_{ij}^2 \right] \equiv 1, \tag{1.27}$$

and successfully explains some of the features observed in experiment, for example the cusp in ac susceptibility. However, it soon became clear that it could not be a correct description of the low-temperature phase, where it was found to be at odds with simulation results and furthermore predicted an unphysical *negative* entropy at zero temperature (Kirkpatrick and Sherrington 1978). An important piece of the puzzle was provided by de Almeida and Thouless (1978), who showed that the replica-symmetric solution of the SK model becomes unstable for $T < 1$ in zero field.[6] The replica-symmetric solution is therefore not observed, just as the paramagnetic solution of the mean-field Ising model is not observed in the ordered phase. Instead, the replica symmetry is spontaneously broken.

1.3.3 Replica symmetry breaking

The correct *stable* solution of the SK model in the low-temperature phase was discovered and developed by Giorgio Parisi in a series of seminal papers.[7] The

[6] In fact, they show that the replica-symmetric solution is unstable in a region of the T-H plane for $T < 1$ and small fields, thus predicting a line of transitions known as the *de Almeida-Thouless line*.

[7] Parisi (1979), Parisi (1980a), Parisi (1980b), and Parisi (1983)

breakthrough idea was that, to find a stable solution in the low-temperature phase, the replicas can no longer be considered to be equivalent; although the effective Hamiltonian is symmetric under the permutation of replicas, this symmetry is spontaneously broken in the spin-glass phase. More precisely, Parisi considered the *overlap* between the configurations of two replicas α and β, defined as

$$q_{\alpha\beta} = \frac{1}{N} \sum_i \left\langle S_i^\alpha S_i^\beta \right\rangle_n , \tag{1.28}$$

where the average is taken with respect to the n-replica effective Hamiltonian. The replica-symmetric solution of Sherrington and Kirkpatrick assumes that $q_{\alpha\beta}$ is independent of which replicas α and β are chosen, and is just equal to the Edwards-Anderson order parameter $q_{\rm EA}$. By contrast, in Parisi's *replica symmetry breaking* (RSB) solution, the replicas are *not* equivalent; instead, each corresponds to one of an infinite number of distinct pure states[8] in the thermodynamic limit; thus $q_{\alpha\beta}$ depends on which α and β are chosen, giving the overlap between the corresponding pure states. The self-overlap of a replica with itself $q_{\alpha\alpha} = q_{\rm EA}$, but in general $-q_{\rm EA} < q_{\alpha\beta} < q_{\rm EA}$. Note that pure states come in symmetry-related pairs, so for states α, β, the time-reversed versions $\overline{\alpha}$, $\overline{\beta}$ are also pure states, and $q_{\alpha\beta} = -q_{\overline{\alpha}\beta} = q_{\alpha\overline{\beta}}$. Thus the distribution of the overlap q between two independent equilibrium spin configurations is an even function, consisting of a superposition of delta functions with weights and positions which depend on the disorder realization $\mathcal{J}$,

$$P_{\mathcal{J}}(q) = \sum_{\alpha\beta} W_\alpha W_\beta \, \delta(q - q_{\alpha\beta}), \tag{1.29}$$

where W_α and W_β are the probabilities ("weights") of the states α and β respectively. Now we consider what this looks like at low temperature, where presumably

[8] That is, thermodynamic states in which connected correlations vanish in the limit of large distance; the "up" and "down" states of the ferromagnetic phase are examples of pure states.

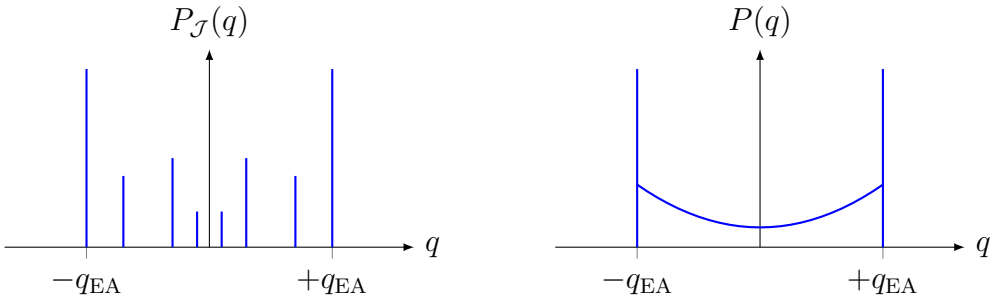

(a) single sample (b) disorder average

Figure 1.3: Sketches of the overlap distribution for (a) a single sample and (b) the sample average, according to replica symmetry breaking (RSB) theory. The support in the region $-q_{\mathrm{EA}} < q < q_{\mathrm{EA}}$ in the disorder-averaged $P(q)$ in (b) comes from the many pairs of pure states for each sample, *e.g.* in (a).

only a few of the (infinite number of) pure states have significant weight. The distribution is bimodal, with the largest weights occurring at $\pm q_{\mathrm{EA}}$; these correspond to self-overlaps, and thus have weight $\sum_\alpha W_\alpha^2$. Between $-q_{\mathrm{EA}}$ and q_{EA} are smaller peaks corresponding to overlaps of distinct pairs of pure states α, β with weights $W_\alpha W_\beta$. This is sketched in Fig. 1.3a.

One surprising result of RSB theory is that the overlap distribution for a single disorder realization $P_{\mathcal{J}}(q)$ is non-self-averaging, meaning that it depends on $\mathcal{J}$ even in the thermodynamic limit. This is at first a little unsettling, because the whole procedure of carrying out the disorder average is justified by the thermodynamic assumption that we can determine the properties of a macroscopic system as an average over subsystems. But this turns out not to be contradictory, as all *observable* properties are self-averaging within the RSB framework (Stein and C. M. Newman 2013). Carrying out the disorder average, we obtain an overlap distribution that has two delta-function peaks at $\pm q_{\mathrm{EA}}$ and is finite everywhere in between. This is sketched in Fig. 1.3b. The weight of the sample-averaged distribution at $q = 0$ is found to be a constant independent of system size for large L.

The RSB solution appears to be the correct description of the low-temperature phase of the SK model, and several of its predictions (although notably not the non-self-averaging of the overlap distribution) have more recently been proven rigorously for the SK model (Talagrand 2003). This has led Parisi and others to conjecture that RSB also provides an accurate description spin-glass phase in more realistic, short-range models such as the Edwards-Anderson model. This is at odds with other competing theories of the spin-glass phase in short-range models.

1.3.4 Theories of short-range spin glasses

The RSB solution of the Sherrington-Kirkpatrick mean-field model predicts several surprising features, such as non-self-averaging of the order parameter distribution and the existence of a line of transitions in nonzero field (*i.e.* the de Almeida-Thouless line), that are not observed in systems without disorder. It has been a controversial issue whether these exotic features, which certainly exist in the SK model, persist in more realistic models with short-range interactions, or whether they are artifacts of the infinite-range interactions, and the nature of the spin-glass phase in short-range models can be explained by a simpler phenomenological picture.

One well-known alternate scenario is the "droplet picture" (DP) introduced by Fisher and Huse (D. S. Fisher and Huse 1986; D. S. Fisher and Huse 1987; D. S. Fisher and Huse 1988), based on the phenomenological scaling arguments of McMillan (1984). The central *ansatz* is that lowest-energy excitations of a ground state which have spatial extent L have an energy cost which scales as L^θ, where θ is a positive ("stiffness") exponent. Consequently, in the thermodynamic limit, excitations which flip a finite fraction of the spins cost an infinite amount

of energy. Additionally, the excitations are predicted to have a fractal surface, with dimension $d_s < d$. Both of these statements are at odds with the predictions of RSB, according to which excitations have an energy which is independent of L and hence excitations which flip a finite fraction of spins can have *finite* energy cost in the thermodynamic limit; also, excitations in RSB are predicted to be space-filling, *i.e.* to have a dimension $d_s = d$.

Further analysis reveals that, in the droplet picture, there can be only a single time-reversed pair of pure states in the thermodynamic limit, in contrast to the infinitely-many predicted by RSB theory. Hence the droplet picture predicts an overlap distribution which is sharply different from the prediction of RSB in the thermodynamic limit. As discussed previously, RSB theory predicts finite probability everywhere between $-q_{\mathrm{EA}}$ and q_{EA}. In contrast, the droplet picture predicts finite probability in the region $-q_{\mathrm{EA}} < q < q_{\mathrm{EA}}$ only for finite systems; $P(q)$ in this region is expected to vanish as $L^{-\theta}$ (Moore, Bokil, and Drossel 1998) in the thermodynamic limit, leaving a trivial distribution with two delta functions at $\pm q_{\mathrm{EA}}$ and vanishing weight in between. Both distributions are sketched in Fig. 1.4.

Because $P(q)$ is relatively easy to measure in simulations, many numerical studies[9] have attempted to find evidence for one picture or the other by studying the overlap distribution near $q = 0$ for a range of system sizes L and looking for a $L^{-\theta}$ decay as predicted by the droplet picture. The results appear consistent with RSB in that $P(0)$ varies only very slowly with L; however, it has been argued that the sizes accessible to simulation are too small to observe the asymptotic behavior, and the droplet picture cannot be ruled out (Moore, Bokil, and Drossel 1998; Middleton 2013). In Chapter 4 of this thesis we study alternate statistics of the overlap distributions of individual samples, $P_{\mathcal{J}}(q)$, in an attempt to distinguish

[9] *e.g.* Marinari, Parisi, Ricci-Tersenghi, et al. (2000), Reger, Bhatt, and A. P. Young (1990), Katzgraber, Palassini, and A. P. Young (2001), and Katzgraber and A. P. Young (2003)

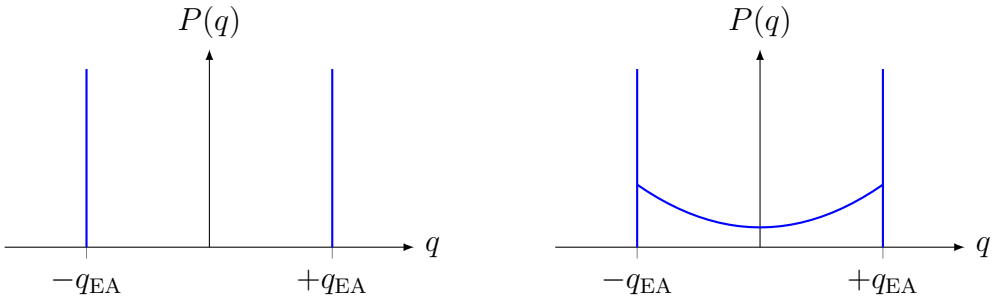

(a) droplet picture (b) RSB picture

Figure 1.4: Comparison of disorder-averaged overlap distributions in the thermodynamic limit for (a) the droplet picture and (b) the RSB picture. The droplet $P(q)$ is trivial in the thermodynamic limit, with two delta functions at $\pm q_{\rm EA}$. In contrast, the RSB $P(q)$ has finite weight everywhere in the region $-q_{\rm EA} < q < q_{\rm EA}$.

the behavior as RSB-like or droplet-like.

C. M. Newman and Stein (1996) lend some support for the argument that RSB is not a realistic description of short-range spin glasses with a proof that non-self-averaging *cannot* occur based on simple symmetry considerations. Thus the "standard" RSB scenario, in which the single-sample overlap distribution is non-self-averaging, cannot be correct for short-range spin glasses. Newman and Stein (NS) argue that a flaw lies in the assumption of convergence to a unique mixed state [*i.e.* a unique distribution $P_{\mathcal{J}}(q)$] in the thermodynamic limit; instead, they argue, the mixed state which is observed has the property of *chaotic size dependence* (C. M. Newman and Stein 1992), meaning that it wanders continually with increasing L, sampling from all possible mixed states. The fundamental object, then, is the probability distribution which is sampled, called the "metastate." In Chapter 5 we investigate the connection between the metastate and the sampling of pure states generated by nonequilibrium dynamics.

Within the metastate description, C. M. Newman and Stein (1997) show that it is possible to recover the many-states picture of RSB, *i.e.* an overlap distribution $P(q)$ like that shown in Fig. 1.4b. In this "non-standard RSB" (which is actually

the only viable form of RSB for short-range spin glasses), the disorder-averaged overlap distribution of standard RSB theory is instead obtained from a metastate average for a *single* disorder realization. Thus the NS description avoids the property of non-self-averaging which is the downfall of the standard RSB picture applied to short-range spin glasses.

While NS have provided an interpretation of RSB which is viable for short-range spin glasses, results concerning the invariance of the metastate under a change of boundary conditions strongly suggest that it cannot occur in realistic spin glasses, and instead a simpler picture (which is still consistent with chaotic size dependence) holds (C. M. Newman and Stein 1998). One such proposal is the *chaotic pairs* picture (C. M. Newman and Stein 1996) which, like the droplet picture, predicts a trivial structure for the sample-averaged overlap distribution, with a pair of delta function peaks at $\pm q_{\mathrm{EA}}$ (*i.e.* the same as Fig. 1.4a). However, in contrast to the droplet picture, in the chaotic pairs picture this distribution arises from a pair of pure states which exhibit chaotic size dependence but whose *overlaps* converge to $\pm q_{\mathrm{EA}}$ in the thermodynamic limit.

1.4 Organization of the dissertation

In Chapter 2 we give an overview of the numerical methods used in the research.

In Chapter 3, we study one-dimensional long-range (1DLR) spin glass models to fill in a previously unexplored region of parameter space in which the interactions become sufficiently long-range that they must be rescaled with the system size to maintain the thermodynamic limit. We find strong evidence that detailed behavior of the 1DLR models everywhere in this "nonextensive regime" is identical to that of the Sherrington-Kirkpatrick model, lending support to a recent

conjecture.

In Chapter 4 we attempt to distinguish the RSB and droplet pictures by studying recently-proposed observables based on the statistics of individual disorder samples, rather than simply averaging over the disorder as is most frequently done in previous studies. We compare Monte Carlo results for 1DLR models which are proxies for short-range models in 3, 4, and 10 dimensions with previously-obtained data for the 3D and 4D short-range models and the SK model. For one statistic, which is expected to sharply distinguish between the two pictures in the thermodynamic limit, we find that larger system sizes than those currently feasible to simulate are needed to obtain an unambiguous result. We also find that two other recently-proposed statistics, the median of the cumulative overlap distribution and the "typical" overlap distribution, are not particularly helpful in distinguishing between the RSB and droplet pictures.

In Chapter 5 we study the evolution of dynamical correlations in a 1DLR model which is a proxy for a short-range model in $d = 8$ dimensions. We find that the spatial decay of the correlations at distances less than the dynamical correlation length $\xi(t)$ agrees quantitatively with the predictions of the metastate theory, evaluated according to the RSB picture. We also compute the dynamic exponent defined by $\xi(t) \propto t^{1/z(T)}$ and find that it is compatible with the mean-field value of the critical dynamical exponent for short-range spin glasses.

Finally, in Chapter 6 we present a unified view of finite-size scaling (FSS) in dimensions d above the upper critical dimension d_u, for both free and periodic boundary conditions. For $d > d_u$, a dangerous irrelevant variable is responsible for both the violation of hyperscaling and the violation of "standard" FSS. We find that the modified hyperscaling proposed to allow for this applies only to $\boldsymbol{k} = \mathbf{0}$ fluctuations, while standard FSS applies to $\boldsymbol{k} \neq \mathbf{0}$ fluctuations. Hence

the exponent η describing the power-law decay of correlations at criticality is unambiguously $\eta = 0$. With free boundary conditions, the finite-size "shift" is greater than the rounding. Nonetheless, using $T - T_L$, where T_L is the finite-size pseudocritical temperature, as the scaling variable, the data do collapse onto a scaling form that includes the behavior both at T_L, where the susceptibility χ diverges like $L^{d/2}$, and the bulk T_c, where it diverges like L^2. We support these claims with data from large-scale simulations of the five-dimensional Ising model.

Chapter 2

Numerical methods

2.1 Importance sampling

The aim of numerical simulations in statistical physics is often to compute the probability distribution of some observable X when a system, described by a Hamiltonian $\mathcal{H}$, is in equilibrium with a heat bath at temperature $T \equiv 1/\beta$,

$$P(x) = \frac{\operatorname{Tr} \delta(\hat{X} - x) \exp(-\beta \mathcal{H})}{\operatorname{Tr} \exp(-\beta \mathcal{H})}, \tag{2.1}$$

where $\delta(\hat{X} - x)$ is a projection onto the subspace of states where X has the particular value x. But computing Eq. (2.1) as written, that is, by summing over all the states of the system, is infeasible in practice. This is because the volume of the phase space over which we must average grows at least exponentially in the size of the system (for quantum systems the situation is even worse, with the *dimension* of the Hilbert space growing exponentially). To have any hope of studying systems with more than just a few degrees of freedom, we need an approximate method that doesn't require considering all of the possible states.

Importance sampling exploits the observation that most of the states of the system have vanishingly small probability for a given temperature, and thus most

of the terms in Eq. (2.1) can be neglected. By averaging over only the most probable states, which represent a small fraction of the overall phase space, we can in practice get an excellent approximation of the equilibrium probability distribution.

2.2 Markov Chain Monte Carlo

But how do we determine which states are the most probable without first enumerating all the possible states and computing the probability of each one? A solution is provided by *Markov Chain Monte Carlo* methods, which are essentially random walks in phase space where, at each iteration, the system transitions to a new state drawn from a probability distribution which depends only on the current state of the system. If the system is in a state l at time t, then the probability of a transition to state m at time $t+1$ is written $w_{l\to m}$. The the *change* in the probability that the system is in state l after one iteration is given by

$$P_l(t+1) - P_l(t) = \sum_{m:\, m\neq l} \left(P_m(t)\, w_{m\to l} - P_l(t)\, w_{l\to m} \right), \tag{2.2}$$

called the "master equation" in the literature. This can be understood intuitively by considering a large number of random walkers traversing the phase space according to the transition probabilities $w_{l\to m}$. We then interpret $P_l(t)$ as the fraction of walkers at state l at time t. Then the first term on the right represents the *gain* in probability from walkers transitioning *into* l, while the second term represents the *loss* in probability from walkers transitioning *out of* l.

It turns out that, after an initial "relaxation time," the random walkers will sample states from a steady-state distribution π_l which depends on the transition probabilities $w_{l\to m}$. Given a target distribution π_l, how do we choose the transition probabilities to achieve this? Clearly, a *necessary* condition is that the target

distribution π_l be a fixed point of Eq. (2.2), *i.e.*

$$\sum_{m:\, m\neq l} (\pi_m w_{m\to l} - \pi_l w_{l\to m}) = 0. \tag{2.3}$$

A stronger condition is obtained by requiring that each term in the sum vanish, *i.e.*

$$\pi_m w_{m\to l} = \pi_l w_{l\to m} \tag{2.4}$$

for all l, m. Although not strictly necessary for convergence, $w_{l\to m}$ is often chosen to satisfy the latter condition, called *detailed balance*. Note that Eq. (2.4) does not uniquely determine the transition probabilities, but only the ratio $w_{l\to m}/w_{m\to l}$ of the probability of a transition to the probability of the reverse transition. Of the many ways to satisfy Eq. (2.4), one of the most useful is the choice of Metropolis et al. (1953),

$$w_{l\to m} = \min\left\{1,\, \pi_m/\pi_l\right\} \quad \text{(Metropolis)}. \tag{2.5}$$

Another useful choice is the "heat-bath" probability,

$$w_{l\to m} = \frac{1}{1+\pi_l/\pi_m} \quad \text{(heat bath)}, \tag{2.6}$$

which has the nice property of being a smooth function of probability ratio. However, with a few exceptions, the "Metropolis probability" of Eq. (2.5) is most frequently used in practice because it leads to higher transition probabilities (see Fig. 2.1) and hence faster convergence. For Monte Carlo simulations in statistical physics, the target distribution is often the Boltzmann distribution, $\pi_l \propto \exp(-\beta E_l)$. In this special case the Metropolis transition probability is given by

$$w_{l\to m} = \min\left\{1,\, e^{-\beta(E_m - E_l)}\right\}. \tag{2.7}$$

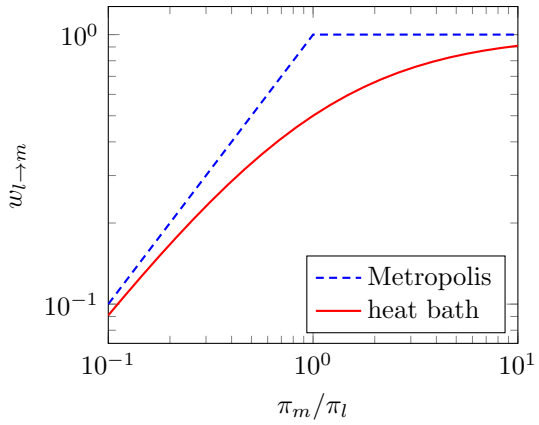

Figure 2.1: Comparison of the Metropolis and heat-bath transition probabilities as a function of the probability ratio of two states in the stationary distribution, π_m/π_l. Note that use of the Metropolis probability leads to larger transition probabilities and thus faster convergence to the stationary distribution.

2.2.1 Constructing a Markov chain

Clearly the detailed balance condition (2.4) is insufficient for convergence, as can be seen by considering the trivial case $w_{l\to m} = 0$. It turns out that convergence also requires *ergodicity*, which is the property that for any pair of states (l, m) it is possible to reach l from m in a finite number of steps.

Note that it is possible for *most* of the $w_{l\to m}$ to be zero while maintaining ergodicity. In other words, rather than considering moves from the current state to *every other* state at each iteration, we can consider just a handful of "neighboring" states. It is useful to imagine a graph where each vertex corresponds to a state of the system and an edge is drawn between two vertices if there is a nonzero probability of transition between the corresponding states. Then, as long as there is a path between every pair of vertices (states), the system is ergodic, and if the transition probabilities additionally satisfy Eq. (2.3), the Markov process will converge to the desired steady-state distribution. Monte Carlo algorithms in statistical physics exploit this fact because it is computationally infeasible to

consider transitions to all possible states at each iteration (actually, this would be no more efficient than directly computing Eq. (2.1)) and in any case the transition probabilities are vanishingly small for the vast majority of them.

In practice, Monte Carlo algorithms in statistical physics usually split each iteration into two parts: first, starting from initial state l, the algorithm selects or "proposes" a transition to state m with some probability $g_{l\to m}$; the proposed move is then accepted with probability $A_{l\to m}$, so that the overall probability of a transition from l to m is the product $w_{l\to m} = g_{l\to m}A_{l\to m}$ (E. J. Newman and Barkema 1999). To satisfy detailed balance (2.4) we must have

$$\frac{g_{l\to m}A_{l\to m}}{g_{m\to l}A_{m\to l}} = \frac{\pi_m}{\pi_l} = e^{-\beta(E_m - E_l)}. \tag{2.8}$$

In order for the algorithm to converge, the selection probabilities $g_{l\to m}$ must allow for ergodicity; that is, there must be a path between every pair of states such that at each step the selection probability is nonzero. The acceptance probabilities $A_{l\to m}$ can then be adjusted to satisfy, *e.g.*, detailed balance. This allows us considerable freedom in the choice of the selection probabilities; however, this choice is paramount to efficiency—the algorithm should propose moves that have reasonably large acceptance probabilities, otherwise it will waste many iterations "stuck" in the same state. On the other hand, the proposed moves should take us "far enough" in phase space that we explore the relevant regions efficiently . The tradeoff between these somewhat vague notions will be clarified in the following two examples of Monte Carlo algorithms for the Ising model.

2.3 Algorithms for the Ising model

Recall from Section 1.2 that the Ising model in d dimensions consists of N classical spins S_i, $i \in \{1, \ldots, N\}$, which take values $S_i = \pm 1$. The spins are put on a

hypercubic lattice of linear size L so that the number of spins $N = L^d$. The system is described by the Hamiltonian

$$\mathcal{H} = -\frac{1}{2}\sum_{ij} J_{ij} S_i S_j - \sum_i H_i S_i, \tag{2.9}$$

where $J_{ij} = J$ if i and j are nearest neighbors and zero otherwise, and H_i is the external field.

2.3.1 Single-spin flip dynamics

The classic example of a Monte Carlo method in statistical physics is the *Metropolis algorithm*, introduced by Metropolis et al. (1953). In this algorithm the proposed states differ from the current state by a single spin flip (*i.e.* $S_i \to -S_i$) and have uniform probability. That is,

$$g_{l\to m} = \begin{cases} 1/N & l \text{ and } m \text{ differ by a spin flip,} \\ 0 & \text{otherwise.} \end{cases} \tag{2.10}$$

Note that, because of the symmetry $g_{l\to m} = g_{m\to l}$, the selection probabilities drop out of detailed balance condition (2.8); consequently the acceptance probabilities satisfy detailed balance,

$$\frac{A_{l\to m}}{A_{m\to l}} = e^{-\beta(E_m - E_l)}. \tag{2.11}$$

Suppose $m[i]$ differs from l by a flip of S_i. Then the change in energy is

$$E_{m[i]} - E_l = 2\left(J\sum_{j\in\mathcal{N}[i]} S_j + H\right) S_i, \tag{2.12}$$

where the sum is over the neighbors of i. Finally, using the Metropolis convention (2.5) we obtain the acceptance probabilities

$$A_{l\to m[i]} = \min\left\{1,\, e^{-\beta(E_{m[i]} - E_l)}\right\}. \tag{2.13}$$

Since the allowed moves are given uniform probability independent of the state of the system, it makes no difference whether updates are done randomly or sequentially; for simplicity we usually update the spins sequentially. A single iteration over the N spins is called a *sweep* and is often taken as the basic unit of Monte Carlo time. Algorithm 1 is a minimal implementation of a Metropolis sweep, the core of the algorithm.

Algorithm 1 Minimal implementation of the Metropolis sweep.

procedure METROPOLIS-SWEEP(S)
  for $i \leftarrow 1, N$ **do**
    $H_S \leftarrow J \sum \{S_j : j \text{ neighbor of } i\}$ ▷ sum neighbor spins
    $\Delta E \leftarrow 2\,(H_S + H)\,S_i$ ▷ compute change in energy
    if $\Delta E < 0$ **or** RAND $< \exp\left(-\Delta E/T\right)$ **then**
      $S_i \leftarrow -S_i$ ▷ flip i-th spin
    end if
  end for
end procedure

2.3.2 Cluster dynamics

Another important class of Monte Carlo algorithms are *cluster algorithms*, which flip not just a single spin at a time but clusters of many spins. One of the first algorithms to make use of this idea is that of Swendsen and Wang (1987). Recall that in the Metropolis algorithm, the selection step is trivial and the physics enters through the acceptance probabilities. On the other hand, the Swendsen-Wang (SW) algorithm has a nontrivial selection step in which the spins are divided into clusters by a method that depends on the temperature and couplings, while the acceptance step is relatively simple: each cluster is flipped with probability 1/2.

Cluster algorithms such as SW are especially effective at temperatures near the

transition temperature, where the correlation length becomes large. Here cluster algorithms have a significant advantage over single-flip algorithms because they are able to realize long-distance correlations in a single move (by flipping large clusters of spins) whereas single-flip algorithms take many moves to propagate the effective interaction between two spins separated by a large distance. Thus cluster algorithms avoid the slow dynamics associated with the phenomenon of *critical slowing down* near a critical point. Farther from a critical point, cluster algorithms lose this advantage and in fact may become less efficient than single-flip algorithms: at high temperatures cluster algorithms essentially reduce to single-flip algorithms (with the additional overhead of rejected cluster-growth attempts); at low temperatures, clusters become comparable to the size of the system and, considering the up-down symmetry of the Ising model, the overall effect is to flip only a few spins at each iteration. In the latter case, the efficiency of the cluster algorithm is much worse than that of a single-flip algorithm, because each move involves an $O(N)$ cluster-growth procedure to essentially flip a few spins.

A variant of the SW algorithm which is simpler to implement but with similar good performace near the critical point is due to Wolff (1989). In this algorithm, we choose a random "seed" spin and "grow" a cluster outwards, adding like spins adjacent to the cluster with a probability $p_{\text{add}}(T/J)$ which depends only on the (dimensionless) temperature. When cluster growth is complete, all of the spins in the cluster are flipped.

To derive the value of p_{add} corresponding to a given temperature, we return to the detailed balance condition (2.4). Note that it is the *ratio* of selection probabilities of the forward and reverse moves that is relevant. In general there are many ways to grow the same cluster; for example, the seed spin could be any spin in the cluster. Following E. J. Newman and Barkema (1999), we consider a

particular way of growing the cluster which takes us from state $l \to m$, that is a particular seed spin and sequence of additions to the cluster. Consider also the particular reverse move which takes us from $m \to l$ starting from the same seed spin and with the same sequence of additions to the cluster.

Now, the change in energy when the cluster is flipped depends only on the relative orientations of the spins at its boundary. Suppose that n_f bonds are "broken" by the forward move, meaning that n_f pairs of spins that were formerly aligned are anti-aligned after the cluster flip, and n_r bonds are broken by the reverse move. Then the change in energy in going from $l \to m$ is $2J(n_f - n_r)$. To see this, note that broken bonds each contribute $2J$ to the energy, and also that the changes of energy of the forward and reverse moves must sum to zero. Thus, to satisfy detailed balance, we must have

$$\frac{g_{l\to m} A_{l\to m}}{g_{m\to l} A_{m\to l}} = e^{-2\beta J(n_f - n_r)}. \tag{2.14}$$

We now compute the selection probability for forward and reverse moves in terms of the parameter p_{add}. Broken bonds represent like spins that were rejected for addition to the cluster. Since the probability of each rejection is $1 - p_{\text{add}}$, the probability of selecting a cluster with n broken bonds is $(1 - p_{\text{add}})^n$. Thus, the *ratio* of selection probabilities for the forward and reverse moves is $(1-p_{\text{add}})^{n_f - n_r}$. Finally, we insert this into Eq. (2.14) to find the relationship between p_{add} and the ratio of acceptance probabilities,

$$(1 - p_{\text{add}})^{n_f - n_r} \frac{A_{l\to m}}{A_{m\to l}} = e^{-2\beta J(n_f - n_r)}. \tag{2.15}$$

Then comes a remarkable simplification: if we set

$$p_{\text{add}} = 1 - e^{-2\beta}, \tag{2.16}$$

Equation (2.15) is satisfied with $A_{l\to m}/A_{m\to l} = 1$. This means that we can simply accept all moves and still satisfy detailed balance!

A minimal implementation of the Wolff cluster update is given in Algorithms 2 and 3. This is a recursive implementation which uses a *depth-first search* to grow the cluster. The choice of search order makes no difference in the overall efficiency of the algorithm (E. J. Newman and Barkema 1999), but comparison of results obtained using different search orders can be a useful check for correctness, and some hybrid approaches are more memory-efficient (Martın-Herrero 2004).

Note that spins are flipped as the cluster is grown rather than at the end of cluster growth. This is equivalent to the procedure described above, but does not require an additional size $O(N)$ buffer to keep track of the cluster.

Algorithm 2 Minimal implementation of the Wolff cluster algorithm.

```
procedure WOLFF-CLUSTER-UPDATE(S)
    p ← 1 − e^{−2/T}          ▷ probability to add a spin to the cluster
    i ← RAND-INT(1, N)        ▷ choose random spin to seed the cluster
    σ ← S_i                   ▷ save the cluster spin
    GROW-CLUSTER(S, i)        ▷ grow a cluster starting from the seed
end procedure
```

Algorithm 3 Recursive cluster-growth procedure for the Wolff algorithm.

```
procedure GROW-CLUSTER(S, i)
    S_i ← −S_i                                  ▷ flip spin
    for all j ∈ neighbors of i do
        if S_j = σ and RAND < p then            ▷ check if like spin and flip coin...
            GROW-CLUSTER(S, j)                  ▷ recurse...
        end if
    end for
end procedure
```

2.4 Convergence to equilibrium

Having seen several practical applications of Markov Chain Monte Carlo algorithms in statistical physics, in this section we return to the general problem of

convergence. We have seen how to choose transition probabilities $w_{l\to m}$ to guarantee that the target distribution π_l is a fixed point of the master equation, Eq. (2.2). But so far there has been no guarantee that, starting from an arbitary inital distribution, the iterations will converge to the desired steady-state distribution. As we stated earlier, this will only be the case if the system is ergodic, which is the only case we consider here.

It is convenient to define the *transition probability matrix* $\mathbf{\Gamma}$ with off-diagonal elements $\Gamma_{lm} = w_{l\to m}$ and diagonal elements $\Gamma_{ll} = 1 - \sum_{m\neq l} w_{l\to m}$ representing the probability to stay in state l. The rows of $\mathbf{\Gamma}$ are probability distributions and therefore must sum to one,

$$\sum_m \Gamma_{lm} = 1. \tag{2.17}$$

Using this notation we can write Eq. (2.2) in a form suggestive of matrix multiplication,

$$P_l(t+1) = \sum_m P_m(t)\Gamma_{ml}. \tag{2.18}$$

Let $\boldsymbol{P}_t$ be the (row) vector with components $P_l(t)$. Then $\boldsymbol{P}_{t+1} = \boldsymbol{P}_t\mathbf{\Gamma}$, and the steady-state vector $\boldsymbol{\pi}$ is a left-eigenvector of $\mathbf{\Gamma}$ with eigenvalue one,

$$\boldsymbol{\pi}\mathbf{\Gamma} = \boldsymbol{\pi}. \tag{2.19}$$

The assumption of ergodicity is then equivalent to the statement that there exists some power p such that $\mathbf{\Gamma}^p$ has strictly positive entries

$$(\mathbf{\Gamma}^p)_{lm} > 0. \tag{2.20}$$

Then p can be interpreted as the minimum number of steps required for a random walker to reach state m from state l, maximized over all pairs l, m.

One strategy to prove the convergence of Eq. (2.18) is to show that $\mathbf{\Gamma}^p$ has a one-dimensional eigenspace, spanned by $\boldsymbol{\pi}$, with eigenvalue one, and all other

eigenvalues less than one in magnitude. Then, as long as $\boldsymbol{P}_0$ has some nonzero projection onto $\boldsymbol{\pi}$ (which is necessarily the case in classical Monte Carlo simulations[1]), the components of $\boldsymbol{P}_t$ orthogonal to $\boldsymbol{\pi}$ will decay exponentially in t and, because right-multiplication by $\boldsymbol{\Gamma}$ conserves probability according to Eq. (2.17), $\boldsymbol{P}_t \to \boldsymbol{\pi}$ as $t \to \infty$. We now proceed with the proof.

First, note that the column vector of ones $\mathbf{1}$ is a right eigenvector of $\boldsymbol{\Gamma}$ with eigenvalue one. Given an arbitrary vector $\boldsymbol{u}$, note that Eqs. (2.17) and (2.20) imply that each component of $\boldsymbol{\Gamma}^p \boldsymbol{u}$ is a convex combination[2] of the components of $\boldsymbol{u}$, and thus can be no larger in magnitude than the largest component of $\boldsymbol{u}$. That is,

$$\left| \sum_j \left(\boldsymbol{\Gamma}^p\right)_{ij} u_j \right| \leq \max_k \left\{ |u_k| \right\} \tag{2.21}$$

for all i. But equality for *any* i implies that the components of $\boldsymbol{u}$ are all equal, or, in other words, $\boldsymbol{u}$ is an element of the one-dimensional eigenspace spanned by $\mathbf{1}$. Therefore $\boldsymbol{\Gamma}^p \boldsymbol{u} = \lambda \boldsymbol{u}$ implies that either $\boldsymbol{u} \propto \mathbf{1}$ or $|\lambda| < 1$.

The above argument unfortunately doesn't appear to have a clear interpretation in terms of random walkers moving between states. Narayan and A. P. Young (2001) give a direct proof in this language, which also provides the intuition that *deviations* from the stationary probability of each state eventually meet and annihilate as long as the system is ergodic, so that the overall distribution eventually converges to the stationary distribution.

[1] In classical Monte Carlo simulations, we start in some initial state m so $P_l(0) = \delta_{l\,m}$. By the assumption of ergodicity, Eq. (2.20), the stationary state π must have all components nonzero and thus $P(0)$ has a nonzero projection onto π.

[2] That is, a linear combination in which the coefficients are all positive and sum to one.

2.4.1 Estimating the relaxation time

We have argued that Monte Carlo simulations of ergodic systems *eventually* converge to a steady state, but in practice we need to estimate the number of Monte Carlo steps necessary to achieve convergence. This is called the *relaxation time* or *equilibration time* and is denoted in the following by τ.

By the above arguments the rate of convergence is related to the magnitude of the second-largest eigenvalue λ_2 of $\mathbf{\Gamma}$, which controls the exponential decay of the components of $\boldsymbol{P}_t$ orthogonal to $\boldsymbol{\pi}$. Thus *in theory* τ can be estimated by

$$\tau \sim -\frac{1}{\log|\lambda_2|}. \tag{2.22}$$

In practice, the number of states in a typical Monte Carlo simulation is far too large to calculate λ_2, and we instead estimate τ empircally.

A simple but effective way to estimate τ is to plot thermal averages of the quantity of interest, $\langle x \rangle$, against the Monte Carlo time and estimate τ from the onset of a plateau. In one particulary useful scheme, we start with some initial number of updates M_0 without computing any averages. We then do an additional M_0 updates, computing the average $\langle x \rangle_1$. Finally, we compute $\langle x \rangle_n$ by averaging between $t = 2^{n-1}M_0$ and $t = 2^n M_0$. In other words, $\langle x \rangle_n$ represents the average taken over the last half of the updates. We then plot $\langle x \rangle_n$ as a function of n (which is just the logarithm of the Monte Carlo time) to estimate τ.

While the simple method of estimating τ from a plateau is often adequate, a more robust approach is possible if we can find an "indicator" quantity that necessarily vanishes in equilibrium, but is nonzero in the initial, nonequilibrium state. The vanishing of the indicator, in conjunction with a plateau in the quantity of interest, provides additional evidence for equilibration. This method has proven useful in the study of spin glasses with Gaussian couplings, for which such

a quantity is known (Katzgraber and A. P. Young 2003). Below we derive the *equilibrium* relationship between measurable quantities on which this indicator is based.

2.4.2 Equilibration test for Gaussian spin glasses

Consider the equilibrium energy per spin averaged over samples,

$$U = -\frac{1}{2N} \sum_{ij} \left[J_{ij} \left\langle S_i S_j \right\rangle \right]_{\text{av}} \equiv -\frac{1}{2N} \sum_{ij} U_{ij}, \tag{2.23}$$

For Gaussian J_{ij} with mean zero and variance σ_{ij}^2, we can compute the bond average in closed form to obtain an equilibrium relationship between measurable quantities. Integrating by parts with respect to J_{ij}, noting that the boundary term vanishes,

$$U_{ij} = \frac{\sigma_{ij}^2}{\sqrt{2\pi\sigma_{ij}^2}} \int \mathrm{d}x \, e^{-x^2/2\sigma_{ij}^2} \, \frac{\mathrm{d}}{\mathrm{d}x} C_2(x), \tag{2.24}$$

where $C_2(J_{ij}) \equiv \left\langle S_i S_j \right\rangle$, and thus

$$U = -\frac{1}{2N} \sum_{ij} \sigma_{ij}^2 \left[\frac{\mathrm{d}}{\mathrm{d}J_{ij}} \left\langle S_i S_j \right\rangle \right]_{\text{av}}. \tag{2.25}$$

In equilibrium at temperature $T \equiv 1/\beta$,

$$\left\langle S_i S_j \right\rangle = \frac{\operatorname{Tr} S_i S_j e^{-\beta \mathcal{H}}}{\operatorname{Tr} e^{-\beta \mathcal{H}}}. \tag{2.26}$$

Taking the derivative and using the identity $\frac{\mathrm{d}}{\mathrm{d}J_{ij}} e^{-\beta\mathcal{H}} = \beta S_i S_j e^{-\beta\mathcal{H}}$, we find

$$T \frac{\mathrm{d}}{\mathrm{d}J_{ij}} \left\langle S_i S_j \right\rangle = 1 - \left\langle S_i S_j \right\rangle^2. \tag{2.27}$$

Thus we find the *equilibrium* relationship

$$\begin{aligned} U &= -\frac{1}{2NT} \sum_{ij} \sigma_{ij}^2 \left(1 - \left[\left\langle S_i S_j \right\rangle^2 \right]_{\text{av}} \right) \\ &= -\frac{\left(T_c^{\text{MF}}\right)^2}{2T} \left(1 - \frac{1}{N} \sum_{ij} \frac{\sigma_{ij}^2}{\left(T_c^{\text{MF}}\right)^2} \left[\left\langle S_i S_j \right\rangle^2 \right]_{\text{av}} \right) \end{aligned} \tag{2.28}$$

where in the second line we use the identity $\left(T_c^{\rm MF}\right)^2 = (1/N)\sum_{ij}\sigma_{ij}^2$. The second term in the parentheses,

$$q_l \equiv \frac{1}{N}\sum_{ij}\frac{\sigma_{ij}^2}{\left(T_c^{\rm MF}\right)^2}\left[\left\langle S_i S_j\right\rangle^2\right]_{\rm av}, \tag{2.29}$$

is a generalized form of the *link overlap*, so named because the average $\left\langle S_i S_j\right\rangle^2$ measures the tendency for a bond, or "link", to be simultaneously satisfied in independent replicas. Equation (2.28) can be rewritten as

$$U = -\frac{\left(T_c^{\rm MF}\right)^2}{2T}\left(1 - q_l\right), \tag{2.30}$$

or

$$\Delta(U, q_l) \equiv U + \frac{\left(T_c^{\rm MF}\right)^2}{2T}\left(1 - q_l\right) = 0 \quad \text{(equilibrium)}. \tag{2.31}$$

However, for a *nonequilibrium* state at time t with link overlap $q_l(t)$ and energy $U(t)$, the quantity $\Delta(t) \equiv \Delta\left[U(t), q_l(t)\right]$ does not necessarily vanish. For example, consider putting the system in a random state at $t = 0$ by flipping each spin with probability 1/2 (which is how we typically initialize Monte Carlo simulations). Then $q_l(t = 0) \approx 0$, less than the *equilibrium* value $q_l(t \to \infty)$, and furthermore $U(t = 0) > U(t \to \infty)$. Thus

$$\Delta(t = 0) > 0, \tag{2.32}$$

and, from Eq. (2.31),

$$\Delta(t \to \infty) = 0. \tag{2.33}$$

Therefore a useful test for equilibration is to plot $\Delta(t)$ and infer the time at which the system reaches equilibrium from the onset of a plateau at $\Delta = 0$. An example of such an "equilibration plot" is shown in Fig. 2.2.

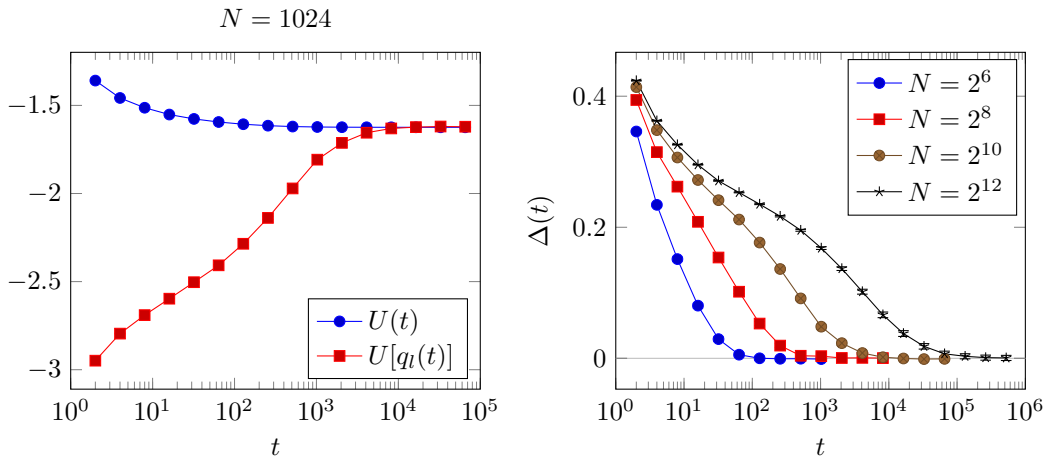

Figure 2.2: Example equilibration plots for the one-dimensional diluted spin glass with $\sigma = 0.6$. On the left, the left- and right-hand sides of Eq. (2.30), computed from Monte Carlo averages, as a function of sweeps t on a log-linear scale. The plateau of both quantities at a common value is consistent with the onset of equilibrium. On the right, the quantity Δ, defined in Eq. (2.31), as a function of t for different sizes on a log-linear scale. Here, the plateau at zero is consistent with the onset of equilibrium.

2.5 Parallel tempering

For systems with slow dynamics and at low temperatures, the rate of convergence is significantly improved by *parallel tempering* (also known as *replica exchange*) Monte Carlo, introduced by Hukushima and Nemoto (1996). The idea is to simultaneously simulate several copies (replicas) of the system, each at a different temperature, and, in addition to the usual (*e.g.* spin-flip) updates, allow a new type of "replica exchange" update which swaps the *entire spin configurations* of a pair of replicas.

The advantage of parallel tempering is realized in systems with "rough" energy landscapes, with many local optima separated by energy barriers on many scales. Replicas at low temperatures tend to settle into local minima which are difficult to escape, leading to slow dynamics. Parallel tempering helps by allowing "stuck" replicas at low temperature to "jump up" to a higher temperature where they are

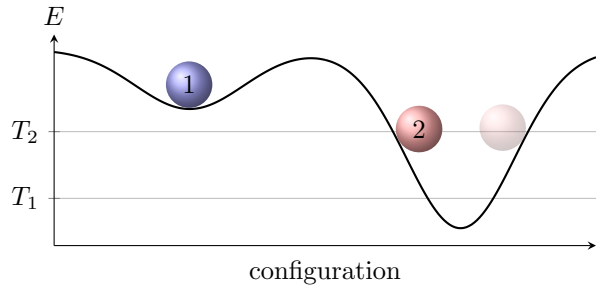

Figure 2.3: Replicas at different temperatures $T_1 < T_2$ exploring a non-convex energy landscape. In this scenario, the replica at the lower temperature T_1 has become trapped in a local minimum. At the next iteration of parallel tempering, the configurations of the two replicas will be swapped with high probability (corresponding to exchanging the positions of "1" and "2" in the figure). The replica at temperature T_1 will then be able to explore the low-energy region.

able to escape local minima and more efficiently explore the phase space. Once a region of lower energy is found, a replica can then "drop down" to a lower temperature. See Fig. 2.3.

We now derive the transition probabilities for the replica exchange moves assuming detailed balance. Suppose we have two replicas in states l, m and at temperatures β_1, β_2 respectively. According to the Boltzmann distribution, the joint probability of this configuration is

$$P(l, \beta_1)P(m, \beta_2) \propto e^{-\beta_1 E_l - \beta_2 E_m}. \tag{2.34}$$

Exchanging l and m, we obtain for the ratio of joint probabilities

$$\frac{P(m, \beta_1)P(l, \beta_2)}{P(l, \beta_1)P(m, \beta_2)} = \frac{\exp\left(-\beta_1 E_m - \beta_2 E_l\right)}{\exp\left(-\beta_1 E_l - \beta_2 E_m\right)} = e^{(\beta_1 - \beta_2)(E_l - E_m)}. \tag{2.35}$$

To define a Markov process which converges to a distribution satisfying Eq. (2.34), it is sufficient to satisfy the detailed balance condition and, using the Metropolis convention of Eq. (2.5), we obtain for the transition probability

$$w_{X \to X'} = \min\left\{1, e^{(\beta_1 - \beta_2)(E_l - E_m)}\right\}. \tag{2.36}$$

where the configuration $X = \big\{(\beta_1, l), (\beta_2, m)\big\}$ and $X' = \big\{(\beta_1, m), (\beta_2, l)\big\}$.

Note that the *average* transition probability of a replica exhange move depends on the amount of overlap of the energy distributions of the two replicas. In other words, the condition for parallel tempering to be effective is $\Delta E/\delta E \lesssim 1$, where ΔE is the difference between the average energies and δE is the width of the distributions. This is sketched in Fig. 2.4. Differentiating the partition function we find $Nc_V = (\delta E)^2/T^2$, where c_V is the heat capacity per spin. Combining this with $\Delta E = Nc_V \Delta T$, the condition becomes

$$\frac{\Delta T}{T} \lesssim \frac{1}{\sqrt{Nc_V}}. \tag{2.37}$$

Thus, at least in cases where the specific heat c_V doesn't vary too much over the temperature range we wish to study, a geometric series of temperatures is an appropriate choice.[3] In practice, we usually adjust $\Delta T/T$ to obtain acceptance probabilities for swaps between each pair of neighboring temperatures of about 20–30%, near optimal values found by Rathore, Chopra, and Pablo (2005) and Kone and Kofke (2005). Recently Katzgraber, Trebst, et al. (2006) have proposed an adaptive method which optimizes the round-trip time for a replica to explore the entire temperature space, which avoids bottlenecks in swap probabilities that may occur for example if the heat capacity exhibits singular behavior within the range of temperatures studied.

2.6 Finite-size scaling

Using state-of-the-art Monte Carlo algorithms running on modern hardware we can (optimistically) simulate systems of sizes up to roughly $N \sim 10^9$, limited by

[3] One must use caution for example in the vicinity of a critical point, where the specific heat may diverge, leading to vanishingly small transition probabilities between pairs of replicas near the critical point.

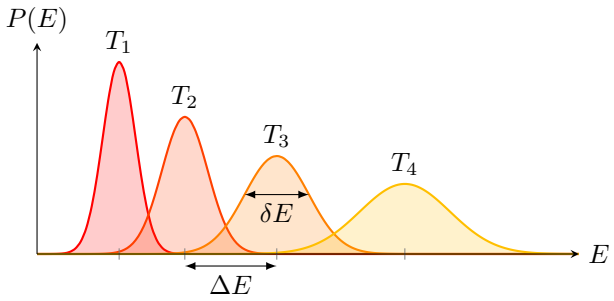

Figure 2.4: Overlap of energy distributions of replicas of a system at nearby temperatures. For parallel tempering to be effective, temperatures must be chosen such that the difference ΔE between average energies of neighboring replicas is of the order (or smaller than) the width of the energy distributions δE.

available processing speed and memory. For equilibrium simulations of systems glassy systems, this number is much smaller, about 10^4, as the time required to equilibrate the system grows rapidly with size. There is a big gap between the sizes we are able to simulate and $N \sim 10^{23}$ observed in laboratory experiments! Thus it would be very useful to know in which situations finite-size effects become important and how to use results for finite systems obtained from simulations to extrapolate the behavior in the thermodynamic limit.

A very important result of the theory of phase transitions is that *phase transitions can only occur in the thermodynamic limit*, *i.e.* for infinite systems. This is because the non-analytic behavior at a critical point observed in infinite (or near-infinite, macroscopic) systems, for example the divergence of the susceptibility as $\chi \propto (T - T_c)^{-\gamma}$, cannot arise from a partition function which is a sum of a finite number of (analytic) terms. In finite systems what is actually observed is a "rounding" effect, whereby the measured critical exponents initially approach the their true asymptotic values as $T \to T_c$, but then enter a "crossover" regime close to T_c, where the behavior of the quantity which is singular in the thermodynamic limit smoothly transitions to the asymptotic behavior below T_c.

Plausibly, finite-size effects become important when the relevant length scale of the fluctuations, *i.e.* the correlation length ξ, becomes large relative to the linear size of the system L. The basic assumption of *standard* finite-size scaling (FSS) theory is that finite-size corrections only involve the ratio of the bulk correlation length ξ (*i.e.* the correlation length that would be observed in an infinite system) to the size L. This assumption is correct for systems below the upper critical dimension, $d < d_u$. Above the upper critical dimension, $d > d_u$, this simple picture is complicated by the presence of a "dangerous irrelevant variable," (Binder, Nauenberg, et al. 1985) and we have to proceed more carefully using a renormalization group approach. This situation is discussed in detail in Chapter 6. Here we will assume $d < d_u$, so that standard FSS applies.

Finite-size effects are particularly important near a critial point, which is marked by the divergence of the bulk correlation length ξ. Near the critial temperature T_c, the correlation length scales like $\xi \sim t^{-\nu}$, where $t = T - T_c$, so by the basic assumption of FSS, the size dependence enters only through the ratio $t^{-\nu}/L$, or, equivalently, through $L^{1/\nu}t$. For a susceptibility which diverges (in the bulk) like $\chi \sim t^{-\gamma}$ at the critial temperature, we then infer the finite-size scaling form

$$\chi(L,t) \sim L^{\gamma/\nu}\widetilde{\chi}\left(L^{1/\nu}t\right), \tag{2.38}$$

where $\sim$ indicates asymptotic equality for large L, and $\widetilde{\chi}$ is a *scaling function* which depends on L only through its argument. The prefactor $L^{\gamma/\nu}$ is justified by the assumption that $\chi(\infty,t) \sim t^{-\gamma}$, which requires that $\widetilde{\chi}(x) \to x^{-\gamma}$ as $x \to \infty$.

The FSS form is particulary simple for *dimensionless* quantities since there can be no prefactor power of L. For a dimensionless quantity g, the FSS form is simply

$$g(L,t) \sim \widetilde{g}\left(L^{1/\nu}t\right) \tag{2.39}$$

One commonly-studied dimensionless quantity is the "Binder ratio," defined as a ratio of moments of the order parameter m,

$$g = \frac{1}{2}\left(3 - \frac{\langle m^4 \rangle}{\langle m^2 \rangle^2}\right). \tag{2.40}$$

Equation (2.39) is useful in practice to estimate the the bulk transition temperature T_c, because the right-hand side is independent of L only at $T = T_c$ (*i.e.* $t = 0$). Thus we can estimate T_c from the temperature at which data for different sizes intersect. However, note that Eq. (2.39) is only asymptotically correct—in practice corrections to scaling are significant and data for different sizes do not all intersect at a single temperature. However, if the form of the leading correction to scaling is known, for example as in Section 3.3, we can extrapolate to estimate the bulk T_c, see Eq. (3.27).

Remarkably, the scaling functions $\widetilde{X}$, $\widetilde{g}$ predicted to be universal (up to non-universal factors multiplying argument and $L^{\gamma y_t}$. This follows from the renormalization-group derivation of the scaling relationships.

2.7 Statistical error analysis

In this section we briefly review some of the most important statistical methods used in the research. The derivations presented here closely follow P. Young (2015), to which we refer the reader for an in-depth discussion.

In experimental physics and in numerical simulations, we typically have a set of N independent measurements $\{x_i\}$ of some quantity X. We assume the data are sampled from the same (unknown) underlying distribution with probability density $p(x)$, and our goal is to estimate the mean of the underlying distribution,

$$\mu \equiv \int \mathrm{d}x\, x\, p(x), \tag{2.41}$$

and determine the statistical error in the estimate. For the purpose of discussing *bias* and *statistical error* it is useful to imagine performing many identical experiments, each time obtaining a new set of N measurements $\{x_i\}$. The average of x_i over an infinite number of experiments, which we denote $\langle x_i \rangle$, is equal to the true mean, *i.e.* $\langle x_i \rangle = \mu$. The assumption of independence means that $\langle x_i x_j \rangle = \langle x_i \rangle \langle x_j \rangle$ if $i \neq j$.

An *unbiased* estimator of the true mean μ is the *sample mean*,

$$\overline{x} \equiv \frac{1}{N} \sum_{i=1}^{N} x_i. \tag{2.42}$$

By unbiased we mean that the average over many identical experiments of the sample mean $\overline{x}$ converges to true mean $\langle x \rangle$, because

$$\langle \overline{x} \rangle = \frac{1}{N} \sum_{i=1}^{N} \langle x_i \rangle = \mu. \tag{2.43}$$

The variance of the sample mean is

$$\begin{aligned} \sigma_{\overline{x}}^2 &\equiv \langle \overline{x}^2 \rangle - \langle \overline{x} \rangle^2 \\ &= \frac{1}{N^2} \sum_{ij} \left(\langle x_i x_j \rangle - \langle x_i \rangle \langle x_j \rangle \right) \\ &= \frac{1}{N^2} \sum_{i} \left(\langle x_i^2 \rangle - \langle x_i \rangle^2 \right) \\ &\equiv \frac{\sigma^2}{N}. \end{aligned} \tag{2.44}$$

Thus, to give an statistical error in our estimation of the true mean μ by the sample mean $\overline{x}$, we also need to estimate σ^2, a parameter of the underlying distribution. We expect this to be related to the *sample variance*,

$$s^2 \equiv \frac{1}{N} \sum_{i=1}^{N} \left(x_i - \overline{x} \right)^2, \tag{2.45}$$

which can also be written as $s^2 = (1/N) \sum_i x_i^2 - (1/N^2) \sum_{ij} x_i x_j$. To find the relationship between the sample variance s^2 and the variance of the underlying

distribution σ^2, we evaluate

$$\begin{aligned}\left\langle s^2 \right\rangle &= \frac{1}{N}\sum_i \left\langle x_i^2 \right\rangle - \frac{1}{N^2}\sum_{ij}\left\langle x_i x_j \right\rangle \\ &= \left\langle x^2 \right\rangle - \left(\frac{1}{N}\left\langle x^2 \right\rangle + \frac{N-1}{N}\left\langle x \right\rangle^2\right) \\ &= \frac{N-1}{N}\left(\left\langle x^2 \right\rangle - \left\langle x \right\rangle^2\right) \\ &= \left(\frac{N-1}{N}\right)\sigma^2, \end{aligned} \tag{2.46}$$

where in the second line we split the double summation into a sum of N terms with $i = j$ and $N(N-1)$ terms with $i \neq j$, and use the assumed independence of the data. Thus we find that $Ns^2/(N-1)$ is an unbiased estimator of σ^2. Combining Eqs. (2.44) and (2.46), our final result for the estimate of the true mean μ from the data is

$$\mu \sim \overline{x}, \qquad \sigma_{\overline{x}} \sim \sqrt{\frac{s^2}{N-1}}, \tag{2.47}$$

where, in this section, "$\sim$" means "is an unbiased estimator of."

2.7.1 Manual error propagation

Often we would like to estimate the value of a function f evaluated at the mean μ. In general, $f(\overline{x})$ is *not* an unbiased estimator of $f(\mu)$, unless f is linear. In fact,

$$\left\langle f(\overline{x}) \right\rangle = f(\mu) + \frac{1}{2}f''(\mu)\left\langle \delta^2 \right\rangle + \cdots \tag{2.48}$$

where $\delta \equiv \overline{x} - \mu$ and we have used that $\langle \delta \rangle = 0$, but $\left\langle \delta^2 \right\rangle$ and higher moments do not generally vanish. In fact, $\left\langle \delta^2 \right\rangle = \sigma_{\overline{x}}^2$ and thus, using Eq. (2.47), we can eliminate the leading bias by estimating

$$f(\mu) \approx f(\overline{x}) - \frac{s^2}{2(N-1)}f''(\overline{x}). \tag{2.49}$$

The statistical error in our estimate follows from the variance,

$$\left\langle f(\overline{x})^2 \right\rangle - \left\langle f(\overline{x}) \right\rangle^2 = [f'(\mu)]^2 \sigma_{\overline{x}}^2 + \cdots \tag{2.50}$$

and hence

$$\sigma_{f(\overline{x})} \approx \left(\frac{s^2}{N-1} \right)^{1/2} f'(\overline{x}). \tag{2.51}$$

The correction term in Eq. (2.49) is usually unnecessary in practice because the bias falls off like $1/N$ asymptotically, so for reasonably large N it is insignificant compared to the statistical error, which is seen to fall off like $1/\sqrt{N}$. If N is sufficiently large, as is usually the case, we can ignore the bias and estimate $f(\mu)$ and the associated statistical error by

$$f(\mu) \approx f(\overline{x}), \qquad \sigma_{f(\overline{x})} \approx \left(\frac{s^2}{N-1} \right)^{1/2} f'(\overline{x}). \tag{2.52}$$

This result generalizes straightforwardly to functions of multiple averages. For example, consider a function $f(x, y)$ and suppose we want to estimate $f(\mu_x, \mu_y)$, where $\mu_x = \langle x_i \rangle$ and $\mu_y = \langle y_i \rangle$. As before, bias arises from the quadratic terms in the expansion of f about the mean values,

$$\left\langle f(\overline{x}, \overline{y}) \right\rangle = f(\mu_x, \mu_y) + \frac{1}{2} f_{xx}^{\mu} \left\langle \delta_x^2 \right\rangle + f_{xy}^{\mu} \left\langle \delta_x \delta_y \right\rangle + \frac{1}{2} f_{yy}^{\mu} \left\langle \delta_y^2 \right\rangle + \cdots \tag{2.53}$$

where *e.g.* f_{xx}^{μ} is shorthand for the second derivative $\partial_x^2 f(x, y)$ evaluated at μ_x, μ_y. The average in the cross term, $\left\langle \delta_x \delta_y \right\rangle$, is equal to the *covariance* of the sample means, $\sigma_{\overline{xy}}^2$. Analogously to Eq. (2.44), we find $\sigma_{\overline{xy}} = \sigma_{xy}/N$. The covariance σ_{xy} is related to the *sample covariance*, defined by

$$s_{xy}^2 = \frac{1}{N} \sum_{i=1}^{N} (x_i - \overline{x})(y_i - \overline{y}). \tag{2.54}$$

Analogously to Eq. (2.46) we find

$$\left\langle s_{xy}^2 \right\rangle = \left(\frac{N-1}{N} \right) \sigma_{xy}^2. \tag{2.55}$$

Finally, we can eliminate the leading bias by estimating $f(\mu_x, \mu_y)$ as

$$f(\mu_x, \mu_y) \approx f(\overline{x}, \overline{y}) - \frac{1}{2(N-1)} \left(s_{xx}^2 f_{xx}^\mu - 2 s_{xy}^2 f_{xy}^\mu - s_{yy}^2 f_{yy}^\mu \right). \tag{2.56}$$

As before, the leading statistical error arises from the first derivatives, and we find

$$\sigma_{f(\overline{x},\overline{y})}^2 = \frac{1}{N-1} \left(s_x^2 f_x^\mu + s_y^2 f_y^\mu \right). \tag{2.57}$$

2.7.2 Resampling methods

In practice, the function f can be complicated, making manual computation of the derivatives required for error propagation a tedious and error-prone process. In some cases we may not be able to compute the necessary derivatives analytically, and must resort to numerical approximation, for example when the function we are evaluating involves a complex nonlinear fit. Therefore we would like to have an "automatic" numerical procedure that can be used to compute an unbiased estimate of $f(\mu)$ and associated statistical error, which does not require computing the derivatives directly. Here we briefly summarize two such methods, called *resampling methods*, which were used extensively in the research presented in this thesis. The basic idea is to generate from the original N data points $\{x_i\}$ a number of *resampled* data sets $\{x_i^\alpha\}$ similar to those that would be obtained by performing the experiment many times. We can then use averages computed from these resampled data sets to form an unbiased estimate of $f(\mu)$ and obtain a statistical error in the estimate. For a detailed discussion we refer the reader to P. Young (2015).

Jackknife

Using the *jackknife* method, we generate N resampled data sets $\{x_i^\alpha\}$, $\alpha \in \{1 \dots N\}$ simply by leaving out a single point of the original data set in each

one. That is, $\{x_i^\alpha\} \equiv \left\{x_j : j \in \{1 \ldots N\}, i \neq j\right\}$ We call the averages of the resampled data sets *jackknife averages*,

$$\overline{x^\alpha} \equiv \frac{1}{N-1} \sum_{i \neq \alpha} x_i, \tag{2.58}$$

which is just the average over the original data set leaving out data point x_α. We then estimate $f(\mu)$ by the average

$$\overline{f} \equiv \frac{1}{N} \sum_{\alpha} f(\overline{x^\alpha}). \tag{2.59}$$

Note that $(1/N) \sum_{\alpha=1}^{N} \overline{x^\alpha} = \overline{x}$. If f is linear, then $\overline{f} = (1/N) f\left(\sum_\alpha \overline{x^\alpha}\right) = f(\overline{x})$. However, if f is not linear, then $\overline{f} \neq f(\overline{x})$ and both are biased estimates of $f(\mu)$. From Eq. (2.48) we note that $\left\langle f(\overline{x}) \right\rangle$ has an expansion of the form

$$\left\langle f(\overline{x}) \right\rangle = f(\mu) - \frac{A}{N} - \frac{B}{N^2} - \cdots \tag{2.60}$$

Following P. Young (2015) we note that, since the jackknife data sets x^α have the same distribution as the original data set (after all, they *are* the original data set with one point left out), the coefficients A and B are the same in the expansion of $\left\langle \overline{f} \right\rangle$, only N is replaced with $N-1$. Thus we can eliminate the leading $\mathcal{O}(1/N)$ bias by estimating

$$f(\mu) \approx N f(\overline{x}) - (N-1)\overline{f}. \tag{2.61}$$

We define the variance of the jackknife estimates by

$$s_f^2 \equiv \overline{f^2} - \overline{f}^2. \tag{2.62}$$

With some algebra, it can be shown that, to leading order in N,

$$\sigma_{\overline{f}}^2 \approx (N-1) s_f^2. \tag{2.63}$$

Thus we obtain an estimate of $f(\mu)$ and statistical error equivalent to Eq. (2.52) without the need to compute partial derivatives. Relative to other resampling

methods, such as bootstrap, jackknife is simple and efficient. However, roundoff error can be a problem with large data sets, where the jackknife averages will be very close together. In particular, the computation of the standard deviation, which involves subtracting large, almost-equal numbers when N is large, is susceptible to roundoff error.

In the work presented here we have mainly used jackknife to obtain error bars for estimates of ratios of various moments. The most frequently-occurring example is the Binder ratio

$$g \equiv \frac{1}{2}\left(3 - \frac{\langle x^4 \rangle}{\langle x^2 \rangle^2}\right), \tag{2.64}$$

for which we compute an estimate and error bar from Eqs. (2.59) and (2.63).

Bootstrap

Using the bootstrap method, we generate M resampled data sets $\{x_i^\alpha\}$, each with N points, by random selection with replacement from the original data set. Here we state the results which are useful for estimating $f(\mu)$ and the statistical error from the bootstrap data sets. For the derivations we refer the reader to P. Young (2015). As for the jackknife method, the bootstrap estimate of $f(\mu)$ is given by Eq. (2.59), with $\overline{x^\alpha}$ here denoting the averages of the *bootstrap* data sets. The statistical error in this estimate is given by

$$\sigma_{\overline{f}} = \sqrt{\frac{N}{N-1}}\, s_f \tag{2.65}$$

where s_f is defined as in Eq. (2.62) but with the averages done over the bootstrap data sets. When N is large, the square-root factor can be neglected, so that the bootstrap estimate of the error is just the standard deviation of the bootstrap estimates $f(\overline{x^\alpha})$.

The chief advantage of the bootstrap method compared with jackknife is that it samples the full range of the distribution of $f(\overline{x})$. It is thus useful to produce error bars on fits when (a) the statistical errors are non-Gaussian or (b) we fit a nonlinear model and the variance of the distribution is sufficiently large that an effective linear model is not applicable P. Young (2015).

Chapter 3

Nonextensive spin glasses

3.1 Motivation

In the study of phase transitions, it is often desirable to study models in a range of spatial dimensions between the lower critical dimension d_l, below which there is no finite-temperature transition, and the upper critical dimension d_u, above which the critical behavior is mean-field-like, meaning that the critical exponents are determined by mean-field theory.

But numerical simulations with large d are difficult because the number of spins, and hence the time and space required for the simulation, grows rapidly with size as $N = L^d$. For glassy systems, situation is especially difficult because the characteristic time scales, and thus the amount of simulation time required to equilibrate the system, also grows rapidly with size. Presently the best-known Monte Carlo methods for glassy systems are able to equilibrate up to about 10^4 spins in a reasonable amount a computer time, which limits system sizes at $d_u = 6$ to $L \lesssim 10$. For such small sizes finite-size scaling analysis is difficult or impossible, not only because we lose the ability to study a *range* of L from which to infer the

bulk behavior, but also because corrections to scaling become significant for small L.

3.1.1 Long-range interactions

Some of these difficulties can be avoided by instead studying one-dimensional models with long-range interactions, as proxies for higher-dimensional models with short-range interactions. For example, consider the Ising chain with only nearest-neighbor interactions, which is below the lower critical dimension $d_l = 2$ for the Ising ferromagnetic transition and therefore does not have a finite-temperature phase transition. However, with the addition of long-range interactions falling off as $r^{-\sigma}$, there *is* a finite-temperature transition for $\sigma \leq 2$ and, furthermore, the critical behavior is mean-field-like for $\sigma < 4/3$ (Dyson 1969). Thus we establish a correspondence between the lower- and upper-critical dimensions $d_l = 2$ and $d_u = 4$ of the short range model, and the lower- and upper-critical *ranges* $\sigma_l = 2$ and $\sigma_u = 4/3$ of the chain with long-range interactions. The *continuous* parameter σ of the chain plays a role analagous to the dimensionality d of the short-range model (Katzgraber and A. P. Young 2003), which is plausible because both parameters essentially control the degree of the coupling between spins.

Note that increasing σ *decreases* the range of the interactions, and thus plays a similar role of reducing the connectivity of the spins as decreasing d. The extreme case $\sigma = 0$ is the "infinite-range" model which is solved exactly by mean-field theory, while the opposite extreme $\sigma \to \infty$ is the short-range model. We define the "effective dimension" $d_{\text{eff}}(\sigma)$ such that a one-dimensional model with long-range interactions falling off as $r^{-\sigma}$ has the same critical behavior as the equivalent short-range model with $d = d_{\text{eff}}$. In the mean-field regime (*e.g.* $\sigma < 4/3$ for the Ising ferromagnet) we can derive $d_{\text{eff}}(\sigma)$ in closed form by equating the singular

parts of the free energy density for the two models (Larson et al. 2010). This is discussed in Section 3.1.3, where we compute $d_{\text{eff}}(\sigma)$ for the one-dimensional spin glass with long-range interactions.

One-dimensional models with long range interactions have the important advantage that, since $N = L$, there is no difficulty in studying many different sizes for finite-size scaling (FSS) analysis. But although we can feasibly study large L using this method, it is important to note that finite-size effects are not reduced—we have traded small L and short-range interactions for large L and long-range interactions, so that the ratio of the length scale of fluctuations to the system size is essentially unchanged.

3.1.2 Nonextensive regime

Considering the general case of a d-dimensional model with long-range interactions falling off as $r^{-\sigma}$, we note that, if $0 \leq \sigma \leq d$, the free energy is nonextensive, *i.e.* grows faster than N in the thermodynamic limit. We call this region of parameter space the *nonextensive regime*.

For example, the mean-field transition temperature for an Ising ferromagnet with long-range interactions, given by

$$T_c^{\text{MF}} \equiv \sum_j J_{ij} = c \sum_{j \neq i} r_{ij}^{-\sigma}, \tag{3.1}$$

behaves asymptotically like

$$T_c^{\text{MF}}/J \sim \int \mathrm{d}^d r \, r^{-\sigma} \propto \begin{cases} 1 + a_1 L^{d-\sigma} & \text{if } d \neq \sigma, \\ 1 + a_2 \log L & \text{if } d = \sigma, \end{cases} \tag{3.2}$$

where a_1 and a_2 are constants. Therefore if we take c in Eq. (3.1) to be independent of N, the mean-field transition temperature diverges in the thermodynamic limit

unless $\sigma > d$. Nevertheless it is possible to define a model with $\sigma \leq d$ and a sensible thermodynamic limit provided we also take $c \to 0$ in such a way that the mean-field transition temperature remains finite (Cannas and Tamarit 1996). For $\sigma < d$ we require

$$c = c(\sigma, N) \propto N^{\sigma/d-1}. \tag{3.3}$$

To fix the constant of proportionality we adopt the convention $T_c^{\mathrm{MF}} = 1$, which for the ferromagnet gives

$$J_{ij} = \frac{c(\sigma, N)}{r_{ij}^{\sigma}}, \qquad c(\sigma, N) = \left(\sum_{j \neq i} r_{ij}^{-\sigma} \right)^{-1}. \tag{3.4}$$

The nonextensive regime for *ferromagnets* has already been explored. In one of the earliest studies of ferromagnets with long-range interactions, Hiley and Joyce (1965) showed that the transition temperature approaches the mean-field prediction in the limit $\sigma \to d$ from above. This led Cannas and Tamarit (1996) to conjecture that, for a ferromagnetic model in which the interactions are appropriately scaled in the nonextensive regime, the mean-field transition temperature is exact not only for $\sigma = 0$ and $\sigma \to d^+$, but in the entire range $0 \leq \sigma \leq d$. This conjecture was subsequently verified numerically (Cannas, De Magalhães, and Tamarit 2000; Campa, Giansanti, and Moroni 2000).

It is interesting to ask if the same is true for spin glasses. Mori (2011) argues that this is the case; that is, the behavior throughout nonextensive regime is identical to that of the mean-field model of spin glasses, provided the couplings are appropriately scaled so that the mean-field transition temperature is independent of system size. Our motivation will be to test this conjecture using Monte Carlo simulation. First, we introduce a long-range spin glass model and define the corresponding nonextensive regime.

3.1.3 Spin glasses with long-range interactions

Long-range spin glass models may be defined by taking the variance of the interactions to fall off with distance. Such a model was first studied by Kotliar, Anderson, and Stein (1983), who considered a one-dimensional Ising chain with the Hamiltonian

$$\mathcal{H} = -\frac{1}{2}\sum_{i,j} J_{ij} S_i S_j, \qquad J_{ij} = \epsilon_{ij}/r_{ij}^{\sigma}, \tag{3.5}$$

where ϵ_{ij} are independent, identically-distributed Gaussian random variables. For this model they found a finite-temperature phase transition for $\sigma < 1$ and mean-field behavior for $1/2 < \sigma < 2/3$; that is, $\sigma_l = 1$ and $\sigma_u = 2/3$.

The extreme case $\sigma = 0$ corresponds to the Sherrington-Kirkpatrick mean-field model (see Section 1.3.2), for which the transition temperature is exactly

$$\left(T_c^{\mathrm{MF}}\right)^2 \equiv \sum_j \left[J_{ij}^2\right]_{\mathrm{av}} = c\sum_{j\neq i} r_{ij}^{-2\sigma}, \tag{3.6}$$

where $[\cdots]_{\mathrm{av}}$ denotes an average over bonds. Compared with Eq. (3.1) for the ferromagnet, note that J_{ij} ($\propto 1/r_{ij}^{\sigma}$), which is zero on average for a spin glass, is replaced by the variance $\left[J_{ij}^2\right]_{\mathrm{av}}$ ($\propto 1/r_{ij}^{2\sigma}$).

For $0 \leq \sigma \leq 1/2$ the free energy diverges in the thermodynamic limit unless the interactions are scaled by an inverse power of the system size.

Again adopting the convention $T_c^{\mathrm{MF}} = 1$, the analog of Eq. (3.4) for the spin glass is

$$\left[J_{ij}^2\right]_{\mathrm{av}} = \frac{c(\sigma, N)}{r_{ij}^{2\sigma}}, \qquad c(\sigma, N) = \left(\sum_{j\neq i} r_{ij}^{-2\sigma}\right)^{-1}. \tag{3.7}$$

In the mean-field regime ($\sigma < 4/3$) we can make a precise connection between the power σ of the one-dimensional long-range (1D LR) model and the dimensionality d of the short-range (SR) model by equating the singular parts of the free energy density for the two models (Larson et al. 2010). The singular part of

the free energy density scales with L like

$$\frac{1}{L^d}\widetilde{f}\left(L^{y_T}t,\, L^{y_H}h,\, L^{y_u}u\right) \tag{3.8}$$

where $\widetilde{f}$ is a scaling function, $t = (T - T_c)/T_c$ is the reduced temperature, and h is the magnetic field. Eliminating L (using $N = L$ for the LR model and $N = L^d$ for the SR model) and equating the resulting expressions for the two models gives the following relationship between the LR and SR exponents:

$$y^{\mathrm{LR}}(\sigma) = y^{\mathrm{SR}}(d)/d. \tag{3.9}$$

In the mean field regime, where the FSS exponents for the SR and LR models are given by

$$\begin{aligned} y_T^{\mathrm{SR}} &= 2 & y_T^{\mathrm{LR}} &= 2\sigma - 1 \\ y_H^{\mathrm{SR}} &= (d+2)/2 & y_H^{\mathrm{LR}} &= \sigma \\ y_u^{\mathrm{SR}} &= (6-d)/2 & y_u^{\mathrm{LR}} &= 3\sigma - 2 \end{aligned}$$

(Harris, Lubensky, and Chen 1976; Kotliar, Anderson, and Stein 1983), we obtain the following relationship between the power σ of the 1D LR model and the corresponding effective dimension,

$$d_{\mathrm{eff}} = \frac{2}{2\sigma - 1}, \tag{3.10}$$

consistently for each pair of exponents.

3.2 Models

We study the Hamiltonian

$$\mathcal{H} = -\frac{1}{2}\sum_{i,j} J_{ij} S_i S_j \tag{3.11}$$

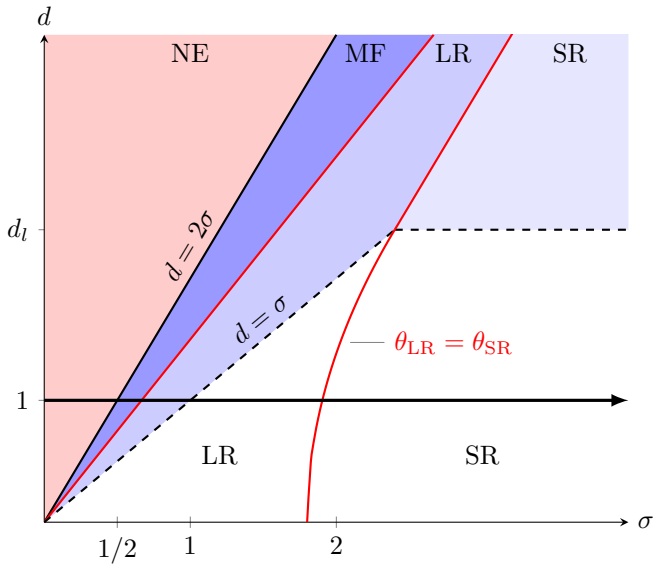

Figure 3.1: *Adapted from Katzgraber and A. P. Young (2003).* Schematic phase diagram in the d-σ plane for the one-dimensional Ising spin glass with power-law interactions, following D. S. Fisher and Huse (1988). In the shaded regions there is a transition with $T_c > 0$. The line $d = 2\sigma$ separates the nonextensive (NE) region from the mean-field (MF) region. The critical exponents in both the NE and MF regions are those of mean-field theory. The line $d = 3\sigma/2$ (red) separates the mean-field region from the long-range (LR) region where the critical exponents differ from mean-field theory, but the dominant contribution to the energy comes from the long-range interactions. On the far right are the short-range (SR) regions where the energy is dominated by the short-range interactions. These are separated from the long-range regions by the curve $\theta_{\rm LR} = \theta_{\rm SR}$ (red), where $\theta_{\rm LR}$ and $\theta_{\rm SR}$ are the stiffness exponents corresponding to the long- and short-range interactions respectively, see Section 1.3.4.

where the couplings J_{ij} are sampled from a distribution with mean zero and variance that falls off with a power of the distance r_{ij},

$$\left[J_{ij}\right]_{\rm av} = 0, \qquad \left[J_{ij}^2\right]_{\rm av} \propto r_{ij}^{-2\sigma}, \tag{3.12}$$

where to define r_{ij} we put the spins on a ring and use the chord distance,

$$r_{ij} = \frac{L}{\pi} \sin\left(\frac{\pi|i-j|}{L}\right) \tag{3.13}$$

(see Fig. 3.2).

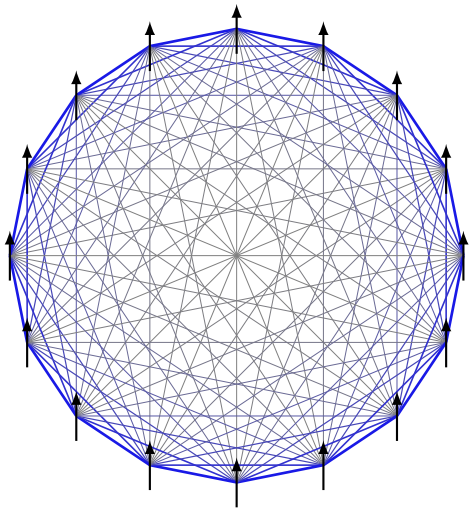

Figure 3.2: Representation of the (undiluted) one-dimensional long-range spin glass with r_{ij} defined as the chord distance when the spins are arranged on a ring.

We choose a particular distribution $P(J_{ij})$, introduced by Leuzzi et al. (2008), that satisfies Eq. (3.12) asymptotically while allowing for efficient computer simulation. In the resulting model, which we refer to as the *diluted model*, the interaction matrix J_{ij} is sparse, with the mean number of neighbors of a given spin fixed to an arbitrary constant z (here we choose $z = 6$). The nonzero elements of J_{ij} are drawn from a Gaussian distribution with zero mean and unit variance. The second part of Eq. (3.12) is then satisfied by letting the *probability* of an interaction between spins i and j fall off with distance like $r^{-2\sigma}$. That is, the interactions are distributed according to

$$P(J_{ij}) = \left(1 - p_{ij}\right) \delta\left(J_{ij}\right) + p_{ij} \frac{1}{\sqrt{2\pi}} e^{-J_{ij}^2/2}, \tag{3.14}$$

where $p_{ij} \propto r_{ij}^{-2\sigma}$.

To sample from this distribution we use the following algorithm. Choose a site i at random from a uniform distribution. Then choose a site j with probability $\widetilde{p}_{ij} = A/r_{ij}^{2\sigma}$, where A is determined by normalization. If there is not already a bond between i and j, take J_{ij} from a Gaussian distribution with zero mean and

unit variance.[1] Repeat until $Nz/2$ bonds have been generated in total, at which point the number of neighbors of a given spin has a Poisson distribution with mean z.

The transition temperature for the diluted model with $\sigma = 0$ was shown by Viana and Bray (1985) to be given by the solution of

$$\frac{1}{\sqrt{2\pi}} \int_{-\infty}^{\infty} \mathrm{d}x \, e^{-x^2/2} \tanh^2 \left(\frac{x}{T_c} \right) = \frac{1}{z}. \tag{3.15}$$

For our chosen value $z = 6$, we find

$$T_c(z = 6) \approx 2.0564 \quad \text{(diluted)}. \tag{3.16}$$

3.3 Method

We perform Monte Carlo simulations of the models described in Section 3.2. To speed up equilibration, we use the parallel-tempering Monte Carlo method described in Section 2.5.

To ensure that measurements are performed in equilibrium we use the equilibration test for Gaussian spin glasses described in Section 2.4.1. That is, we successively double the number of Monte Carlo sweeps, each time averaging over the last half of the sweeps, until (at least) the last three data points for $\Delta(\widetilde{U}, \widetilde{q}_l)$ are consistent with zero. The total number of sweeps used in this check is shown as N_{equil} in Tables 3.1 and 3.2. We perform the equilibration test only for the largest sizes (which account for most of the overall simulation time) and use the same value of N_{equil} for the smaller sizes.

We then do measurement runs where, after an initial N_{equil} sweeps to ensure the system has reached equilibrium, we do an additional 10 to 20 times as many

[1] Note that if $\widetilde{p}_{ij} \ll 1$, then p_{ij} in Eq. (3.14) is given by $p_{ij} = z\widetilde{p}_{ij}$. Otherwise there will be corrections due to the rejection of bonds when there is already a bond between i and j.

σ	L	N_{samp}	N_{equil}	N_{meas}	T_{min}	T_{max}	N_T
0	64	16000	1000	10000	0.5	1.65	47
0	128	16000	1000	10000	0.5	1.6	45
0	256	16000	1000	10000	0.5	1.6	45
0	512	16000	1000	10000	0.75	1.55	33
0	1024	8000	1000	10000	0.75	1.5	31
0	2048	4000	1000	10000	0.75	1.5	31
0	4096	4000	2000	10000	0.85	1.525	28
0.25	64	16000	1000	10000	0.5	1.65	47
0.25	128	16000	1000	10000	0.5	1.6	45
0.25	256	16000	1000	10000	0.5	1.6	45
0.25	512	8000	1000	10000	0.5	1.525	42
0.25	1024	8000	1000	10000	0.75	1.5	31
0.25	2048	4000	1000	10000	0.75	1.5	31
0.25	4096	4000	2000	10000	0.85	1.525	28

Table 3.1: Simulation parameters for the undiluted models. N_{samp} is the number of samples; N_{equil} and N_{meas} are the numbers of sweeps used for the equilibration and measurement phases respectively. We simulate N_T logarithmically-spaced temperatures between T_{min} and T_{max}.

sweeps during which measurements are performed. The detailed parameters of the simulations are given in Tables 3.1 and 3.2. To avoid bias in measurements with distinct thermal averages, e.g. Eq. (3.19), each thermal average is evaluated on a separate replica of the system with the same realization of the random couplings. Since the quantities of interest have no more than two distinct thermal averages, we simulate two copies of the system at each temperature.

We consider moments of the spin glass order parameter,

$$q = \frac{1}{L} \sum_i S_i^{(1)} S_i^{(2)}, \tag{3.17}$$

where "(1)" and "(2)" refer to independent replicas of the system with the same realization of the random couplings. Of particular interest are the spin-glass susceptibility

$$\chi_{\text{SG}} = L \left\langle q^2 \right\rangle \tag{3.18}$$

σ	L	N_{samp}	N_{equil}	N_{meas}	$T_{\min}$	$T_{\max}$	N_T
0	256	8000	400	8000	1.85	2.5	27
0	512	8000	800	16000	1.85	2.5	27
0	1024	8000	2000	40000	1.85	2.5	27
0	2048	4000	2000	40000	1.85	2.5	27
0	4096	4000	2000	40000	1.9	2.5	25
0	8192	2000	4000	80000	1.9	2.5	25
0	16384	2000	4000	80000	2	2.5	14
0.25	256	8000	800	16000	1.85	2.5	27
0.25	512	8000	800	16000	1.85	2.5	27
0.25	1024	8000	1200	24000	1.85	2.5	27
0.25	2048	4000	2000	40000	1.85	2.5	27
0.25	4096	4000	2000	40000	1.9	2.5	25
0.25	8192	2000	4000	80000	1.9	2.5	25
0.25	16384	2000	4000	80000	2	2.5	14
0.375	256	32000	1200	24000	1.863	4	24
0.375	512	32000	1200	24000	1.863	4	26
0.375	1024	16000	1200	24000	1.913	4	24
0.375	2048	15998	2000	40000	1.95	4	24
0.375	4096	8000	4000	80000	1.962	4	28
0.375	8192	7999	4000	80000	1.975	4	34
0.375	16384	4000	4000	80000	2	2.51	18

Table 3.2: Simulation parameters for the diluted models.

and the Binder ratio,

$$g = \frac{1}{2}\left(3 - \frac{\langle q^4 \rangle}{\langle q^2 \rangle^2}\right), \tag{3.19}$$

where $\langle \cdots \rangle$ indicates a thermal average and an average over the disorder.

Because the Binder ratio is dimensionless, its finite-size scaling behavior is simple (see Section 2.6). The models considered here are all in the mean-field regime, in which the scaling relation takes the form

$$g \sim \widetilde{g}\left[L^{1/3}\left(T - T_c\right)\right] \tag{3.20}$$

(where $\sim$ indicates asymptotic equivalence for large L). Although the spin-glass susceptibility is not dimensionless, its scaling form is also known exactly in the

mean-field regime,[2]

$$\chi_{\mathrm{SG}} \sim L^{1/3}\widetilde{\chi}\left[L^{1/3}\left(T - T_c\right)\right]. \tag{3.21}$$

Thus, at least asymptotically for large L, *the Binder ratio g and scaled susceptibility $\chi_{\mathrm{SG}}/L^{1/3}$ are independent of L at $T = T_c$.* We can exploit this to estimate T_c from the intersections of the data for different sizes when plotted against T. However, we will find that the data for different pairs of sizes do not intersect at a common temperature (see, for example, Fig. 3.3), but rather that data for each pair (L_1, L_2) intersect at a size-dependent temperature $T^*(L_1, L_2)$. This is because the corrections to the asymptotic scaling relations become significant for the range of sizes we are able to simulate.

According to standard finite-size scaling the spin-glass susceptibility scales near the critical point as

$$\chi_{\mathrm{SG}}(t, L) = L^a\left[f(L^b t) + L^{-\omega}g(L^y t) + \cdots\right] + c_0 + c_1 t + \cdots, \tag{3.22}$$

(Privman and M. E. Fisher 1983), where $t = T - T_c$, $a = 2 - \eta$ ($= 2\sigma - 1$ here), and $b = 1/\nu$. The $L^{-\omega}$ term is the leading *singular* correction to scaling and c_0 is the leading *analytic* correction to scaling.

In the mean-field regime, $\sigma < \sigma_u = 2/3$, the exponents a and b are independent of σ and take their values at σ_u for all $1/2 < \sigma < \sigma_u$.[3] Although the $L^{2\sigma-1}$ term is therefore replaced as the *largest* term by an $L^{1/3}$ term, we expect the former not to disappear but instead become a correction to scaling. Therefore, for $\sigma < \sigma_u$ we

[2]For a discussion of how standard finite-size scaling is modified in the mean-field regime, see, for example, (Binder, Nauenberg, et al. 1985; Luijten, Binder, and H. W. Blöte 1999; Jones and A. P. Young 2005; Brézin 1982; Brézin and Zinn-Justin 1985)

[3]This is explained by the presence of a "dangerous irrelevant variable," see Binder, Nauenberg, et al. (1985), Luijten, Binder, and H. W. Blöte (1999), and Jones and A. P. Young (2005) and also the discussion in Section 6.1.

replace Eq. (3.22) with

$$\chi_{\rm SG}(t,L) = L^{1/3}\left[f(L^{1/3}t) + L^{-\omega}g(L^{1/3}t) + \cdots\right] \tag{3.23}$$

$$+ d_0 L^{2\sigma-1}h(L^{1/3}t) + c_0 + c_1 t + \cdots . \tag{3.24}$$

The correction exponent ω can be obtained in the mean-field regime from the work of Kotliar, Anderson, and Stein (1983) and is given by $\omega = 2 - 3\sigma$. Thus, in the nonextensive regime $\sigma < 1/2$, the dominant correction to scaling is the constant c_0. Including the dominant correction, Eq. (3.21) becomes

$$\chi_{\rm SG} \sim L^{1/3}\widetilde{\chi}\left[L^{1/3}\left(T - T_c\right)\right] + c_0. \tag{3.25}$$

Data for $\chi_{\rm SG}/L^{1/3}$ for a pair of sizes $(L, 2L)$ will intersect at a temperature $T^*(L, 2L)$ where

$$\widetilde{\chi}\left[L^{1/3}(T^* - T_c)\right] + c_0/L^{1/3} = \widetilde{\chi}\left[(2L)^{1/3}(T^* - T_c)\right] + c_0/(2L)^{1/3}. \tag{3.26}$$

Expanding $\widetilde{\chi}$ to first order and solving for T^*, we obtain the correction to the intersection temperatures corresponding to the dominant correction to scaling,

$$T^*(L, 2L) = T_c + A/L^{2/3} + \cdots , \tag{3.27}$$

where A is a constant. We expect the corresponding result for the Binder ratio g to have the same form. In the following analysis we will fit Eq. (3.27) to the data to estimate the bulk transition temperature T_c.

3.4 Results

We first present our results for the undiluted model. Data for the Binder ratio and the scaled spin glass susceptibility are shown for $\sigma = 0$ (SK model) and $\sigma = 0.25$

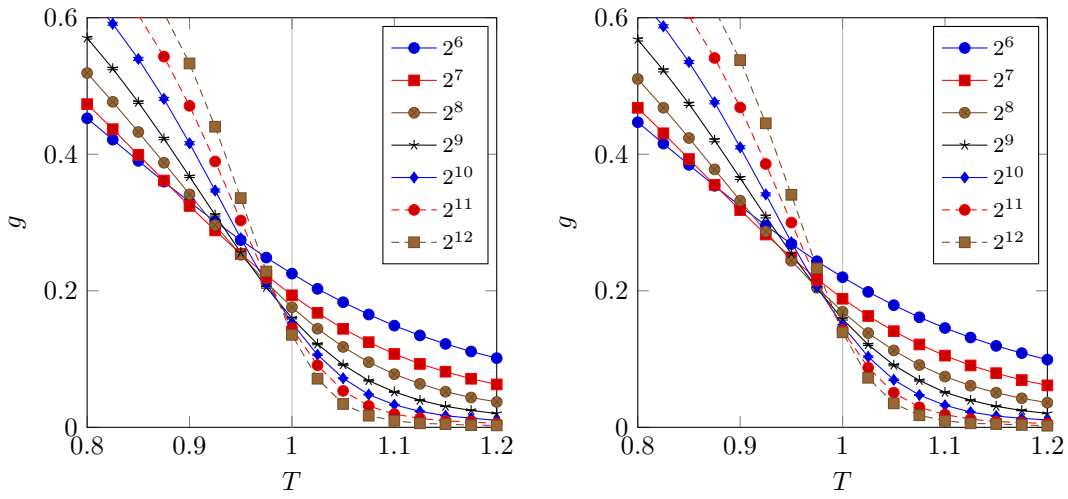

(a) $\sigma = 0$ (b) $\sigma = 0.25$

Figure 3.3: Data for the Binder ratio for the undiluted model. The exact value of the transition temperature for the SK model, $T_c = 1$, is marked with a vertical line.

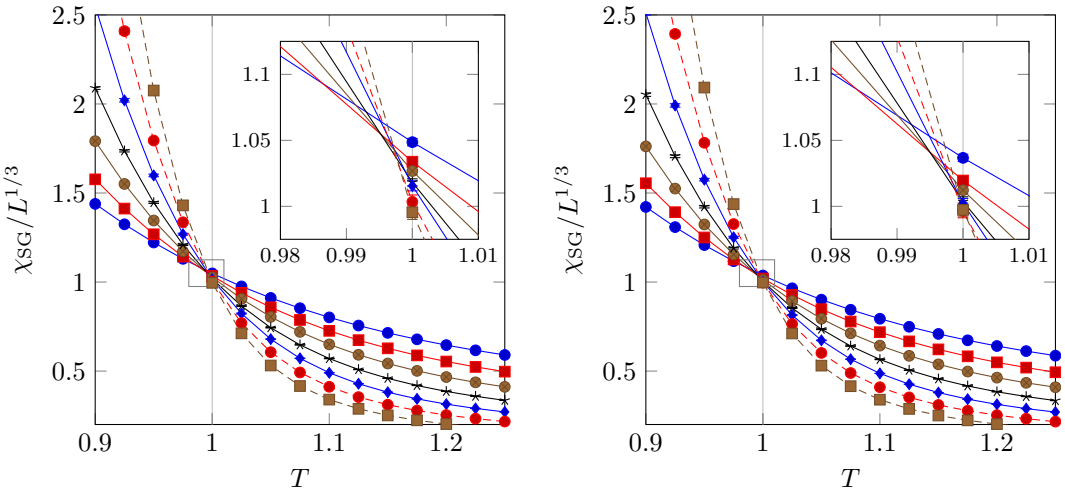

(a) $\sigma = 0$ (b) $\sigma = 0.25$

Figure 3.4: Data for the scaled spin-glass susceptibility for the undiluted model. The exact value of the transition temperature for the SK model, $T_c = 1$, is marked with a vertical line.

in Figs. 3.3 and 3.4. Note the large corrections to scaling for the Binder ratio and the relatively small corrections for the scaled susceptibility.

Figure 3.5 shows the intersection temperatures for the undiluted models, determined by first fitting a cubic spline to the data and finding the intersections of the splines. The error bars were estimated using the bootstrap resampling method (discussed in Section 2.7.2). We then fit Eq. (3.27) to the intersection temperatures to estimate T_c. For *both* values of σ we obtain a value consistent with $T_c = 1$ (with very small errors), the exact value for the SK model. The quality of the fit, as quantified by the goodness of fit parameter Q (Press 2007), is satisfactory except for the Binder ratio data for the SK model. We do not have a good explanation of this, except perhaps that multiple corrections to scaling are significant for the range of sizes studied. In any case we note that the result $T_c = 1$ for the SK model is rigorously correct. The result that $T_c = 1$ also for the model with $\sigma = 0.25$, at the midpoint of the nonextensive region, provides strong evidence for the claim of Mori (2011) that all models in the nonextensive region are identical to the SK model.

The corresponding results for the diluted models with $\sigma = 0$ and 0.25 are shown in Figs. 3.6 to 3.8. For the diluted model we also performed simulations with $\sigma = 0.375$ and show the resulting intersection temperatures in Fig. 3.9. For $\sigma = 0$, the Viana-Bray (VB) model, the transition temperature is given by Eq. (3.15), which, for $z = 6$ taken here, gives the result in Eq. (3.16). Here again we see that the corrections to scaling are larger for the Binder ratio than for the scaled spin glass susceptibility. Fitting Eq. (3.27), we find a predicted value of T_c consistent with the exact value for the VB model for *all* values of σ.

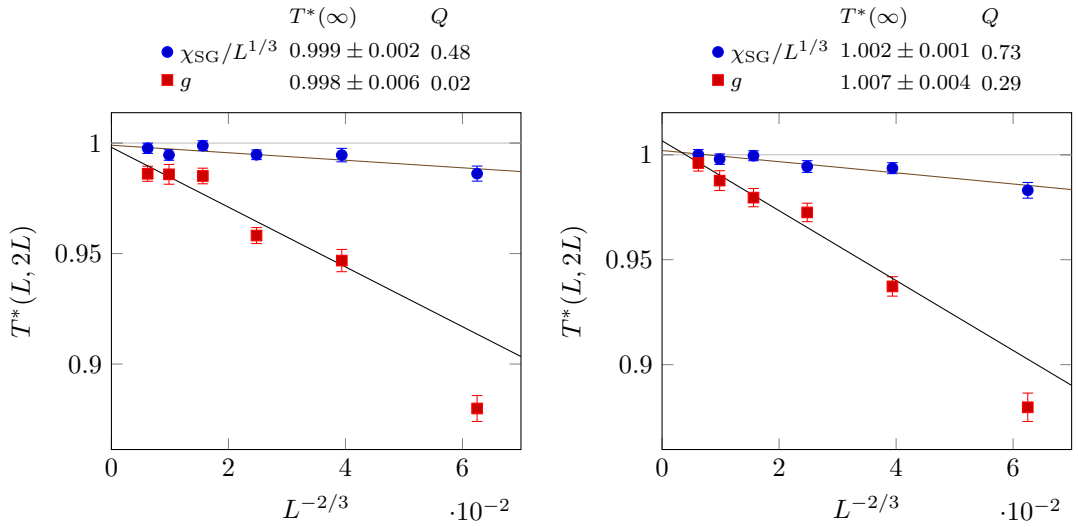

(a) $\sigma = 0$ (b) $\sigma = 0.25$

Figure 3.5: Results for the intersection temperatures for the undiluted model.

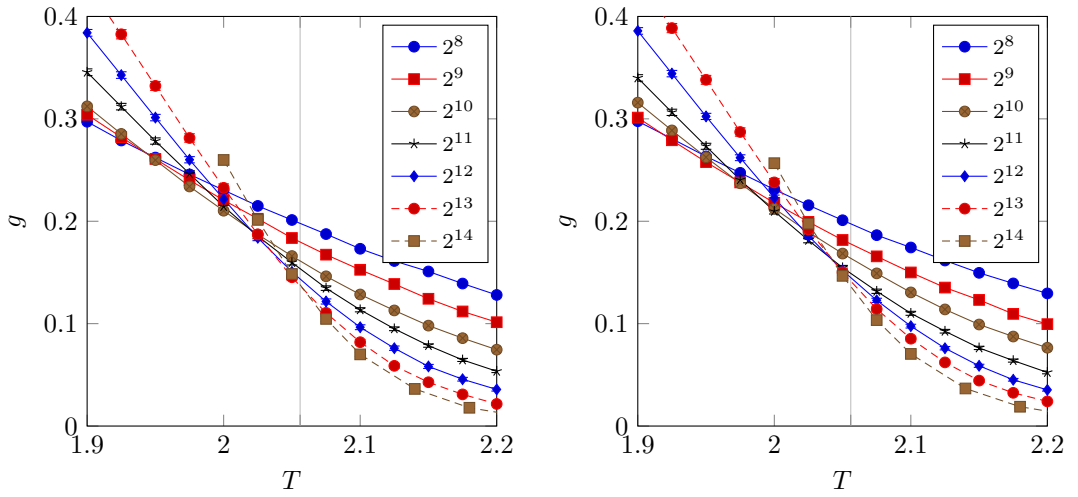

(a) $\sigma = 0$ (b) $\sigma = 0.25$

Figure 3.6: Data for the Binder ratio for the diluted model. The Viana-Bray model transition temperature $T_c \approx 2.056$, obtained from Eq. (3.15), is marked with a vertical line.

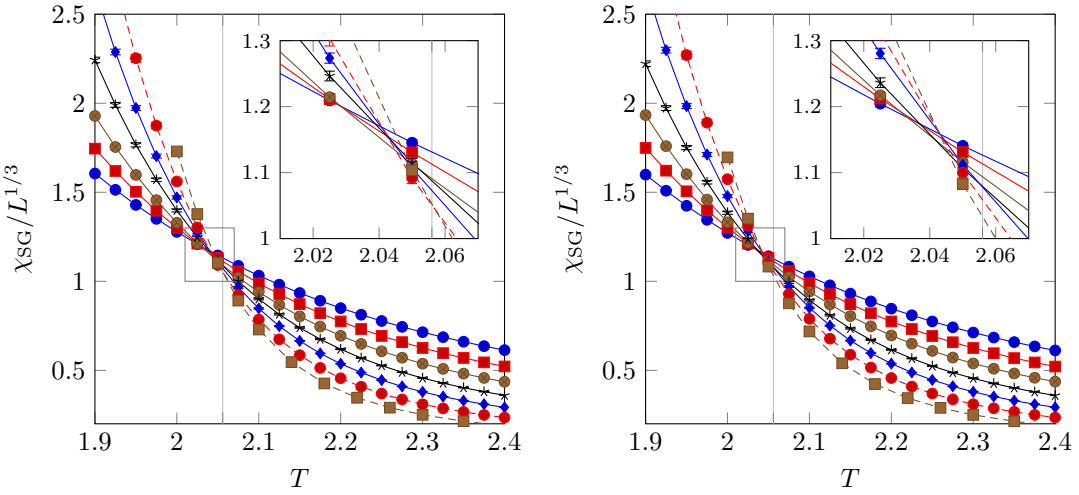

(a) $\sigma = 0$ (b) $\sigma = 0.25$

Figure 3.7: Data for the scaled spin-glass susceptibility for the diluted model. The Viana-Bray model transition temperature $T_c \approx 2.056$, obtained from Eq. (3.15), is marked with a vertical line.

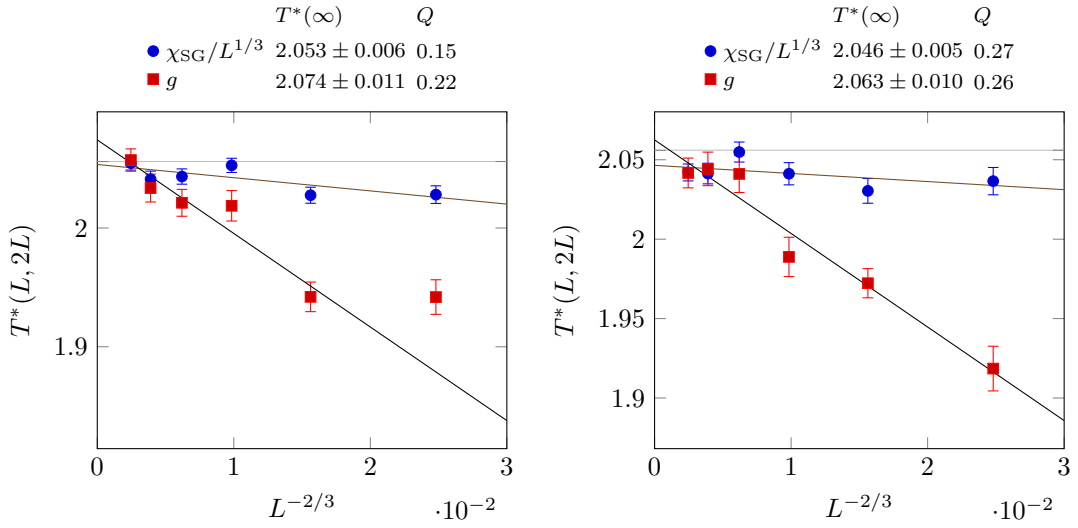

(a) $\sigma = 0$ (b) $\sigma = 0.25$

Figure 3.8: Results for the intersection temperatures for the diluted model.

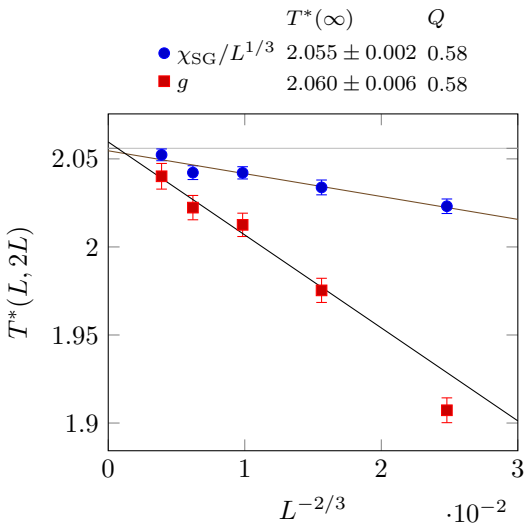

Figure 3.9: Results for the intersection temperatures for the diluted model with $\sigma = 0.375$.

3.5 Conclusions

We have performed Monte Carlo simulations to investigate the transition temperatures of one-dimensional Ising spin glasses, both undiluted and diluted, for several values of σ in the nonextensive regime $0 \leq \sigma < 1/2$. For the undiluted model we studied two values of σ, $\sigma = 0$ and $\sigma = 0.25$. For $\sigma = 0.25$, which lies in the middle of the nonextensive region, we find that the transition temperature agrees to high precision with the exact solution of the SK model. As a check, we also simulated the $\sigma = 0$ case, obtaining results consistent with the exact SK model result, though there seem to be multiple corrections to FSS for some of the data.

For the diluted model we studied three values of σ: $\sigma = 0$, which corresponds to the Viana-Bray model; $\sigma = 0.25$, which lies in the middle of the nonextensive region, and $\sigma = 0.375$. In all cases we found the transition temperature to be consistent with the exact solution of the Viana-Bray model; all results were within ~ 1.5 standard deviations.

To conclude, our results provide confirmation of the proposal (Mori 2011) that the behavior of (undiluted) spin glasses everywhere in the nonextensive regime is identical to that of the SK model. We have also proposed and provided evidence that an analogous result applies to *diluted* spin glass models.

Chapter 4

Statistics of the overlap distribution

4.1 Introduction

Despite much debate, there is still no consensus on the nature of the spin-glass phase. According to the "replica symmetry breaking" (RSB) picture of Parisi discussed in Section 1.3.3, there are many "pure states," a nontrivial order parameter distribution, and a line of transitions in a magnetic field, the de Almeida-Thouless (AT) line. In contrast, according to the droplet theory, there is only a single symmetry-related pair of pure states in zero field (one state in a nonzero field), and thus the order parameter distribution is trivial in the thermodynamic limit and there is no AT line. The nature of the spin glass phase has been investigated in a series of papers by Newman and Stein (see, for example, Stein and C. M. Newman (2013) and references therein), and recently by Read (2014). Marinari, Parisi, Ricci-Tersenghi, et al. (2000) discuss the RSB point of view.

The sample-averaged order parameter distribution, defined in Eqs. (4.6) and (4.7)

below, is predicted to be nonzero in the vicinity of $q = 0$ as the size of the system $N \equiv L^d$ tends to infinity, according to the RSB picture (Parisi 1983), whereas it is expected to *vanish* as $L^{-\theta}$ in the droplet picture, where θ is a positive "stiffness" exponent (D. S. Fisher and Huse 1986). Results from simulations[1] seem close to the predictions of RSB, but it has been argued (Moore, Bokil, and Drossel 1998; Middleton 2013) that the sizes which can be simulated are too small to see the asymptotic behavior.

Consequently, there has recently been interest[2] in studying other quantities related to $P(q)$ but where more attention is paid to the overlap distribution of *individual* samples, $P_{\mathcal{J}}(q)$, rather than just the sample average. Accurately determining $P_{\mathcal{J}}(q)$ for each sample is more demanding numerically than just computing the average, but computer power has advanced to the point where this is now feasible.

Here we will study in detail these new quantities for a *range* of models. In addition to the short-range Edwards-Anderson (EA) spin-glass models in three and four space dimensions, and the infinite-range Sherrington-Kirkpatrick (SK) model, we also study diluted long-range (LR) Ising spin-glass models in one space dimension, described in detail in Section 3.1. The LR models are are useful here because it is important to study models in the mean-field regime ($d \geq 6$), or equivalently $\sigma < 2/3$, but it is difficult to simulate and carry out a finite-size scaling (FSS) analysis of the results for short-range models in high dimensions because the number of spins grows so quickly with L that only a few sizes can be considered. The LR models do not have this difficulty, so we use them to probe the mean-field regime. Finally, verifying the consistency of our results for the SR

[1] Marinari, Parisi, Ricci-Tersenghi, et al. (2000), Reger, Bhatt, and A. P. Young (1990), Katzgraber, Palassini, and A. P. Young (2001), and Katzgraber and A. P. Young (2003)

[2] Middleton (2013), Yucesoy, Katzgraber, and Machta (2012), and Monthus and Garel (2013)

and LR models gives us additional confidence in our numerical results.

4.2 Models

We study several classes of Ising spin-glass models. These are one-dimensional long-range (LR) models, three- and four-dimensional short-range (EA) models, and the infinite-range (SK) model. In all cases the Hamiltonian can be written in the form

$$\mathcal{H} = -\sum_{i,j} J_{ij} S_i S_j, \tag{4.1}$$

where the $S_i \in \{1, 2, \ldots, N\}$ represent Ising spins that take values ± 1, and the J_{ij} are independent, quenched random variables. The summation is defined over all pairs of interacting spins. All of the models studied here have finite-temperature spin-glass transitions. The models differ according to which spins interact and the strength of the couplings.

4.2.1 Edwards-Anderson models on hypercubic lattices

The three- and four-dimensional EA models that we study are defined on (hyper-)cubic lattices with periodic boundary conditions. The nearest-neighbor interactions are taken from a Gaussian distribution with zero mean and unit variance,

$$\left[J_{ij}\right]_{\text{av}} = 0, \quad \left[J_{ij}^2\right]_{\text{av}} = 1, \tag{4.2}$$

where $[\ldots]_{\text{av}}$ indicates a quenched average over the couplings. From numerical studies it is known that the transition temperatures are $T_c = 0.951(9)$ for $d = 3$ (Katzgraber, Körner, and A. P. Young 2006) and $T_c = 1.80(1)$ for $d = 4$ (Parisi, Ricci-Tersenghi, and Ruiz-Lorenzo 1996).

4.2.2 Sherrington-Kirkpatrick model

In the SK model each spin interacts with every other spin. The couplings are taken from a Gaussian distribution with zero mean and variance which is inversely proportional to the size of the system,

$$\left[J_{ij}\right]_{\text{av}} = 0, \quad \left[J_{ij}^2\right]_{\text{av}} = 1/N. \tag{4.3}$$

The latter condition is necessary to ensure that there is a well-defined thermodynamic limit, as discussed in Section 3.1. The transition temperature for this model is $T_c = 1$ (Sherrington and Kirkpatrick 1975).

4.2.3 One-dimensional diluted long-range model

For the LR models the distribution of the interactions satisfies

$$\left[J_{ij}\right]_{\text{av}} = 0, \quad \left[J_{ij}^2\right]_{\text{av}} \propto R_{ij}^{-2\sigma}, \tag{4.4}$$

where σ is a parameter controlling the range of interactions, and R_{ij} is the chord distance between sites i and j when the spins are arranged on a ring, see Fig. 3.2 and Eq. (3.13). The *diluted model* corresponds to a choice of the distribution $P(J_{ij})$ which satisfies Eq. (4.4) while allowing for efficient computer simulation, namely

$$P(J_{ij}) = (1 - p_{ij})\delta(J_{ij}) + p_{ij}\frac{1}{\sqrt{2\pi}}e^{-J_{ij}^2/2}, \tag{4.5}$$

where $p_{ij} \propto R_{ij}^{-2\sigma}$ at large distance. The constant of proportionality is determined by fixing the mean number of neighbors of each spin, z_b. In this work we take $z_b = 6$. The motivation for choosing this distribution and the algorithm used to sample from it are discussed in Section 3.2.

We consider three values of the range parameter: $\sigma = 0.6$, which is in the mean-field regime (Larson et al. 2010), $\sigma = 0.784$, which represents, at least ap-

proximately, a short-range system in four dimensions,[3] and $\sigma = 0.896$, which approximately represents a three-dimensional system.[4] The values of T_c are approximately equal to 1.35 and 0.795 for $\sigma = 0.784$ and 0.896, respectively (Larson et al. 2013). For $\sigma = 0.6$ we find $T_c \approx 1.953$.

4.3 Methods

We have carried out parallel-tempering (replica-exchange) Monte Carlo simulations of the models described in Section 4.2. In parallel tempering, N_T replicas of the system with the same couplings are each simulated at a different temperature in the range between $T_{\min}$ and $T_{\max}$. In addition to standard Metropolis sweeps at each temperature, there are parallel tempering moves that allow replicas to be exchanged between neighboring temperatures. Parallel tempering moves permit replicas to diffuse from low temperatures, where equilibration is very slow, to high temperatures, where it is easy, and back again. The result is greatly accelerated equilibration relative to an algorithm that only performs Metropolis sweeps. See Section 2.5 for more on the theory and implementation the parallel tempering algorithm.

The simulation parameters are given in Tables 4.1 to 4.4. A single "sweep" consists of a Metropolis sweep at each temperature, followed by parallel tempering moves between each pair of neighboring temperatures. The parameter b determines the number of sweeps: 2^b for equilibration followed by 2^b for data collection. The parameter N_{sa} is the number of disorder samples simulated. For each model we have chosen the lowest temperature to be less than or equal to $0.4T_c$,

[3] Larson et al. (2010), Alvarez Baños, Fernandez, et al. (2012), Katzgraber and Hartmann (2009), and Larson et al. (2013)

[4] See Footnote 3.

σ	N	b	$T_{\min}$	$T_{\max}$	N_T	N_{sa}
0.6	64	24	0.82	3	50	4992
0.6	128	24	0.82	3	50	4800
0.6	256	24	0.82	3	50	4800
0.6	512	24	0.82	3	50	4684
0.6	1024	25	0.82	3	50	4800
0.784	64	24	0.55	2	50	4377
0.784	128	24	0.55	2	50	5060
0.784	256	24	0.55	2	50	5470
0.784	512	24	0.55	2	50	5207
0.784	1024	25	0.55	2	50	5988
0.896	64	24	0.31	1.2	50	2600
0.896	128	24	0.31	1.2	50	4468
0.896	256	24	0.31	1.2	50	4749
0.896	512	24	0.31	1.2	50	4749
0.896	1024	25	0.31	1.1788	25	4749

Table 4.1: Simulation parameters for the 1D LR models. For each value of σ and size N, N_{sa} samples were equilibrated for 2^b sweeps and then measured for an additional 2^b sweeps, using replica-exchange Monte Carlo with N_T temperatures between $T_{\min}$ and $T_{\max}$.

N	L	b	$T_{\min}$	$T_{\max}$	N_T	N_{sa}
64	4	18	0.2	2	16	4891
216	6	24	0.2	2	16	4961
512	8	27	0.2	2	16	5130
1000	10	27	0.2	2	16	5027
1728	12	25	0.42	1.8	26	3257

Table 4.2: Simulation parameters for the 3D EA spin glass. The parameters are defined as in Table 4.1 except for the linear size L, where $N = L^3$.

the approximate temperature for which we report most of our results.

To test our simulations for equilibration, we use the method discussed in Section 2.4.2. That is, we plot Eq. (2.31) as a function of the number of sweeps and infer the time to reach equilibrium from when $\Delta(t)$ is consistent with zero for a sufficient number of points, see the discussion below. Note that for the SK model, $\left(T_c^{\text{MF}}\right)^2 = T_c^2 = 1$, while for the remaining models $\left(T_c^{\text{MF}}\right)^2 = z$, where z is the

N	L	b	$T_{\min}$	$T_{\max}$	N_T	N_{sa}
256	4	23	0.72	2.38	52	3252
625	5	23	0.9101	2.38	42	4086
1296	6	23	0.72	2.38	52	3282
2401	7	23	0.9101	2.38	42	4274
4096	8	23	0.72	2.38	52	3074
6561	9	24	0.72	2.38	52	3010

Table 4.3: Simulation parameters for the 4D EA spin glass. The parameters are defined as in Table 4.1 except for the linear size L, where $N = L^4$.

N	b	$T_{\min}$	$T_{\max}$	N_T	N_{sa}
64	22	0.2	1.5	48	5068
128	22	0.2	1.5	48	5302
256	22	0.2	1.5	48	5085
512	18	0.2	1.5	48	4989
1024	18	0.2	1.5	48	3054
2048	16	0.4231	1.5	34	3020

Table 4.4: Simulation parameters for the SK spin glass. The parameters are defined as in Table 4.1.

(average) number of neighbors of each site. Thus $z = 2d$ for the EA models and $z = z_b = 6$ for the LR models.

While the method of Section 2.4.2 is a useful criterion for the equilibration of *sample-averaged* quantities, we must be especially careful when studying quantities that may be sensitive to the equilibration of individual samples, such as those considered in Section 4.4. To ensure the equilibration of individual samples, *i.e.* not just sample averages, we run our simulations for many times the number of sweeps needed to satisfy Eq. (2.31); at minimum we require that at least 3 consecutive, logarithmically-spaced times agree within error bars.

Figure 4.1 shows example equilibration tests for (a) the 1D LR model with $\sigma = 0.896$ for the largest size at the lowest temperature, and (b) the 3D EA model with $L = 8$, again at the lowest temperature. In both cases the data plateau at

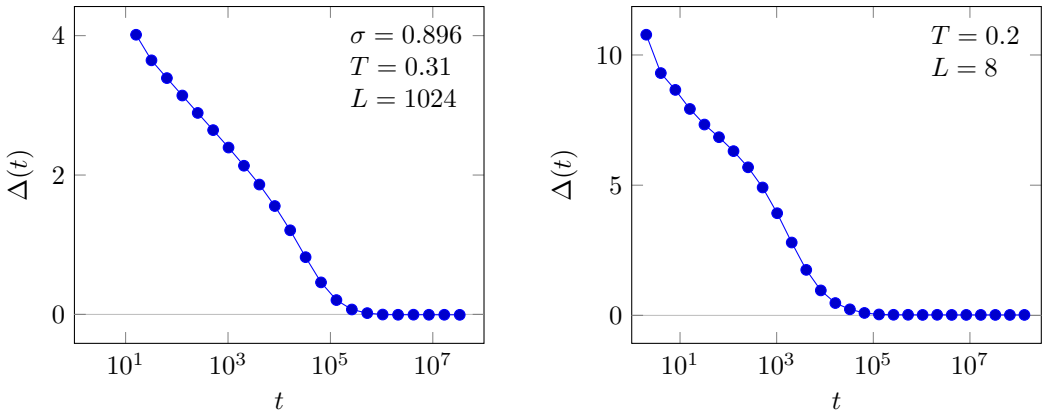

(a) 1D LR model

(b) 3D EA model

Figure 4.1: Plots of the quantity $\Delta(t)$, defined in Eq. (2.31), for (b) the 3D EA model and (a) the 1D LR model. The results shown are for the lowest temperatures studied and intermediate sizes. Note that at large times $\Delta \to 0$, indicating the equilibration of *sample averages*, but the simulations continue well beyond this point to ensure that individual samples are equilibrated. Error bars are smaller than the symbols.

zero (within the error bars) at around 10^5 sweeps, but the simulations continue for much longer than this to ensure that individual samples are equilibrated.

As an additional check of equilibration for the 1D LR models, Fig. 4.2 shows several quantities of interest, defined in Section 4.4, as a function of the number of sweeps on a log scale, for the lowest temperature studied and for each value of σ. The data appear to have saturated. The 3D EA data have also been tested for equilibration using the integrated autocorrelation time, as discussed in Yucesoy, Machta, and Katzgraber (2013).

4.4 Measured quantities

For a single sample $\mathcal{J} \equiv \{J_{ij}\}$, the spin overlap distribution is given by

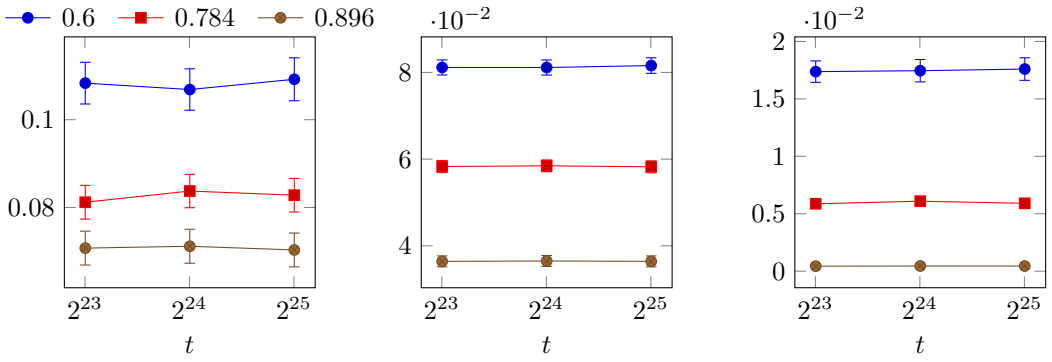

(a) $\Delta(q_0 = 0.2, \kappa = 1)$ (b) $I^{\text{av}}(q = 0.2)$ (c) $I^{\text{med}}(q = 0.2)$

Figure 4.2: Plots of several observables obtained from the overlap distribution, defined in Section 4.4, versus the number of Monte Carlo sweeps for the largest size studied, $N = 1024$, for the long-range model at the lowest temperature simulated for each value of σ. (See Table 4.1.) The data appear to have reached a steady state.

$$P_{\mathcal{J}}(q) = \left\langle \delta \left(q - \frac{1}{N} \sum_{i=1}^{N} S_i^{(1)} S_i^{(2)} \right) \right\rangle , \tag{4.6}$$

where "(1)" and "(2)" refer to two independent copies of the system with the same interactions, and $\langle \cdots \rangle$ denotes a thermal (*i.e.* Monte Carlo) average for a single sample. In most previous work, $P_{\mathcal{J}}(q)$ is simply averaged over disorder samples to obtain $P(q)$ defined by

$$P(q) = \left[P_{\mathcal{J}}(q) \right]_{\text{av}} \tag{4.7}$$

In order to gain additional information that might distinguish the RSB and droplet pictures, several investigators have recently introduced other observables related to the statistics of $P_{\mathcal{J}}(q)$. Yucesoy, Katzgraber, and Machta (2012) proposed a measure that is sensitive to peaks in the overlap distributions of *individual samples*, $P_{\mathcal{J}}(q)$. A sample is counted as "peaked" if $P_{\mathcal{J}}(q)$ exceeds a threshold value κ in the domain $|q| < q_0$. The quantity $\Delta(q_0, \kappa)$ is then defined as the

fraction of peaked samples. More precisely, for each sample let

$$\Delta_{\mathcal{J}}(q_0,\kappa) = \begin{cases} 1 & \text{if } P_{\mathcal{J}}(q) > \kappa \text{ for some } q \text{ where } |q| < q_0, \\ 0 & \text{otherwise.} \end{cases} \tag{4.8}$$

We then define $\Delta(q_0,\kappa)$ to be the sample average,

$$\Delta(q_0,\kappa) = \left[\Delta_{\mathcal{J}}(q_0,\kappa)\right]_{\text{av}}. \tag{4.9}$$

Note that $\Delta(q_0,\kappa)$ is a nondecreasing function of q_0 and a nonincreasing function of κ. A more important property of $\Delta(q_0,\kappa)$ is that its behavior for $N \to \infty$ distinguishes between the RSB and droplet pictures as follows. All of the scenarios for the low-temperature behavior of spin-glass models predict that $P_{\mathcal{J}}(q)$ is a superposition of δ functions as $N \to \infty$. The difference between scenarios lies in the number and positions of these δ functions, see Fig. 1.4. According to the RSB picture, there is a countable infinity of δ functions that densely fill the line between $-q_{\text{EA}}$ and $+q_{\text{EA}}$. Thus, for any q_0 and any κ, $\Delta(q_0,\kappa) \to 1$ for models described by RSB. On the other hand, for models described by the droplet scenario or other scenarios with only a single pair of pure states for $N \to \infty$, $\Delta(q_0,\kappa) \to 0$ for any $q_0 < q_{\text{EA}}$ and any κ. Thus, the quantity $\Delta(q_0,\kappa)$ will sharply distinguish the RSB and droplet scenarios if one can study large enough sizes. We will study the size dependence of Δ numerically for all of our models in Section 4.5.1.

As mentioned above, most previous work evaluated the *average* probability distribution $P(q)$, but recently Middleton (2013) and Monthus and Garel (2013) have proposed measures yielding a *typical* value of the sample distribution $P_{\mathcal{J}}(q)$ with the hope that these measures would provide a clearer differentiation between the RSB and droplet pictures than the average $P(q)$.

Middleton (2013) studied $I^{\text{med}}(q)$, the *median* of the *cumulative* overlap dis-

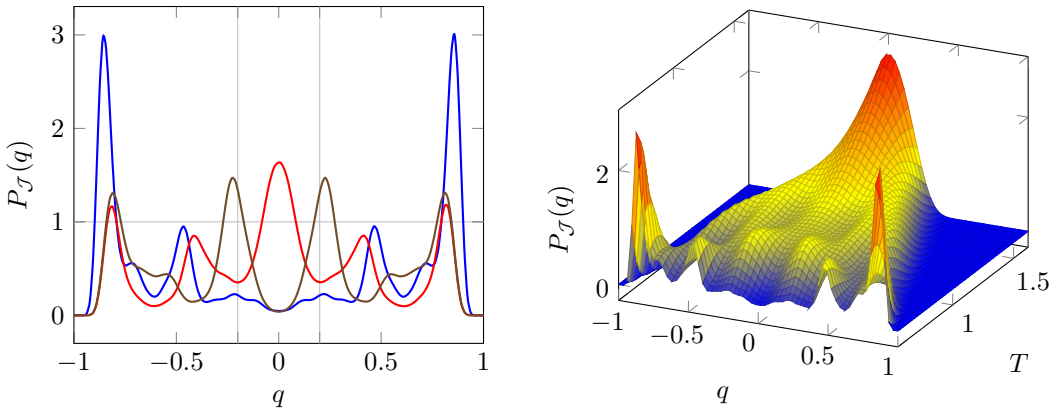

(a) (b)

Figure 4.3: Plots of the overlap distribution $P_{\mathcal{J}}(q)$ for individual disorder samples. Panel (a) shows the overlap distribution obtained for three different samples for the 1D LR model with $\sigma = 0.784$ at the lowest temperature simulated, $T = 0.55$. According to Eq. (4.8) with parameters $q_0 = 0.2$, $\kappa = 1$ (indicated by vertical lines and a horizontal line respectively), two of the three samples contribute to $\Delta(q_0, \kappa)$. Panel (b) shows the overlap distribution $P(q)$ versus temperature for a single disorder sample for the same model, showing the emergence of multiple pairs of peaks below the transition temperature $T_c \approx 1.35$.

tribution of a single sample $I_{\mathcal{J}}(q)$, where $I_{\mathcal{J}}(q)$ is defined by

$$I_{\mathcal{J}}(q) = \int_{-q}^{q} \mathrm{d}q' P_{\mathcal{J}}(q'). \tag{4.10}$$

We also denote by $I^{\mathrm{av}}(q)$ the sample-averaged cumulative distribution, which is given by

$$I^{\mathrm{av}}(q) = \int_{-q}^{q} \mathrm{d}q' P(q'). \tag{4.11}$$

Compared to the average, the median is insensitive to the effect of samples with unusually large values of $I_{\mathcal{J}}(q)$.

For the SK model $P(q)$ tends to a constant as $q \to 0$, and so $I^{\mathrm{av}}(q) \propto q$ for small q. We can obtain a rough idea of how $I^{\mathrm{med}}(q)$ varies with q for small q in the SK model from the results of Mézard et al. (1984). First of all, to obtain a notation which is more compact and is extensively used in other work, we write $x(q) \equiv I^{\mathrm{av}}(q)$. Mézard et al. (1984) argue that, at small q where $x(q)$ is also small,

the probability of a certain integrated value $I_{\mathcal{J}}$ is given by

$$p(I_{\mathcal{J}}) \propto x I_{\mathcal{J}}^{x-1}. \tag{4.12}$$

From Eq. (4.12) we estimate the median in terms of the average as

$$I^{\mathrm{med}}(q) \propto e^{-\ln 2/x(q)} = e^{-\ln 2/\left[2qP(0)\right]} \tag{4.13}$$

for $q \to 0$, where we used that $P(0)$ is nonzero so $x(q) \equiv I^{\mathrm{av}}(q) \simeq 2P(0)q$ in this limit [see Eq. (4.11)]. Therefore the median tends to zero exponentially fast as $q \to 0$, whereas the average only goes to zero linearly.

In the droplet picture, $P(0)$ is expected to vanish with L as $L^{-\theta}$, so $I^{\mathrm{av}}(q) \propto L^{-\theta}q$ for small q. The median value $I^{\mathrm{med}}(q)$ will presumably also vanish for small q as $L \to \infty$, but we are not aware of any precise predictions for this. We will study the median cumulative distribution numerically in Section 4.5.2.

Another measure related to the overlap distribution of individual samples has been proposed by Monthus and Garel (2013). They suggest calculating a "typical" overlap distribution defined by the exponential of the average of the log, *i.e.*

$$P^{\mathrm{typ}}(q) = \exp\left[\ln P_{\mathcal{J}}(q)\right]_{\mathrm{av}}. \tag{4.14}$$

We will study this quantity numerically in Section 4.5.3.

4.5 Results

4.5.1 Fraction of peaked samples, $\Delta(q_0, \kappa)$

Plots of $\Delta(q_0, \kappa)$ for the 1D LR models for various values of q_0 and κ are given in Fig. 4.4; corresponding plots for the 3D and 4D EA models are shown in Fig. 4.5. A comparison with the SK model is made in both cases. The error bars for all

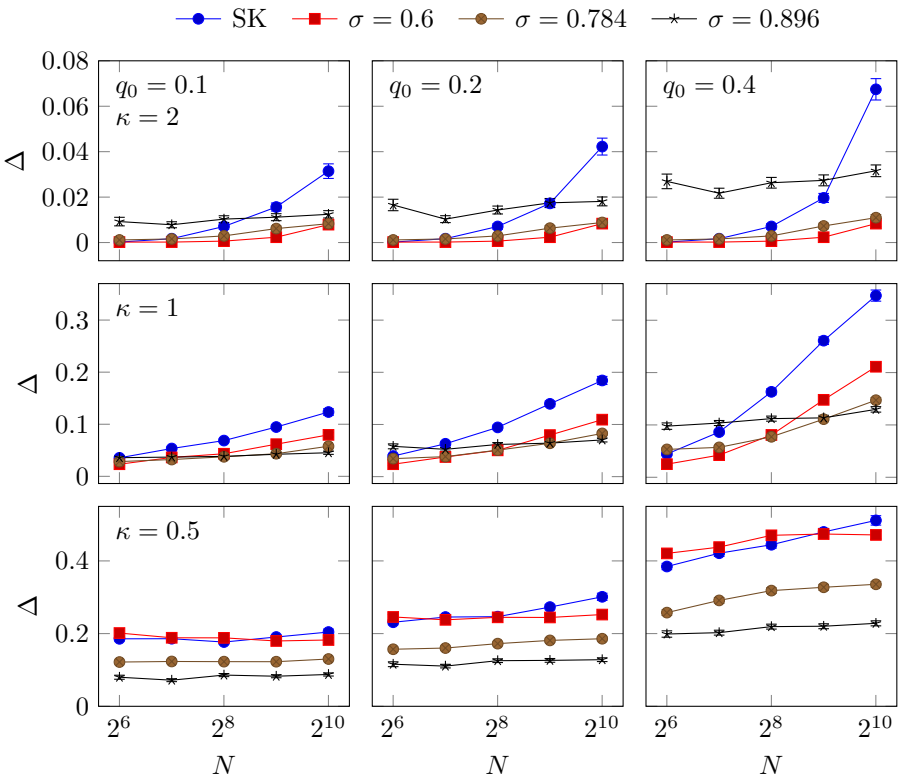

Figure 4.4: $\Delta(q_0, \kappa)$ as a function of system size N for the 1D LR models and the SK model for all available values of σ and various values of the window q_0 and threshold κ. In all cases the temperature is $0.4T_c$. All panels have the same horizontal scale, and all panels in a row have the same vertical scale.

plots in this section are one standard deviation statistical errors due to the finite number of samples. There are also errors in the data for each sample due to the finite length of the data collection. For the EA and SK models, we estimated these errors by measuring $\Delta^+(q_0, \kappa)$ and $\Delta^-(q_0, \kappa)$, defined as in Eqs. (4.8) and (4.9), but from the $q > 0$ and $q < 0$ components of $P_{\mathcal{J}}(q)$, respectively. These are expected to be reasonably independent and their differences provide an estimate of the error due to finite run lengths. For all sizes, the average absolute difference between these quantities, $\left[\left|\Delta^+(q_0, \kappa) - \Delta(q_0, \kappa)\right| + \left|\Delta^-(q_0, \kappa) - \Delta(q_0, \kappa)\right|\right]/2$, is less than the statistical error.

One can draw several qualitative conclusions from these plots. It is apparent

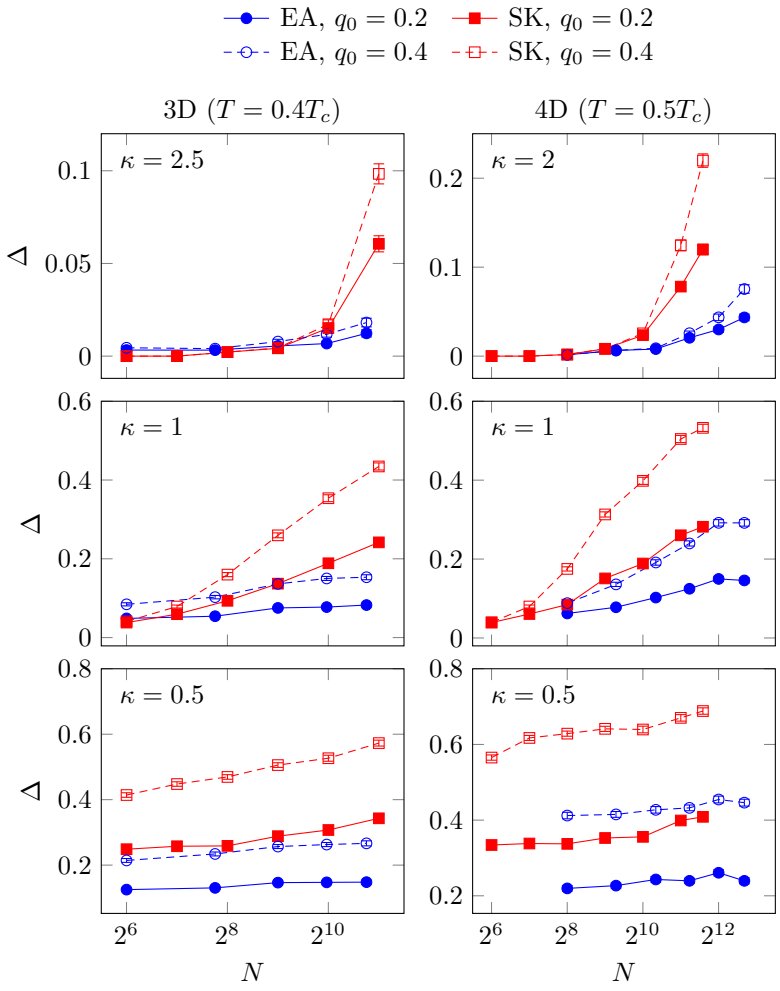

Figure 4.5: $\Delta(q_0, \kappa)$ as a function of system size N for the EA models and the SK model for several values of the window q_0 and threshold value κ. The temperatures are $0.4T_c$ for the 3D data and $0.5T_c$ for the 4D data. All panels in a column have the same horizontal scale.

that $\Delta(q_0, \kappa)$ is an increasing function of N for small N. As the system size increases, we expect $\Delta(q_0, \kappa)$ to increase because all the features of $P_{\mathcal{J}}(q)$ sharpen. For the SK model, which is described by the RSB picture, the number of features and their height should both increase and $\Delta(q_0, \kappa)$ should be a strongly increasing function of N. Indeed, this behavior is seen except for $\kappa = 0.5$, which is a sufficiently small value that $\Delta(q_0, \kappa)$ is effectively measuring whether or not there is a feature in the relevant range, and this quantity increases relatively slowly for the SK model.

However, as σ increases for the 1D LR models, the curves become increasingly flat and the difference between $\sigma = 0.896$ and the SK model is striking; the former is nearly flat while the latter increases sharply (see Fig. 4.4). The same qualitative distinction holds between the 3D EA model and the SK model (see Fig. 4.5). The similarity between the behavior of the 1D model for $\sigma = 0.896$ and the 3D EA model is expected since the two models are believed to have the same qualitative behavior. The distinction between the SK model and the 1D LR model with $\sigma = 0.784$ and the 4D EA model is less striking but qualitatively similar.

It is interesting to compare the results for the SK model with the 1D LR model with $\sigma = 0.6$, which is in the mean-field regime. For $\kappa = 0.5$ the results for the two models are very similar and do not increase much with N, indicating that $\kappa = 0.5$ is too small to give useful information for this range of sizes, as discussed above. For $\kappa = 1$, the SK data increase most rapidly with N, and the $\sigma = 0.6$ data increase less quickly, but still faster than the other values of σ. For $\kappa = 2$, the SK data increase quickly, while for the value of σ furthest from the SK limit, 0.896, the data are moderately large but roughly size-independent over the range of sizes studied. Curiously, for intermediate values of σ (0.6 and 0.784) the data are very small but show an increase for the larger sizes. This increase is particularly sharp

for $\sigma = 0.6$. It seems that there is an initial value of Δ for small N and a growth as N increases. We do not have a good understanding of the initial value, *e.g.*, why it is so small for $\kappa = 2$ and $\sigma = 0.6$, 0.784. The more important aspect of the data is the increase observed, at least for most parameter values, at large sizes. Given the rapid increase in the data for $\sigma = 0.6$, $\kappa = 2$ for the largest size, we anticipate that for still larger sizes, its value for Δ for $\kappa = 2$ would be closer to that of the SK model than that of the intermediate σ values.

There are two possible interpretations of the trends discussed above. If one believes that the RSB picture holds for all of the models studied here, then one can point to the fact that all of the Δ curves are nondecreasing and assert that they will all approach unity as $N \to \infty$, just extremely slowly for the 3D EA model and the 1D LR model with $\sigma = 0.896$. Billoire, Fernandez, et al. (2013) argue that this is the case, and are rebutted by Yucesoy, Katzgraber, and Machta (2013). If, on the other hand, one believes that the droplet scenario or chaotic pairs scenario holds for finite-dimensional spin glasses, then the flattening of the curves for these models is a prelude to an eventual decrease to zero. Unfortunately, the sizes currently accessible to Monte Carlo simulation do not permit one to sharply distinguish between these competing hypotheses. Using an exact algorithm for the two-dimensional (2D) Ising spin glass with bimodal disorder, Middleton (2013) shows that the crossover to decreasing behavior for $\Delta(q_0, \kappa)$ in 2D does occur at large length scales. He also shows, within a simplified droplet model, that the large length scales are needed to see the predictions of the droplet scenario manifest in the 3D EA model. Overall, we see that we need larger sizes to unambiguously determine from $\Delta(q_0, \kappa)$ whether the droplet of RSB picture applies to 3D-like models.

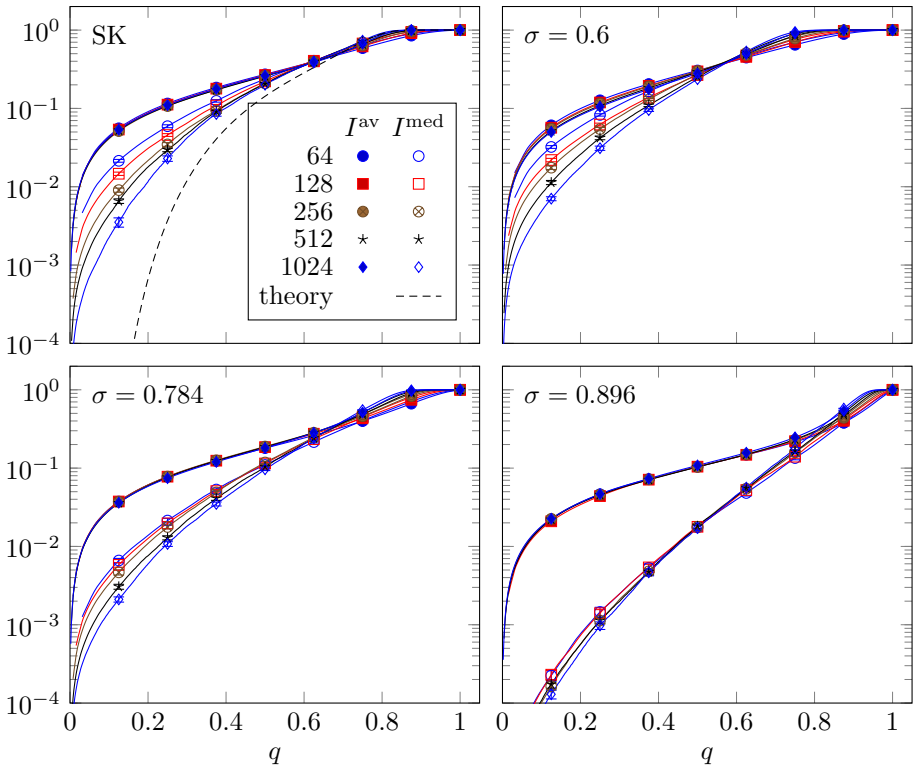

Figure 4.6: Mean and median over samples of the cumulative distribution $I_{\mathcal{J}}(q)$ for the 1D LR models and the SK model. In all cases the temperature is close to $0.4T_c$. For both the SK and the 1D models, the median shows a relatively strong size dependence compared with the mean, this difference being the least pronounced for $\sigma = 0.896$. The "theory" curve for the SK data [Eq. (4.13)] is expected to be valid for small q only. The theory expression can be multiplied by an (unknown) constant which has been set to unity. All panels have the same horizontal and vertical scales. Only a representative set of points is shown but the curves go through all the points.

4.5.2 Median $I^{\rm med}(q)$ and mean $I^{\rm av}(q)$ cumulative overlap distribution

In this section, we compare the mean $I^{\rm av}(q)$ and the median $I^{\rm med}(q)$ of the cumulative overlap distribution. Figure 4.6 shows the results for these two quantities for the SK model and several 1D LR models for a temperature close to $0.4T_c$. Figure 4.7 shows the same quantities for the 3D and 4D EA models.

As noted in earlier work, the results for the average show very little size de-

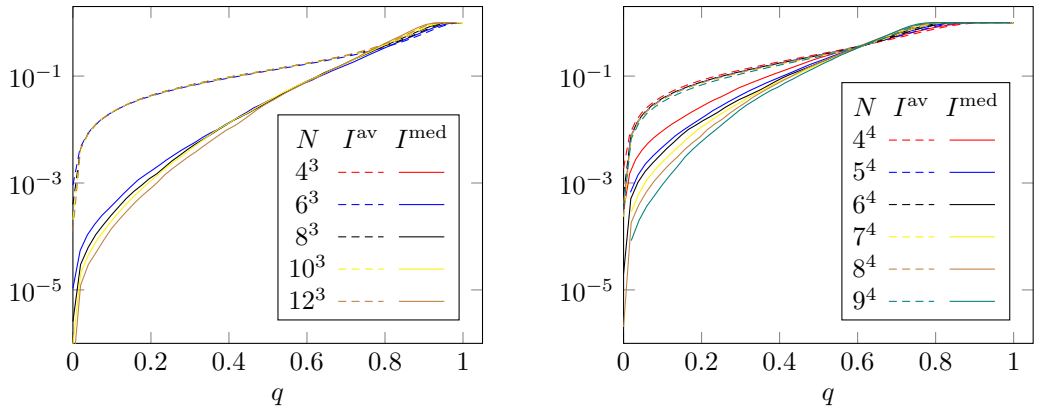

(a) 3D EA (b) 4D EA

Figure 4.7: Log-linear plot of $I^{\mathrm{med}}(q)$ and $I^{\mathrm{av}}(q)$ versus q for (a) the 3D EA model at $T \simeq 0.42$ and (b) the 4D EA model at $T \simeq 0.90$.

pendence for all models. This is a prediction of the RSB picture which certainly applies to the SK model. By contrast, in the droplet picture $I^{\mathrm{av}}(q)$ is predicted to vanish as $L^{-\theta}$ (D. S. Fisher and Huse 1986). The observed independence of $I^{\mathrm{av}}(q)$ with respect to L is one of the strongest arguments in favor of the RSB picture for finite-dimensional Ising spin-glass models. However, it has been argued, *e.g.* by Moore, Bokil, and Drossel (1998) and Middleton (2013), that there are strong finite-size corrections and that the asymptotic behavior predicted by the droplet model for $I^{\mathrm{av}}(q)$ would only be seen for sizes larger than those accessible in simulations. For this reason Middleton (2013) proposes the median as an alternative to the mean.

The data for the median of the SK model in Fig. 4.6 show a rapid decrease at small q, which is *very strongly size-dependent*. As discussed in Section 4.4 above, the rapid decrease is expected in the RSB picture since it predicts that $I^{\mathrm{med}}(q)$ is exponentially small in $1/q$ [see Eq. (4.13)]. The theoretical result is shown as a solid line in the SK panel. It is plausible that the data will approach the theory in the large N limit, but there are strong finite-size effects at small q for sizes that

can be simulated, so the data for the largest sizes are still far from the theoretical prediction. This already indicates that the median is not a very useful measure to distinguish the RSB picture from the droplet picture.

The median data for the 1D LR model with $\sigma = 0.6$, which is in the mean-field regime, shows similar trends to that for the SK model. On the other hand, for the long-range model furthest from mean-field theory, $\sigma = 0.896$, the data also decrease rapidly at small q but are less dependent on size. The data for the 3D and 4D EA models in Fig. 4.7 also show a rapid decrease at small q which is quite strongly size-dependent.

We have seen that even for the SK model it would be very difficult to extrapolate the numerical data to an infinite system size. For the 1D LR models, the most likely candidate for droplet theory behavior, according to which the median (such as the average) vanishes in the thermodynamic limit, is $\sigma = 0.896$. However, for this model, the data are not zero for small q and there is rather little size dependence, implying that, if the droplet picture does hold, it will only be seen for much larger sizes than can be simulated. This is the same situation as for the mean (if the droplet picture is correct). Consequently, it does not seem to us that the median of the cumulative order parameter distribution is a particularly useful quantity to distinguish the droplet and RSB pictures.

4.5.3 Typical overlap distribution, $P^{\rm typ}(q)$

Estimating $P^{\rm typ}(q)$, defined in Eq. (4.14) as the exponential of the average of the logarithm from Monte Carlo simulations is problematic because the finite number of observations implies that the result can be precisely zero if the average is comparable to or smaller then ϵ, the inverse of the number of measurements. Such results make the typical value undefined according to Eq. (4.14). One can

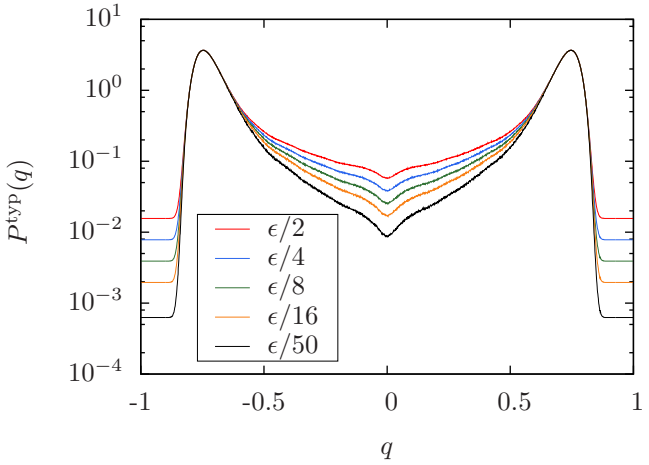

Figure 4.8: Log-linear plot of $P^{\rm typ}(q)$ for the SK model with $N = 2048$, showing the strong dependence on the zero-replacement value ϵ/k.

regularize this problem by replacing zero values of $P_{\mathcal{J}}(q)$ with the small value ϵ/k for a reasonable range of k, with the hope that the result would not be too sensitive to the choice of k. Unfortunately, there is a strong dependence on k, as seen in Fig. 4.8, where $P^{\rm typ}(q)$ is plotted for several values of k a=for the SK model for $N = 2048$. The dependence on k indicates that $P^{\rm typ}(q)$ cannot be reliably measured in Monte Carlo simulations with feasible run lengths.

4.6 Summary and conclusions

We have studied the overlap distribution for several Ising spin-glass models using recently-proposed observables. We consider 1D long-range models, 3D and 4D short-range (Edwards-Anderson) models, and the infinite-range (Sherrington-Kirkpatrick) model. The three observables are all obtained from the single-sample overlap distribution $P_{\mathcal{J}}(q)$. They are the fraction of peaked samples $\Delta(q_0, \kappa)$, the median of the cumulative distribution $I^{\rm med}(q)$, and the typical value of the distribution $P^{\rm typ}(q)$. These observables were proposed to help distinguish between the replica symmetry breaking picture and two-state pictures such as the droplet

model. While none of these unambiguously differentiates between these competing pictures, it appears that Δ does the best job. In particular, there is a qualitative distinction between the behavior for the 3D EA model and the long-range 1D model with $\sigma = 0.896$ that is expected to mimic it, on the one hand, and the mean-field SK model and the 1D model with $\sigma = 0.6$ that is expected to be in the mean-field regime, on the other hand. For a reasonable range of q_0 and κ, the two 3D-like models do not show an increase in Δ for the largest sizes while the mean-field models are sharply increasing for the largest sizes. The increase in Δ for the mean-field model is exactly what we expect from the RSB picture. The results for the 3D-like models are ambiguous because eventually Δ must go either to zero or one. It is possible that for much larger sizes Δ will begin to increase, indicating RSB behavior, but simulating such large systems at very low temperatures is infeasible at present.

The other proposed measures do not appear to be useful in numerical simulations for distinguishing scenarios. The typical value of the overlap distribution, $P^{\rm typ}(q)$ cannot be measured in feasible Monte Carlo simulations, while the median value of the cumulative overlap $I^{\rm med}(q)$ is very small at small q even for the SK model and has a very strong size dependence. For the droplet model $I^{\rm med}(q)$ is presumably zero at small q for $N \to \infty$. However, the strong size dependence of the results in this region of small q makes it impossible to tell numerically if the data are going to zero or just to a very small value, even for the SK model. Curiously, there is *less* size dependence for the 3D model and the equivalent 1D LR model with $\sigma = 0.896$ than for the SK model.

In contrast to the findings of Billoire, Maiorano, et al. (2014) that the data for $I^{\rm med}(q)$ for the SK model "converge nicely to some limiting curve when N increases" and that "trading the average for the median does make the analysis

more clear-cut," we find a strong size-dependence for $I^{\rm med}(q)$ for te SK model in the important small-q region (clearly visible in a logarithmic scale) and largely because of this we do not find that the median is particularly helpful in distinguishing between the droplet and RSB pictures.

Chapter 5

Connection between dynamics and statics in spin glasses

5.1 Introduction

Theoretical calculations in statistical physics often involve *equilibrium averages* over a thermodynamic ensemble, for example the canonical ensemble, where it is assumed that the system is in equilibrium with a heat bath at fixed temperature. In contrast, experiments and simulations usually measure steady-state *time averages*. While such *static* and *dynamic* averages are usually equivalent, this equivalence can break down.

One case where this may occur is in the ordered phase of a system that exhibits a phase transition with spontaneous symmetry breaking. For example, consider an Ising ferromagnet in zero field. As the system is cooled below the transition temperature, the symmetry of the paramagnetic phase is broken and subsequent observation will find the system in one of two ordered states, "up" or "down,"

corresponding to the sign of the net magnetization.[1] These "up" and "down" states have the property that spatial correlations of fluctuations vanish at long distances, *i.e.*

$$\lim_{r_{ij}\to\infty}\left(\left\langle S_i S_j\right\rangle - \left\langle S_i\right\rangle\left\langle S_j\right\rangle\right) = 0. \tag{5.1}$$

Equation (5.1) is called a "clustering property" and states that satisfy it are called "pure" states (C. M. Newman and Stein 2003). The set of pure states is "complete" in the sense that *any* thermodynamic state can be expressed as a linear combination of pure states. More precisely, correlation functions evaluated in an arbitrary thermodynamic state ρ may be decomposed as a convex combination[2] of correlation functions, each evaluated in a pure state ρ_α,

$$\left\langle S_{i_1}\dots S_{i_n}\right\rangle_\rho = \sum_\alpha W_\alpha \left\langle S_{i_1}\dots S_{i_n}\right\rangle_{\rho_\alpha}, \tag{5.2}$$

where we say that W_α is the "weight" of ρ_α in ρ. If a state ρ does not satisfy Eq. (5.1), more than one of the W_α will be nonzero and we say that ρ is a "mixed" state.

Returning now to the ferromagnet, in an experiment we will find either the "up" or "down" state. However, the Boltzmann distribution does not exhibit the broken symmetry of the ordered phase and includes equal contributions of both states, giving a net magnetization of zero. Thus Eq. (5.1) is not satisfied and the canonical ensemble corresponds to a *mixed* state.

However, in spin glasses, which have disorder and "frustration," the situation is more complicated. Below the spin glass transition temperature T_c, a macroscopic spin glass is not in thermal equilibrium because relaxation times are far

[1] Here, by "state" we mean a *thermodynamic* state, corresponding to a probability distribution over the microscopic configurations.

[2] That is, a linear combination where all coefficients are nonnegative and the sum of the coefficients is one.

longer than any experimental time scale. Rather, in a typical experiment the system is "quenched" from a high temperature to a temperature below T_c and the subsequent dynamical evolution of the system is observed. The state (or states) of thermal equilibrium are very complicated and are not related to any symmetry. As for the ferromagnet we would like to find a *static* calculation which will predict the experimental behavior, at least to some extent. Below we show *quantitatively* that the theoretical construct called the "metastate" (C. M. Newman and Stein 1997; Aizenman and Wehr 1990), combined with the technique of "replica symmetry breaking" (RSB, see Section 1.3.3), provides such a description for spin glasses, at least in dimensions above the upper critical dimension d_u, where the critical behavior is described by mean-field theory.

Pure states, those states that satisfy Eq. (5.1), are convenient objects of study for several reasons. As in the case of the ferromagnet with its "up" and "down" states, finding the pure states of the ordered phase of a system provides insight into the nature of the broken symmetry. Furthermore, *pure states are observed in experiment*, while mixed states (for example, the canonical ensemble for the ferromagnet, which has zero magnetization even below T_c) are not. For these reasons we would like to also describe spin glasses in terms of pure states. This can be done (in principle) by taking a very large system, applying boundary conditions on it, and studying the correlations in a relatively small window of size W (with $W \ll L$) far from the boundary (C. M. Newman and Stein 2003; Read 2014). The assumption is that the correlations within the window will be described by a single pure state; in a many-states picture, different states may be observed by varying boundary conditions at the (distant) boundary.

The question of whether there are many pure states or just one (a time-reversed

pair in the absence of a magnetic field) in spin glasses has been very controversial.[3] If there are many, one needs to do some sort of statistical average over them, which is called a "metastate," for which different but equivalent formulations have been given by C. M. Newman and Stein (1997) and by Aizenman and Wehr (1990). The former (NS) metastate corresponds to the distribution of states generated in a small window W distant from the boundary by varying the boundary conditions, as described above. In the latter (AW) metastate, one considers the scale M, intermediate between the window size W and the system size L. The metastate-averaged state (MAS) is obtained by computing correlation functions in a window in which an average is performed not only over the spins but also over the bonds in the "exterior" region between M and L. The setup is sketched in Fig. 5.1.[4] Parisi's exact solution of the infinite-range Sherrington-Kirkpatrick (SK) model using RSB predicts many pure states (see Section 1.3.3) in a sense that was later clarified by C. M. Newman and Stein (1997).

The critical behavior of a realistic spin glass is expected to be the same as that of the SK model in dimension d greater than the upper critical dimension, $d_u = 6$. However, this does not necessarily mean that the RSB description of the spin glass phase *below* T_c also applies for $d > 6$.[5] Nonetheless, Read (2014) has computed the spatial fluctuations in a finite-dimensional model below T_c, assuming mean-field (Gaussian) fluctuations, and the metastate description from Parisi's RSB solution of the SK model. Spin correlations are found to fall off with a power of distance, due to averaging over many pure states (which are unrelated by symmetry) in the

[3] See, for example, Parisi (1980b), Parisi (1983), D. S. Fisher and Huse (1987), D. S. Fisher and Huse (1988), and Moore and Bray (2011)

[4] For more details see Aizenman and Wehr (1990), Read (2014), and Manssen and Hartmann (2015).

[5] See C. M. Newman and Stein (1997), D. S. Fisher and Huse (1987), D. S. Fisher and Huse (1988), and Moore and Bray (2011).

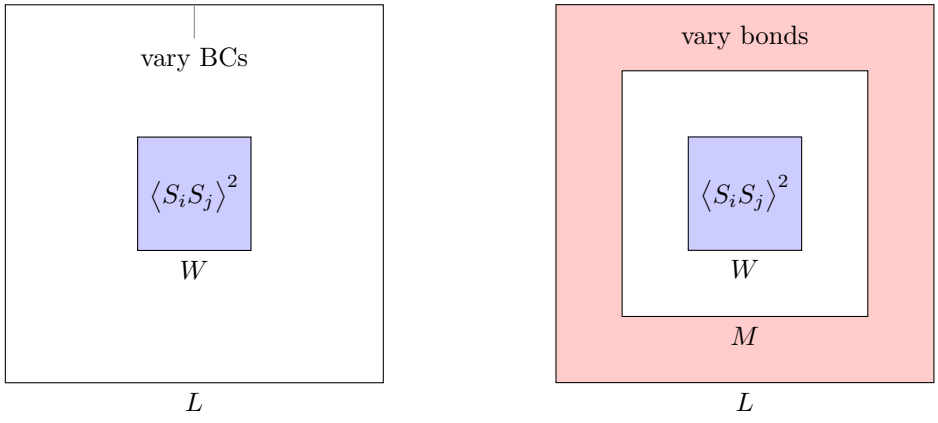

(a) NS metastate ($W \ll L$) (b) AW metastate ($W \ll M \ll L$)

Figure 5.1: Sketch of the setups for two different (but presumably equivalent) formulations of the metastate given by (a) C. M. Newman and Stein (1997) and by (b) Aizenman and Wehr (1990).

metastate, *i.e.*

$$\langle S_i S_j \rangle^2_{\text{MAS}} \propto r_{ij}^{-\alpha_s} \qquad \alpha_s = d - 4, \tag{5.3}$$

where "s" stands for "static," "MAS" stands for metastate-averaged state, and sites i and j are in the window far from the boundary. For a detailed discussion of how to do the metastate average see Read (2014).

We emphasize that the calculation leading to Eq. (5.3) is a *static* one. Is it possible to relate Eq. (5.3) to experiments (or numerical simulations), which concern (non-equilibrium) dynamics? Many simulations[6] have been carried out in which a spin glass is quenched to below T_c and the resulting dynamics analyzed. It is found that fluctuations can equilibrate (or at least reach a steady state) on length scales smaller than a dynamical correlation length $\xi(t)$ which is found, empirically, to grow with a power of t like

$$\xi(t) \propto t^{1/z(T)}, \tag{5.4}$$

[6] *e.g.* Manssen and Hartmann (2015), Rieger (1993), and Marinari, Parisi, Ruiz-Lorenzo, et al. (1996)

where the non-equilibrium dynamical exponent $z(T)$ varies, roughly, like $1/T$ and becomes close to the critical dynamical exponent z_c for $T = T_c$, *i.e.*

$$1/z(T) \simeq (T/T_c)z_c. \tag{5.5}$$

At distances less than $\xi(t)$ correlations are observed to fall off with a power of distance, leading to the following scaling hypothesis,

$$C_4(r_{ij}, t) \equiv \left[\left\langle S_i(t)S_j(t)\right\rangle^2\right]_{\rm av} = r_{ij}^{-\alpha_d} f\left(\frac{r}{\xi(t)}\right), \tag{5.6}$$

where "d" stands for "dynamic." Here the square of the thermal average, $\langle\cdots\rangle^2$, is performed by simulation two copies of the system with the same interactions, initialized with different random spin configurations. Use of two copies provides an unbiased estimate of this thermal average. The second average, $[\cdots]_{\rm av}$, is over the bonds. We will also average over all pairs of sites a given distance r apart.

For $r_{ij} \ll \xi(t)$, $f(x)$ approaches a constant as $x \to 0$, so

$$C_4(r_{ij}, t) \propto r_{ij}^{-\alpha_d} \quad (r_{ij} \ll \xi(t)). \tag{5.7}$$

In the opposite limit, $r_{ij} \gg \xi(t)$, *i.e.* large x, $f(x)$ decreases exponentially for short-range systems.

Clearly, the nonequilibrium dynamics is generating a sampling the pure states. To our knowledge, White and D. S. Fisher (2006) were the first to point out the similarity of this sampling to the metastate average for statics. They use the term "maturation metastate" to describe the ensemble of states generated dynamically on scales less than $\xi(t)$ following a quench, and "equilibrium metastate" for the static metastate discussed earlier. Here we will use the terms "dynamic" and "static" to describe these two metastates. Subsequently Manssen, Hartmann, and A. P. Young (2015) emphasized the similarity between the two metastates and

suggested that they might actually be equivalent, in which case α_s in Eq. (5.3) would equal α_d in Eq. (5.7).

The rationale behind this hypothesis is that thermal fluctuations of the spins outside the window at a distance $\xi(t)$ and greater, which are not equilibrated with respect to spins in the window, effectively generate a random noise to the spins in the window which is similar to the random perturbation coming from changing the bonds in the outer region according to the AW metastate.

For the three-dimensional spin glass, Alvarez Baños et al. (2010a) and Alvarez Baños et al. (2010b) have shown that a static calculation in the zero spin overlap sector gives a power-law decay for the spin correlations, as in Eq. (5.3), with a value of α_s consistent with that obtained from dynamcs following a quench by Belletti et al. (2009). These are both numerical results. Here we consider the mean-field regime, $d > 6$, because there is an exact *analytic* result in RSB theory, $\alpha_s = d - 4$, with which we can compare our numerical results.

5.2 Model

Unfortunately, it is difficult to carry out Monte Carlo simulations of spin glasses in in six dimensions (see the discussion in Section 3.1). Instead, we study the *diluted* one-dimensional models with long-range interactions described in Section 3.2, which we briefly review here. The one-dimensional diluted model is described by the Hamiltonian

$$\mathcal{H} = -\sum_{i,j} J_{ij} S_i S_j, \tag{5.8}$$

where the sites $i \in \{1, 2, \ldots, N\}$ lie on a one-dimensional ring with periodic boundary conditions, as shown in Fig. 3.2. The variables $S_i = \pm 1$ are Ising spins, and the

interactions J_{ij} are independent random variables with a distribution satisfying

$$\left[J_{ij}\right]_{\text{av}} = 0, \qquad \left[J_{ij}^2\right]_{\text{av}} \propto R_{ij}^{-2\sigma}, \tag{5.9}$$

where R_{ij} is taken to be the chord distance between sites i and j, see Fig. 3.2. We vary the parameter σ to control the range of the interactions.

The *diluted* model corresponds to a particular choice of the distribution $P(J_{ij})$ that satisfies Eq. (5.9) while allowing for efficient simulation, namely

$$P(J_{ij}) = \left(1 - p_{ij}\right)\delta\left(J_{ij}\right) + p_{ij}\frac{1}{\sqrt{2\pi}}e^{-J_{ij}^2/2}, \tag{5.10}$$

where $p_{ij} \propto R_{ij}^{-\sigma}$ at large distance and the constant of proportionality is chosen to fix the mean number of neighbors z_b (= 6 in this work). See Section 3.2 for a detailed discussion of the diluted model and an algorithm to sample from Eq. (5.10).

As discussed in Section 3.1, varying the parameter σ is argued to be analogous to changing the dimension d of a short-range model. In the mean-field regime, $d > d_u = 6$ for the short-range model, a precise connection can be given between σ and an equivalent d, namely

$$d = \frac{2}{2\sigma - 1} \tag{5.11}$$

(see Section 3.1), and thus, for the long-range model, the mean-field regime is $1/2 < \sigma < 2/3$.

The connection between critical exponents of the short-range and corresponding long-range models has been discussed systematically by Alvarez Baños, Fernandez, et al. (2012), who note that an exponent of the short-range model in d dimensions is d times the corresponding exponent of the equivalent one-dimensional long-range model. Thus, to get the exponent $\alpha_s = d - 4$ in the static metastate

for the long-range model we divide by d and, since we will work in the mean-field regime, use Eq. (5.11) to relate d to σ. This gives

$$\alpha_s = 3 - 4\sigma \quad \text{(long-range model)}. \tag{5.12}$$

In this work we focus on a single value of σ in the mean-field regime, $\sigma = 5/8$, which corresponds to $d = 8$ according to Eq. (5.11). Using standard finite-size scaling analysis (see Section 2.6) we find that $T_c = 1.85(2)$ for this model with $z_b = 6$. Here we need to work *well* below T_c so that our data is characteristic of the ordered phase and does not also incorporate critical fluctuations. Thus we take $T = 0.4T_c = 0.74$ for the simulations.

5.3 Method

We quench the system from infinite temperature to $T = 0.74$ at time $t = 0$ and follow the evolution of the system using Monte Carlo simulation with only local (*e.g.* *not* replica exchange) updates. We measure spin correlations, averaging them for times between 2^{k-1} and 2^k, for integer k up to the maximum value. For the largest sizes this was $k = 14$. We find that finite-size effects are very large and we need to study enormously large sizes. We therefore take a range of sizes which also increases geometrically, $N = 2^\ell$ up to $\ell = 26$. We also average over about 1000 samples (the precise number depending on size).

5.4 Results

Figure 5.2 shows our data for the correlation function $C_4(r, t)$, defined in Eq. (5.6), as a function of $r \equiv |i - j|$ at $t = 2^{14}$ for different sizes. Despite the strong finite-

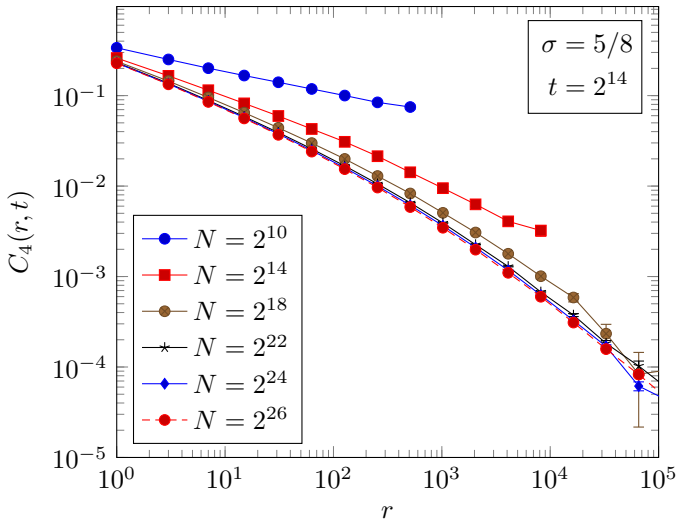

Figure 5.2: Data for the correlation function $C_4(r,t)$, defined in Eq. (5.6), as a function of r for the range of sizes studied. The data is averaged between $t = 2^{13}$ and 2^{14}.

size effects, the data seems to have saturated for the largest sizes, at least for the range of distance presented.

Having established that the largest size, $N = 2^{26}$, is large enough to eliminate finite-size effects for the range of r and t considered, we now discuss the data for this size in detail. Figure 5.3 shows data for $C_4(r,t)$ at different times as a function of r. It is expected to have the scaling form shown in Eq. (5.6). For short-range models, the scaling function $f(x)$ decays exponentially at large x because the correlation function falls off very rapidly once r is greater than the dynamical correlation length. However, in the present model we have interactions of arbitrarily long range which give a "direct" contribution to the correlation function at large distances. Since $C_4(r,t)$ involves the square of the spin-spin correlation function, and is averaged over the interactions, the direct contribution should be proportional to $\left[J_{ij}^2\right]_{\rm av}$, which, according to Eq. (5.9), is proportional to $r^{-2\sigma}$ $(= r^{-5/4}$ for $\sigma = 5/8)$. The data in Fig. 5.3 follow this behavior for short times and large distances, see the dotted line.

By contrast, at small r and large t, where $r \ll \xi(t)$, the data for different times collapse and are consistent with a decay proportional to $r^{-(3-4\sigma)}$ ($= r^{-1/2}$ for $\sigma = 5/8$), see the dashed line in Fig. 5.3. To better estimate the slope at large t and small r we plot in the inset to Fig. 5.4 the "effective" exponent α_{eff}, the slope of the data in Fig. 5.3, as a function of r for different times. The curves are quadratic fits for intermediate r ($7 \leq r \leq 255$). The intercepts of the fits approach $-1/2$ for $r \to 0$ at large t. Thus, according to Eq. (5.7), we have $\alpha_d = 3 - 4\sigma$ (or at least very close to it). However, this is precisely equal to α_s, the corresponding exponent from the *static* metastate according to RSB theory as shown in Eq. (5.12). Thus we see that, in the mean-field regime, the static and dynamic metastates appear to agree and the description appears to be that of RSB. The latter is in agreement with several other studies (Moore and Bray 2011; Katzgraber and A. P. Young 2005) and is of course also implied by those, such as Alvarez Baños et al. (2010a) and Alvarez Baños et al. (2010b), which argue that RSB holds even below six dimensions.

The main part of Fig. 5.4 shows a scaling plot of our data for the largest size according to Eqs. (5.4) and (5.6). The data scale well with $z(T) = 1.4$ and, including estimated error bars, we have the result $z(0.4T_c) = 1.4(2)$ for the dynamical exponent describing the growth of nonequilibrium correlations following a quench. For short-range models it is found empirically[7] that $1/z(T) \propto T$. If we assume the same here then $z(T_c) = 0.56(8)$. Furthermore, still for short-range models it is also found that $z(T_c)$, obtained from nonequilibrium data, is equal to (or at least close to) the equilibrium dynamical exponent z_c. We therefore take $z_c = 0.56(8)$ for our long-range model. To translate this into the exponent for the equivalent short-range model, we multiply by d ($= 8$), as discussed above, so our estimate for

[7]See Manssen and Hartmann (2015), Rieger (1993), Marinari, Parisi, Ruiz-Lorenzo, et al. (1996), and Yoshino, Hukushima, and Takayama (2002).

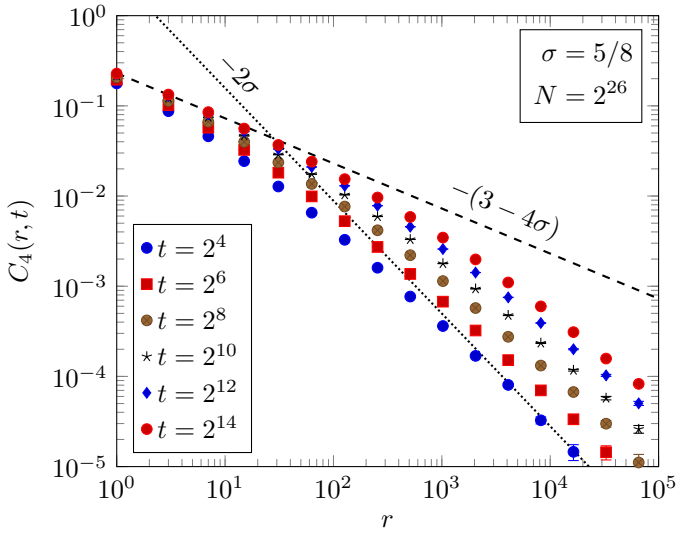

Figure 5.3: Data for the correlation function for the largest size $N = 2^{26}$ as a function of r for different times. A gradual crossover can be seen between two power laws. At long times and short distances $C_4(r,t) \propto 1/r^{\alpha_d}$ with $\alpha_d = 3 - 4\sigma$ (dashed line); at short times and long distances $C_4(r,t) \propto 1/r^{-2\sigma}$ (dotted line) which is just the average of the square of the interactions J_{ij}.

the critical dynamical exponent of the $d = 8$ short-range spin glass is $z_c = 4.5(6)$ ($d = 8$). This model is in the mean-field regime ($d > 6$) for which the dynamical exponent is found to be $z_c = 4$ (Zippelius 1984). Our result is consistent with this.

5.5 Conclusion

We have shown quantitatively that the nonequilibrium dynamics following a quench of a model which is a proxy for a short-range spin glass in dimension $d > 6$ is given, in the steady-state regime where the distance is less than the nonequilibrium correlation length, by the *analytic* result for the *static* metastate calculated according to RSB theory. This suggest that (i) RSB theory applies to spin glasses above the upper critical dimension, $d_u = 6$, and (ii) the dynamic and static metastates are

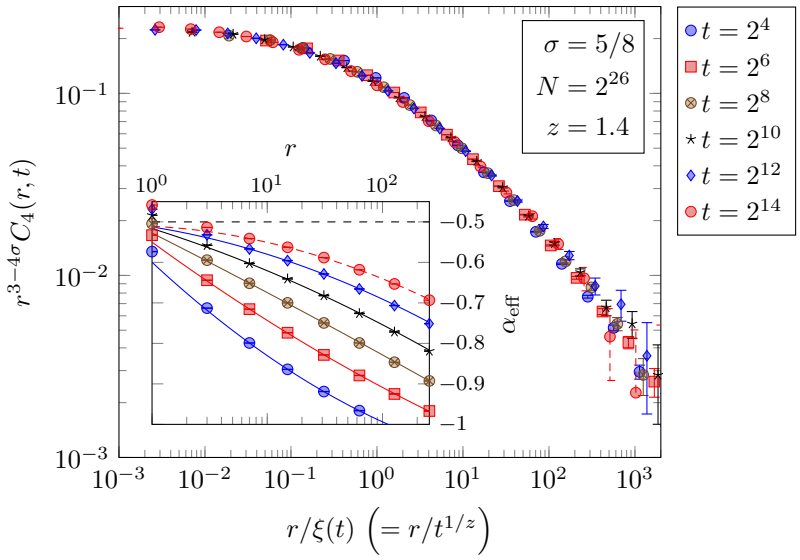

Figure 5.4: Scaling plot of the data for the largest size $N = 2^{26}$ at $T = 0.74$ according to Eq. (5.6). The inset shows the effective exponent α_{eff}, the slope of the curves in Fig. 5.3, as a function of r. The curves in the inset are quadratic fits to the data for intermediate r, $7 \leq r \leq 255$. The intercepts of the fits approach -0.5 at long times.

equivalent (at least in this region).

Chapter 6

Finite-size scaling above the upper critical dimension

6.1 Introduction

The theory of finite-size scaling (FSS) bridges the gap between the critical behavior of *finite* systems and that of infinite (or effectively infinite) systems which are commonly studied in analytical theory and experiment. As such, FSS is ubiquitous in the literature of computational physics, where it is used extensively to extrapolate *bulk* (*i.e.* $L \to \infty$) behavior, which can be compared with analytical or experimental results, from the results of numerical simulation of finite systems (Binder and Luijten 2001).

As discussed in Section 2.6, the central assumption of *standard* FSS is that finite-size corrections only involve the ratio of the system size L to the bulk (*i.e.* infinite system size) correlation length ξ. While this assumption turns out to be correct in dimensions d less than the upper critical dimension d_u, the situation is more complicated *above* the upper critical dimension, $d > d_u$. This is a bit surpris-

ing since for $d > d_u$ the critical exponents are independent of d and are predicted exactly by mean-field theory. Thus, we might naively expect from Eq. (2.38) that, for $d > d_u$, the susceptibility scales with L like

$$\chi(L,T) \sim L^2 \widetilde{\chi}\left[L^2\,(T-T_c)\right], \tag{6.1}$$

where $\widetilde{\chi}$ is a scaling function and we have inserted the mean-field exponents $\gamma = 1$ and $\nu = 1/2$. Unfortunately, it is not that simple, and instead it turns out that the basic assumption of FSS, that L dependence enters only through the ratio L/ξ, is invalid for $d > d_u$. The trouble is related to the observation that, for $d > d_u$, "hyperscaling" relations such as $d\nu = \gamma - 2\beta$ are necessarily violated, since the critical exponents "stick" at their mean-field values for all values of $d > d_u$. It turns out that a "dangerous irrelevant variable" is responsible for both effects. To understand this we need a more sophisticated approach based on the renormalization group (RG).

According to renormalization-group derivations of FSS (Privman and M. E. Fisher 1983), the singular part of the free energy f_L and the correlation length ξ_L have the form

$$f_L = L^{-d}\widetilde{f}\,(tL^{y_t}, hL^{y_h}, uL^{y_u})\,, \tag{6.2}$$

$$\xi_L = L\widetilde{\xi}\,(tL^{y_t}, hL^{y_h}, uL^{y_u})\,, \tag{6.3}$$

where $t \equiv (T - T_c)/T_c$ is the reduced temperature, h is the magnetic field, and u is the quartic coupling of the Landau theory; y_t, y_h, and y_u are the corresponding renormalization-group exponents. For $d < d_u$, u is a relevant variable ($y_u > 0$, see Section 1.2.2) and for $h = 0$ we obtain the scaling forms

$$\chi(L,t) = L^{\gamma y_t}\widetilde{\chi}\,(tL^{y_t}) \tag{6.4a}$$

$$g(L,t) = \widetilde{\chi}\,(tL^{y_t})\,, \tag{6.4b}$$

where $y_t = 1/\nu$, for the susceptibility and Binder ratio [defined in Eq. (6.21)] respectively.

For $d > d_u$, u is irrelevant ($y_u < 0$), but the corresponding derivation is complicated by the fact that the scaling function $\widetilde{f}(x, y, z)$ is singular in the limit $z \to 0$, *i.e.*, u is a *dangerous irrelevant variable*. Therefore we can't simply substitute $z = 0$ in the scaling function, and must instead evaluate the limit $z \to 0$, assuming a particular form of the singularity.

6.1.1 Periodic boundary conditions

For $k = 0$ fluctuations[1] in systems with periodic boundary conditions, Binder, Nauenberg, et al. (1985) show that, for $d > d_u$, the thermal exponent y_t is replaced by y_t^*,

$$\chi(L, t) = L^{y_t^*} \widetilde{\chi}\left(L^{y_t^*} t\right), \tag{6.5a}$$

$$g(L, t) = \widetilde{\chi}\left(L^{y_t^*} t\right), \tag{6.5b}$$

where

$$y_t^* = d/2. \tag{6.6}$$

This is a surprising result because it predicts that finite-size corrections appear not when $\xi \sim L$, as is assumed in standard FSS, but rather only when $\xi \sim L^{d/4}$, a length scale larger than the size of the system.[2] Consequently, the finite-size transition is "rounded out" over a temperature range which scales like $L^{-d/2}$, smaller than L^{-2} predicted by standard FSS.

[1] *i.e.*, fluctuations in the $k = 0$ mode of the order parameter, for example in the (uniform) magnetization, $\sum_i S_i$.

[2] To see this, note that for $d > d_u$, $t \sim \xi^{-1/\nu} = \xi^{-2}$, so the argument of the scaling function $L^{y_t^*} t = L^{d/2} \xi^{-2}$ is of order unity when $\xi \sim L^{d/4}$.

An extensive set of works[3] have shown the validity of Eq. (6.5), though it required large system sizes, good statistics, and appreciation that *corrections* to FSS are large and slowly decaying for the range of sizes that can feasibly be simulated.

6.1.2 Free boundary conditions

As stated above, Eq. (6.5) makes the rather surprising prediction that, for $d > d_u$ and periodic boundary conditions, finite-size effects set in not when $\xi \sim L$, but even closer to criticality, when $\xi \sim L^{d/4}$. It is therefore interesting to ask what is the corresponding behavior for free boundary conditions, where we expect that *something* must happen when the correlation length $\xi \sim L$ (Jones and A. P. Young 2005). In fact, Rudnick, Gaspari, and Privman (1985) have argued analytically that a temperature *shift* of order L^{-2} has to be included with free boundary conditions, in addition to the rounding of order $L^{-d/2}$.

To explain this, note that the exponents y_t in Eq. (6.4) and y_t^* in Eq. (6.5) are "rounding" exponents since they control the temperature range over which a singularity is rounded out. To define the "shift" exponent, we first define, for each size L, a "finite-size pseudocritical temperature" T_L by, for example, the location of the peak in some susceptibility, or the temperature at which the Binder ratio [defined in Eq. (6.21)] has a particular value. The difference $T_c - T_L$ goes to zero for $L \to \infty$ like

$$T_c - T_L = \frac{A}{L^\lambda}, \tag{6.7}$$

defining the shift exponent λ. The precise value of T_L depends on which criterion is used to define it, but the exponent λ is expected to be independent of the

[3]For example, Luijten and H. W. J. Blöte (1996), Parisi and Ruiz-Lorenzo (1996), H. W. J. Blöte and Luijten (1997), Luijten, Binder, and H. W. Blöte (1999), and Binder and Luijten (2001)

definition. Whether or not the amplitude A depends on the quantity used to define the shift will be discussed in Section 6.5.

If λ is less than the rounding exponent, which will turn out to be the case for free boundary conditions, then the shift is *larger* than the rounding, so we need to modify Eq. (6.5) to

$$\chi(L,t) = L^{y_t^*}\widetilde{\chi}\left[L^{y_t^*}(T-T_L)\right], \tag{6.8a}$$

$$g(L,t) = \widetilde{\chi}\left[L^{y_t^*}(T-T_L)\right], \tag{6.8b}$$

in which the argument of the scaling function involves the difference between T and the pseudocritical temperature T_L. We verify Eq. (6.8) in Figs. 6.7 to 6.9 and 6.11 below.

The criterion that the shift is given by the (standard FSS) condition $\xi \sim L$ yields $\lambda = 2$, as proposed by Rudnick, Gaspari, and Privman (1985) and confirmed in simulations by Berche, Kenna, and Walter (2012) and Kenna and Berche (2013). As with Eq. (6.4a) we must have $\widetilde{\chi}(x) \propto x^{-1}$ for $x \to \infty$ in order to recover the correct bulk behavior above T_c. Setting $T = T_c$, we have

$$\chi(L,T_c) = L^{d/2}\widetilde{\chi}(AL^{d/2-2}), \tag{6.9}$$

and therefore, asymptotically for large L,

$$\chi(L,T_c) \propto L^2 \quad \text{(free, } k=0\text{)}, \tag{6.10}$$

a result that has been shown rigorously. Hence, in contrast to Berche, Kenna, and Walter (2012), we propose that the region at the bulk T_c is part of the scaling function. Similarly, for the Binder ratio, $\widetilde{g}(x) \propto x^{-2}$ for $x \to \infty$, which gives

$$g(L,T_c) \propto \frac{1}{L^{d-4}} \quad \text{(free, } k=0\text{)}. \tag{6.11}$$

With periodic boundary conditions, the intersection of the data for g for different sizes provides a convenient estimate of T_c, but, as Eq. (6.11) shows, this method cannot be used for free boundary conditions because g vanishes at T_c for $L \to \infty$. In fact, we will see from the data in Section 6.5 that there are no intersections at all. However, we will not be able to verify the precise form in Eq. (6.11) because the values of g at T_c are very small, below the noise threshold of our simulations.

So far we have discussed only $k = 0$ fluctuations. However, it is also necessary to discuss fluctuations at $\boldsymbol{k} \neq \mathbf{0}$, since we need these to determine the spatial decay of the correlation functions. Of particular importance is the decay of the correlations at T_c, which fall off with distance like $1/r^{d-2+\eta}$, where the mean-field value of the η exponent is zero. In the mean-field regime ($d > d_u$), the fluctuations of the $k = 0$ modes are Gaussian, so the Binder ratio is always zero. For the wavevector-dependent susceptibility, we will argue that *standard* FSS, Eq. (6.4a), holds for both boundary conditions (BCs), *i.e.*

$$\chi(\boldsymbol{k}, L, T) = L^2 \widetilde{\chi}\left[L^2\left(T - T_c\right), kL\right] \quad \text{(both BCs, } \boldsymbol{k} \neq \mathbf{0}\text{)}, \tag{6.12}$$

where we have put the explicit k dependence in a natural way as a second argument of the scaling function. We note that Eq. (6.12) holds for the spherical model[4] with periodic boundary conditions.[5] For free boundary conditions, the Fourier modes are not plane waves (see Section 6.2), and, by $\boldsymbol{k} \neq \mathbf{0}$, we really mean modes that are orthogonal to the uniform ($k = 0$) magnetization and thus do not develop a nonzero expectation value below T_c.

[4]Eq. (22) of Shapiro and Rudnick (1986) and Eq. (37) of Brézin (1982) correspond to Eq. (6.12) with $\widetilde{\chi}(x, y) = \left(x^2 + y^2\right)^{-1}$, at least above T_c.

[5]The spherical model, in which the length constraint $S_i^2 = 1$ on each spin is replaced by a *single* global average constraint, is equivalent to an n-component vector model in the limit of $n \to \infty$ for the case of periodic boundary conditions. For free boundary conditions, however, the correspondence does not hold. In that case, due to a lack of translational invariance, one would need a *different* average constraint on each spin to reproduce the results of the vector model with an infinite number of components.

If we fix $T = T_c$ in Eq. (6.12) and consider $kL \gg 1$, then the size dependence must drop out, so $\widetilde{\chi}(0, y) \propto y^{-2}$ and therefore

$$\chi(\boldsymbol{k}, L, T_c) \propto \frac{1}{k^2} \quad (kL \gg 1). \tag{6.13}$$

How, then, do correlations fall off in real space at criticality? To fully understand this, we have to consider separately the contribution from the $k = 0$ mode, as in Bose-Einstein condensation. If $C(\boldsymbol{r})$ is the spin-spin correlation function at displacement $\boldsymbol{r}$ and $\widetilde{C}(\boldsymbol{k})$ is the Fourier transform (FT), then, as shown in Eq. (6.12),

$$\widetilde{C}(\boldsymbol{k}) \propto \frac{1}{k^2} \tag{6.14}$$

for $k \to 0$. However, for $k = 0$ we note that $\widetilde{C}(k = 0) = \chi(L, T)/L^d$, see Eq. (6.20) below, and from Eq. (6.5a) this gives

$$\widetilde{C}(k = 0) \propto \frac{1}{L^{d/2}}. \tag{6.15}$$

The real-space correlation function at distance $L/2$ is then given by the FT

$$C(\hat{\boldsymbol{z}}L/2) = \left(\frac{L}{2\pi}\right)^d \int_{\boldsymbol{k}\neq\boldsymbol{0}} \mathrm{d}^d k\, \widetilde{C}(\boldsymbol{k}) \exp\left(i\boldsymbol{k} \cdot L\hat{\boldsymbol{z}}/2\right) + \widetilde{C}(k = 0). \tag{6.16}$$

Using Eq. (6.14), which correctly gives the FT at large r, the first term in Eq. (6.16) is proportional, on dimensional grounds, to $1/L^{d-2}$. This is smaller than the second term, which is proportional to $1/L^{d/2}$. Thus, $C(\hat{\boldsymbol{z}}L/2) \propto 1/L^{d/2}$, in agreement with Fig. 1 of Kenna and Berche (2014). Nonetheless, correlations fall off with distance like $1/r^{d-2}$. The resolution of this apparent discrepancy is that the $k = 0$ mode has to be treated separately and gives the dominant contribution to $C(\hat{\boldsymbol{z}}L/2)$. We therefore do not see the need for the second η-like exponent proposed by Kenna and Berche (2014).

While Eq. (6.12) does not seem to have been stated in the literature before, to our knowledge, it is actually quite natural. The dangerous irrelevant variable,

which is the quartic coupling in the Ginzburg-Landau-Wilson effective Hamiltonian, is needed to control the expectation value of the ($k = 0$) order parameter, which leads to nonstandard FSS for $k = 0$ fluctuations. However $\boldsymbol{k} \neq \mathbf{0}$ fluctuations (more precisely, fluctuations that do not acquire a nonzero expectation value) are not directly affected by the dangerous irrelevant variable, and consequently they have standard FSS.

6.2 Model

We consider an Ising model in $d = 5$ dimensions in zero field, described by the Hamiltonian

$$\mathcal{H} = -\frac{1}{2}\sum_{ij} J_{ij} S_i S_j, \tag{6.17}$$

where the $J_{ij} = 1$ if i and j are nearest neighbors and zero otherwise, and the spins S_i take values ± 1. Previous simulations have determined the transition temperature very precisely, finding

$$T_c = 8.77846(3) \tag{6.18}$$

(Luijten, Binder, and H. W. Blöte 1999). We simulate the model efficiently using the Wolff cluster algorithm described in Section 2.3.2, with which we can study sizes up to $L = 64$ (which has about a billion spins).

We calculate various moments of the uniform magnetization per spin,

$$m = \frac{1}{L^d}\sum_{i=1}^{N} S_i, \tag{6.19}$$

including the uniform susceptibility[6]

$$\chi = L^d \left\langle m^2 \right\rangle \tag{6.20}$$

[6]This expression differs from the standard expression for the susceptibility $\chi = \beta L^d \left(\left\langle m^2 \right\rangle - \left\langle m \right\rangle^2 \right)$ in two ways. The first is that we omit the factor of β, which is conventional

and the Binder ratio

$$g = \frac{1}{2}\left(3 - \frac{\langle m^4 \rangle}{\langle m^2 \rangle^2}\right). \tag{6.21}$$

In addition, we compute the wavevector-dependent susceptibilities

$$\chi(\boldsymbol{k}) = L^d \left\langle \left| m(\boldsymbol{k}) \right|^2 \right\rangle, \tag{6.22}$$

in which the wavevector-dependent magnetization, $m(\boldsymbol{k})$, is defined differently for periodic and free boundary conditions as follows.

For periodic boundary conditions, the Fourier modes are plane waves, so we have

$$m(\boldsymbol{k}) = \frac{1}{N}\sum_i e^{i\boldsymbol{k}\cdot\boldsymbol{r}} S_i \quad \text{(periodic)}, \tag{6.23}$$

where

$$k_\alpha = 2\pi n_\alpha / L \quad \text{(periodic)}, \tag{6.24}$$

where $n_\alpha \in \{0, 1, \ldots, L-1\}$ and α denotes a Cartesian coordinate.

For free boundary conditions, the Fourier modes are sine waves,

$$m(\boldsymbol{k}) = \frac{1}{N}\sum_i \left[\prod_{\alpha=1}^{d} \sin\left(k_\alpha, r_{i,\alpha}\right)\right] S_i \quad \text{(free)}, \tag{6.25}$$

where

$$k_\alpha = \pi n_\alpha / (L+1) \quad \text{(free)}, \tag{6.26}$$

where $n_\alpha \in \{1, 2, \ldots, L\}$ and the components of the lattice position $r_{i,\alpha}$ also take values between 1 and L. There is zero contribution to the sum in Eq. (6.25) if we set $r_{i,\alpha} = 0$ or $L+1$, so Eqs. (6.25) and (6.26) correctly incorporate free boundary conditions.

---

in studies of critical phenomena. Secondly, and less trivially, we ignore the subtracted term, which is hard to compute reliably in Monte Carlo simulations since one would have to apply a field h (to break the symmetry) and take the limit $h \to 0$ *after* the limit $L \to \infty$. Thus the quantity we call χ is really only the susceptibility for $T > T_c$. It is, nonetheless, a convenient quantity to study, and it has the claimed scaling behavior.

Note that $k = 0$ is not an allowed mode with free boundary conditions, so the uniform magnetization in Eq. (6.19) does not correspond to a single Fourier mode in this case. Note also that modes with *all* n_α odd have a projection onto the uniform magnetization and so will acquire a nonzero expectation value below T_c in the thermodynamic limit. Such modes will therefore be subject to the nonstandard FSS in Eq. (6.5). However, if any of the n_α are even, there is no projection onto the uniform magnetization, so they will not acquire an expectation value below T_c and will therefore be subject to the standard FSS in Eq. (6.12).

6.3 Quotient method

The discussion in Section 6.1 assumed that the sizes are sufficiently large and T sufficiently close to T_c that corrections to FSS are negligible. For free boundary conditions, however, a substantial fraction of the spins lie on the surface, so *corrections* to FSS are quite large and need to be included in the analysis. In this section, we describe the method we used to include the *leading* corrections to FSS.

A convenient way to extract the leading scaling behavior from the data, in the presence of corrections, is the quotient method (Ballesteros, Fernandez, et al. 1996), based on the phenomenological scaling of Nightingale (1976). As an example, consider the deviation of the pseudocritical temperature T_L from T_c for which the FSS form is given in Eq. (6.7). Including the *leading* correction to scaling, which involves a universal exponent ω, we have

$$\Delta T(L) \equiv T_c - T_L = \frac{A}{L^\lambda}\left(1 + \frac{B}{L^\omega}\right). \tag{6.27}$$

We determine the quotient $Q\left[\Delta T\right]$ by taking the logarithm of the ratio of the

result for sizes L and sL, where s is a simple rational fraction such as 2 or 3/2,

$$Q_{s,L}\left[\Delta T\right] = \frac{1}{\log s}\log\left(\frac{\Delta T(sL)}{\Delta T(L)}\right). \tag{6.28}$$

According to Eq. (6.27) we have, for large L,

$$Q_{s,L}\left[\Delta T\right] = -\lambda + \frac{C_s}{L^{\omega}} \tag{6.29}$$

where

$$C_s = \frac{s^{-\omega}-1}{\log s}B. \tag{6.30}$$

If the data are of sufficient quality, we can fit all of the unknown parameters. In Eq. (6.29), these are the exponents λ, ω, and the amplitude C_s. In most cases, however, we will need to assume the predicted value for the correction exponent ω (see below) to obtain an unambiguous fit for the remaining parameters.

According to the renormalization group, for $d > d_u = 4$, the leading irrelevant variable has scaling dimension

$$\omega = d - 4. \tag{6.31}$$

However, for $k = 0$ fluctuations and periodic boundary conditions, it was shown by Brézin and Zinn-Justin (1985) that there is an additional, and larger, correction for finite-size effects with an exponent given by

$$\omega' = \frac{d-4}{2}. \tag{6.32}$$

An intuitive way to see this is to note that the "naive" variation of χ with L at the critical point, $\chi \propto L^2$ [see Eq. (6.1)], although not the dominant contribution [which is $L^{d/2}$ as shown in Eq. (6.5a)], is nonetheless still present as a correction. This correction is down by a factor of $L^{2-d/2}$ $(= L^{-\omega'})$ relative to the dominant term. We will therefore use ω' rather than ω in considering corrections to scaling for susceptibilities that scale with L to the power $d/2$ rather than 2.

For some of our data, we will also need subleading corrections to FSS for which there are several contributions. One of these is the square of the leading contribution. To avoid having too many fit parameters, this is the form we will assume, *i.e.*, when we include subleading corrections to scaling we will do a parabolic fit in $1/L^{\omega}$ (or $1/L^{\omega'}$ as the case may be).

A subtlety arises in doing fits to data for quotients, for example to determine the parameters λ, ω, and C_s in Eq. (6.29). The reason is that the same set of simulation data may be used to determine more than one data point in the fit. For example, with $s = 2$ the data for $L = 16$ is used in the computation of quotients for pairs (8, 16) and (16, 32). Furthermore, we will fit the exponents λ and ω simultaneously to quotients for two different values of s ($s = 2$ and $3/2$),[7] so for example we also use the data for $L = 16$ to compute the quotient for the pair (16, 24). This has the advantage of increasing the number of data points in the fit by more than the number of parameters. However, in this case the data being fitted are *not statistically independent*, and therefore the best estimate of the fitting parameters should account for the correlations. (Ballesteros, Fernandez, et al. 1996; Ballesteros, Fernández, et al. 1998; Weigel and Janke 2009). In other words, if a data point is (x_i, y_i) and the fitting function is $u(x)$, which depends on certain fitting parameters, those parameters should be determined by minimizing

$$\chi^2 = \sum_{i,j} \left[y_i - u(x_i)\right] \left(\mathbf{\Sigma}^{-1}\right)_{ij} \left[y_j - u(x_j)\right], \tag{6.33}$$

where

$$\Sigma_{ij} = \left\langle y_i y_j \right\rangle - \left\langle y_i \right\rangle \left\langle y_j \right\rangle \tag{6.34}$$

is the covariance matrix of the data. We determine the elements of the covariance matrix by a bootstrap analysis (see Section 2.7.2). If there are substantial corre-

[7] This is justified since the exponents are universal. The amplitude C_s is, however, nonuniversal, so we include a separate amplitude for each value of s.

lations, the covariance matrix can become singular, and where this happens we replace $\mathbf{\Sigma}^{-1}$ in Eq. (6.33) with the "pseudoinverse" $\mathbf{\Sigma}^{+}$.[8] The effective number of independent data points is then the rank of the covariance matrix (the number of nonzero eigenvalues).

6.4 Results: periodic boundary conditions

We perform Monte Carlo simulations of the model with periodic boundary conditions for sizes $L = 8, 10, 12, 16, 20, 24, 28, 32, 36$.

6.4.1 $k = 0$ fluctuations

Here we show results for completeness, as there is no doubt that the FSS form of Eq. (6.5) is correct for periodic boundary conditions.

Figure 6.1 shows an overview of our data for the Binder ratio g, showing intersections at, or near, the transition temperature T_c given in Eq. (6.18). The right-hand panel is an expanded view near T_c, where it is clear that intersections for different sizes do not occur at exactly the same point, indicating corrections to scaling. In fact, the data for smaller sizes intersect at a value larger than the exact, universal value

$$g_c = \frac{1}{2}\left(3 - \frac{\Gamma^4(\frac{1}{4})}{8\pi^2}\right) \approx 0.40578 \tag{6.35}$$

found by Brézin and Zinn-Justin (1985). However, for larger sizes the intersections occur at smaller values of g. Figure 6.2 shows estimates of the value of g at T_c, plotted against $L^{-\omega'}$ with the correction exponent given by $\omega' = 1/2$ as discussed

[8] This corresponds to projecting the covariance matrix onto the eigenvectors whose eigenvalues are not (close to) zero and inverting the resulting matrix.

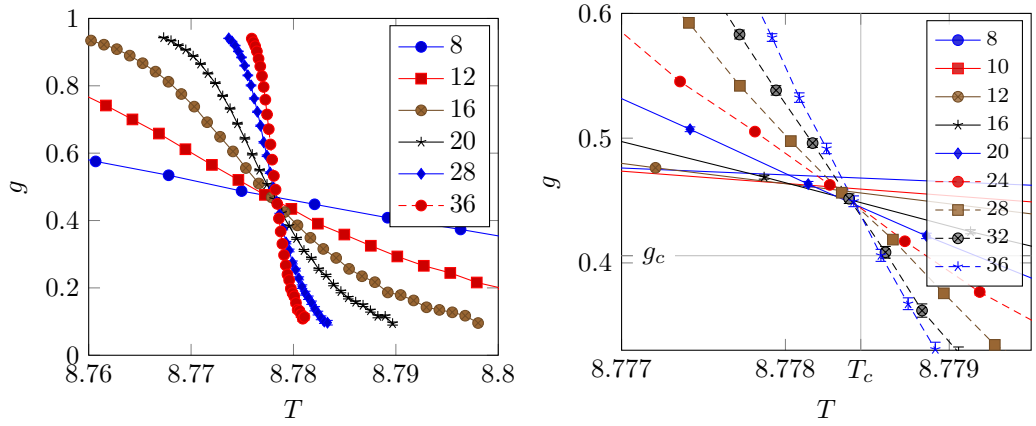

Figure 6.1: The left panel shows an overview of our results for the Binder ratio g for periodic boundary conditions. The right panel is an expanded view near the transition. The transition temperature T_c is marked with a horizontal line, and the universal value of the Binder ratio at the transition temperature, g_c, given by Eq. (6.35), is marked with a vertical line.

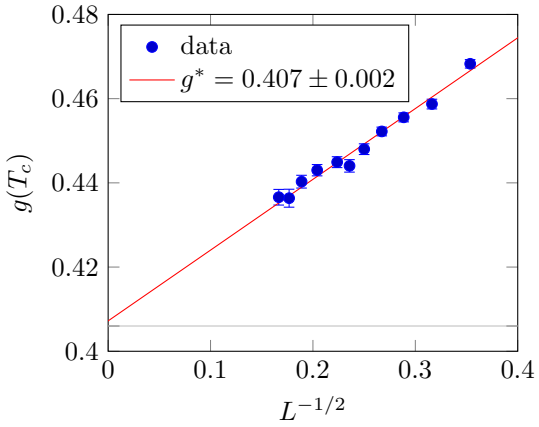

Figure 6.2: Estimates of the Binder ratio g at T_c, plotted against $L^{-\omega'}$ with $\omega' = 1/2$, see Eq. (6.32), and a linear fit indicating an extrapolated value for $L \to \infty$ consistent with the exact result, $g_c \approx 0.406$ (marked with a horizontal line in the figure), see Eq. (6.35). The estimates were obtained from a cubic smoothing spline fit to data at and near T_c, and the error bars were estimated using the bootstrap procedure. The quality of the fit is good, $Q = 0.22$.

in Section 6.3. The data decrease to a value consistent with Eq. (6.35) as $L \to \infty$.

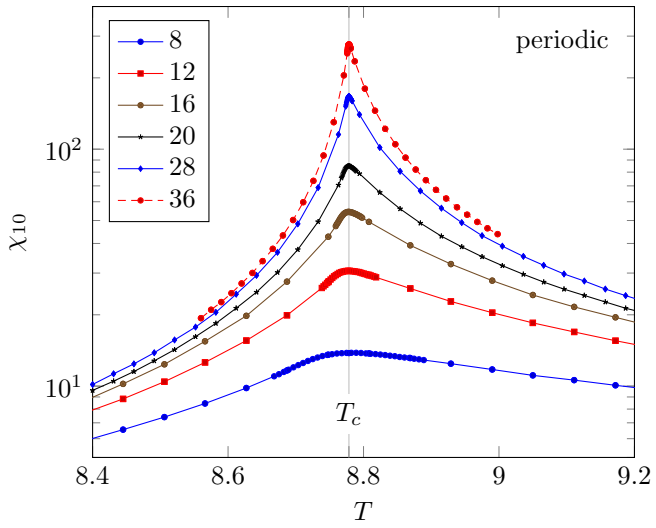

Figure 6.3: Susceptibility $\chi(\boldsymbol{k})$ for $\boldsymbol{k}L = (1, 0, 0, 0, 0)$, which we abbreviate to χ_{10}, for periodic boundary conditions.

6.4.2 $k \neq 0$ fluctuations

The data for $\chi(\boldsymbol{k})$ for $\boldsymbol{k}L/(2\pi) = (1, 0, 0, 0, 0)$ are shown in Fig. 6.3. Note that the Fourier components at nonzero wave vector vanish even in the ordered state below T_c, and so what we define as $\chi(\boldsymbol{k})$ really is the susceptibility below T_c as well as above [unlike the $k = 0$ susceptibility defined in Eq. (6.20)]. Consequently the data have a peak, whereas the uniform "susceptibility" plotted in Fig. 6.6b (for free boundary conditions) continues to increase below T_c.

A scaling plot of the data according to standard FSS of Eq. (6.12) is shown in Fig. 6.4a. Except for the smallest size, $L = 8$, near T_c the data scale very well. Further from T_c on the low-T side, we see bigger corrections. However, this is unsurprising since FSS is only expected to work for T close to T_c.

For larger k values we get a similar picture, albeit with bigger corrections to scaling, as shown in Fig. 6.4b for $\boldsymbol{k}L/(2\pi) = (1, 1, 0, 0, 0)$. It is expected that corrections to scaling become *relatively* bigger for larger k because the signal is less divergent in this case, and so it is more easily affected by corrections.

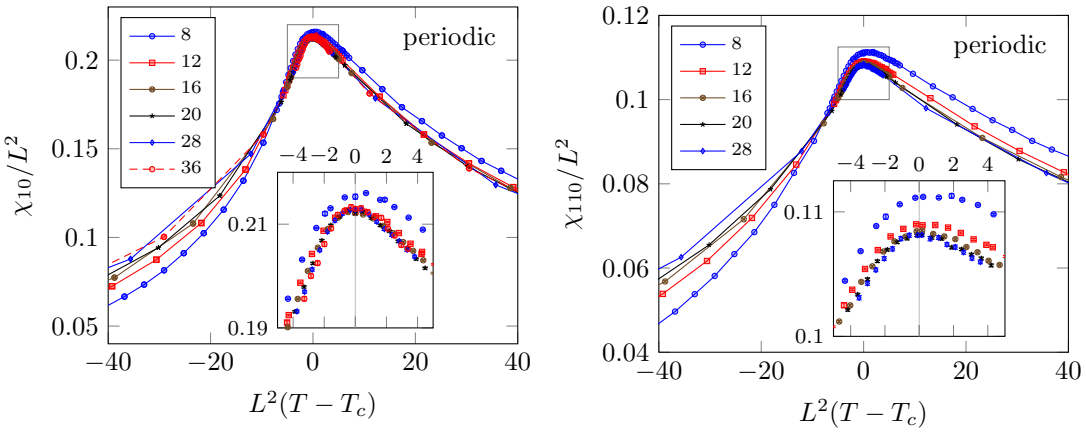

(a) $\boldsymbol{k}L/(2\pi) = (1,0,0,0,0)$ (b) $\boldsymbol{k}L/(2\pi) = (1,1,0,0,0)$

Figure 6.4: Scaling plots of the susceptibility for two nonzero wavevectors. Panel (a) shows the scaled data of Fig. 6.3.

Figure 6.5 shows the behavior of $\chi(\boldsymbol{k})/L^2$ at T_c showing that it is a function of the product kL as expected; see Eq. (6.12). The dashed line has slope -2 indicating that the expected k^{-2} behavior of Eq. (6.13) sets in even for small values of kL.

6.5 Results: free boundary conditions

We perform Monte Carlo simulations of the model with free boundary conditions for sizes $L = 8, 10, 12, 14, 16, 18, 20, 24, 28, 32, 36, 48,$ and 64. The data for the largest two sizes, $L = 48$ and 64, is only for $k = 0$.

Because corrections to scaling are larger for free boundary conditions than for periodic boundary conditions, in this section we make extensive use of the quotient method described in Section 6.3 to incorporate the leading corrections to scaling.

6.5.1 $k = 0$ fluctuations

An overview of our results for the Binder ratio is shown in Fig. 6.6a. We do not

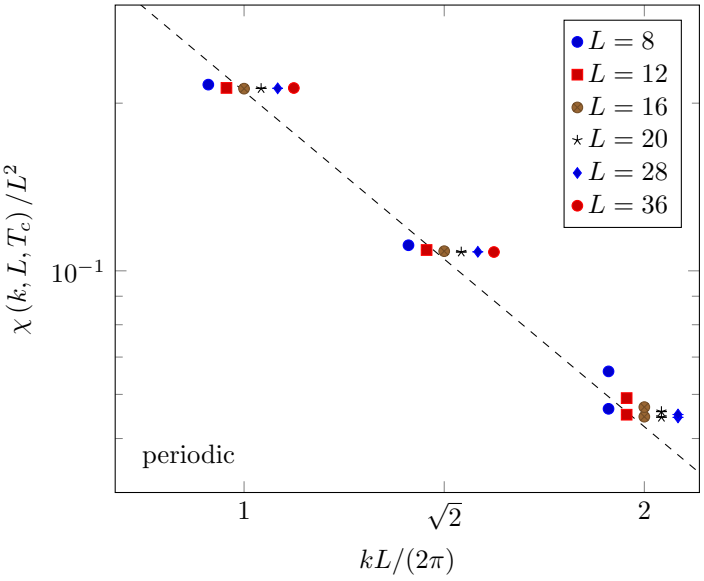

Figure 6.5: Values of $\chi(\boldsymbol{k})/L^2$ at T_c for periodic boundary conditions. Each group of points has the same x coordinate (1, $\sqrt{2}$, or 2), but the points are displaced slightly horizontally so that they can be distinguished. There are two different wavevectors shown for $kL/(2\pi) = 2$, namely $\boldsymbol{k}L/(2\pi) = (2, 0, 0, 0, 0)$ and $(1, 1, 1, 1, 0)$. These two agree well except for the smaller sizes, showing that the fluctuations are isotropic at long wavelength. The dashed line has slope -2, indicating that the expected k^{-2} behavior in Eq. (6.13) sets in even for small values of kL.

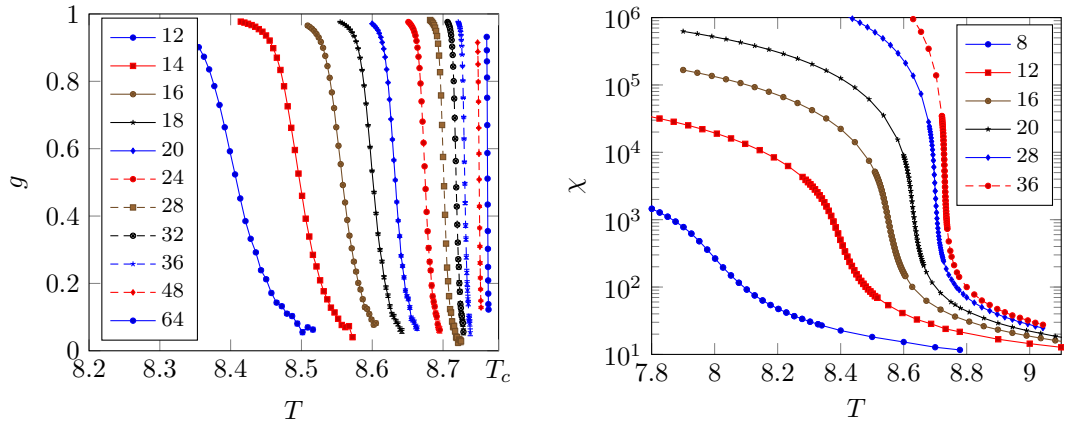

(a) (b)

Figure 6.6: Overview of data for (a) the Binder ratio g and (b) the susceptibility χ, for free boundary conditions, for the different sizes studied. Note the large shift to lower temperatures for the smaller sizes and lack of any apparent intersections of the data for different sizes in (a).

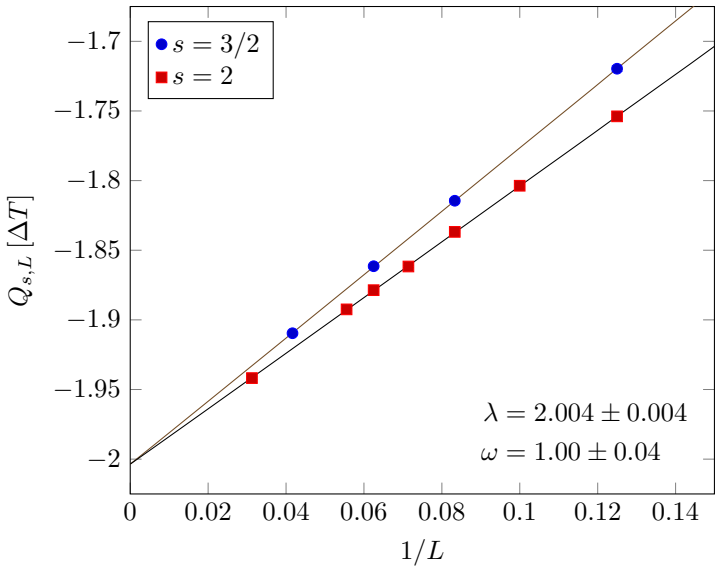

Figure 6.7: Quotients for $\Delta T(L)$, defined in Eq. (6.27), used to determine the shift exponent λ for free boundary conditions. The parameter s is the ratio of the two sizes used to compute the quotient. We fit Eq. (6.29) to the data using as parameters λ, ω (the same for both values of s), and separate amplitudes $C_{3/2}$ and C_2. The quality of the fit is very good, $Q = 0.96$.

find any intersections, and the data are shifted considerably to lower temperatures for smaller sizes.

To determine the shift exponent, we define the pseudocritical temperature T_L to be the temperature at which g takes the value $1/2$, halfway between its limiting values of 0 and 1. We subtract T_c, given in Eq. (6.35), and determine the resulting quotients for $\Delta T(L) \equiv T_c - T_L$ according to Eq. (6.28). We then fit Eq. (6.29) to the quotients, as shown in Fig. 6.7. The quality of the data is very good and we are able to fit all four parameters, λ, ω, and the two amplitudes C_s. We find the values

$$\lambda = 2.004(4), \quad \omega = 1.00(4). \tag{6.36}$$

The value for the shift exponent is in precise agreement with the value $\lambda = 2$ proposed analytically by Rudnick, Gaspari, and Privman (1985) and found numerically by Berche, Kenna, and Walter (2012). There is also excellent agreement

between our value of the correction exponent ω and the RG value of 1.

We estimate the rounding by the range in temperature $\delta T(L)$ over which g varies between 0.25 and 0.75, *i.e.*

$$\delta T(L) = T(g = 0.25) - T(g = 0.75). \tag{6.37}$$

Computing the quotients and fitting the form

$$Q_{s,L}\left[\delta T\right] = -y_t^* + A_s/L^{\omega}, \tag{6.38}$$

we find that the data are insufficient to determine the three parameters, but if we assume the RG value for the correction exponent, $\omega = 1$, then we get a good fit that extrapolates to

$$y_t^* = 2.45(1), \tag{6.39}$$

see Fig. 6.8, close to the prediction $d/2$, see Eq. (6.6). Considering the relatively small statistical error in this estimate, the result is not quite consistent with $d/2$. However, especially in view of the further evidence for $y_t^* = d/2$, discussed below, we believe this discrepancy to be due to subleading corrections to scaling. We note that the quoted error bar *assumes* that the data can be described by Eq. (6.39); in other words, that *subleading* corrections do not affect the fitted data significantly.

Now we consider the scaling of χ in Eq. (6.8a). The data for χ are shown in Fig. 6.6b. From this we estimate the value of χ at T_L (where T_L is determined, as before, from where g takes the value 1/2) and do a quotient analysis, shown in Fig. 6.9. The data are insufficient to determine the correction to the scaling exponent, so we fixed it to the expected value $\omega' = 1/2$, see Eq. (6.32). The amplitude of the correction term is large, but the data extrapolate to a value 2.51(1), consistent with the value of $y_t^* = 5/2$ expected from Eq. (6.8a), and which was found in earlier simulations by Berche, Kenna, and Walter (2012) and Kenna and Berche (2013).

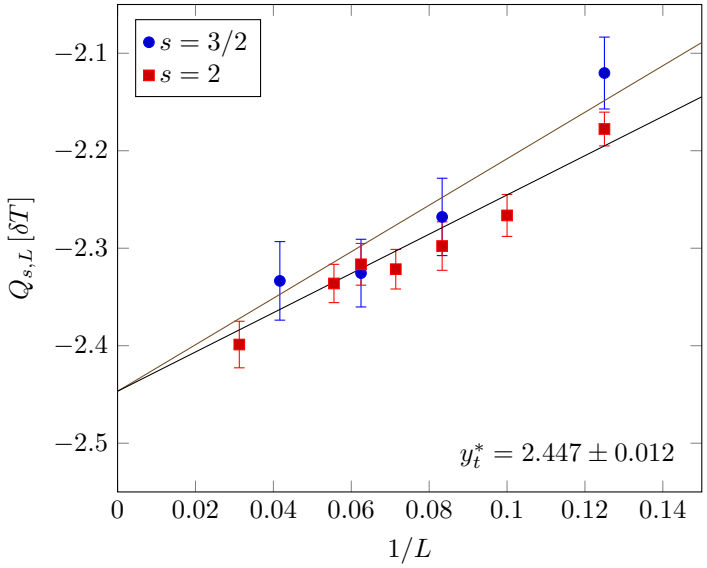

Figure 6.8: Quotients for $\delta T(L)$, defined in Eq. (6.37), used to determine the rounding exponent y_t^* for free boundary conditions. We fit Eq. (6.38) to the data using as parameters y_t^*, (the same for both values of s) and separate amplitudes. The value of the correction exponent is fixed to $\omega = 1$.

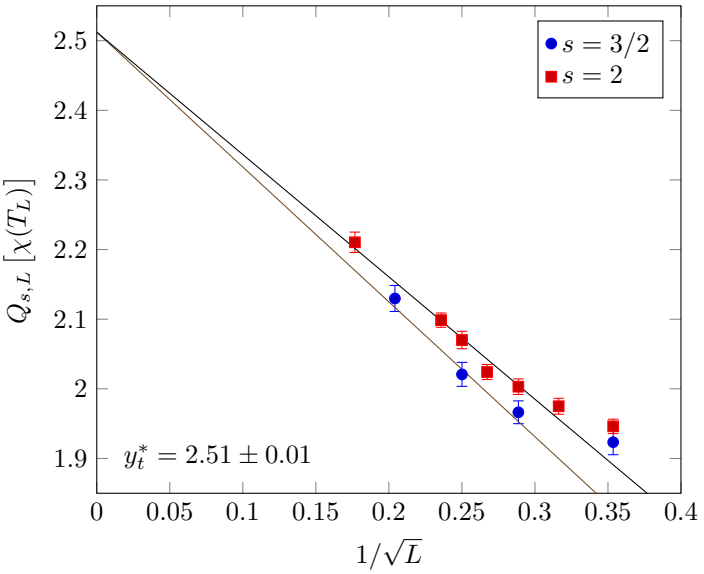

Figure 6.9: Quotients for the value of χ at T_L for free boundary conditions plotted against $L^{-\omega'}$, where the correction to scaling exponent ω' is fixed to the value $1/2$. According to Eq. (6.5a), the quotients should extrapolate to the value y_t^* $(= 5/2)$ for $L \to \infty$. The linear fit omits the right-hand point for each of the two data sets. There are three fitting parameters: y_t and two amplitudes for the correction, one for each value of s. The quality of fit is good, $Q = 0.21$.

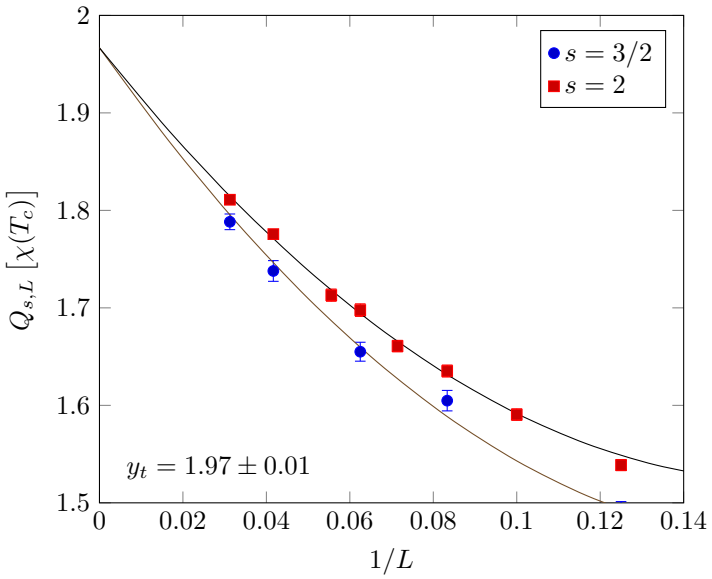

Figure 6.10: Quadratic fit to the quotients for the value of χ at the bulk T_c for free boundary conditions against $1/L^{\omega}$ where the correction to scaling exponent ω is fixed to the value 1. According to Eq. (6.10), the quotients should extrapolate to the value of y_t $(= 2)$. There are five fitting parameters: y_t and the amplitudes of the linear and quadratic corrections for each s value. The quality of fit is good, $Q = 0.23$.

We also measure χ at the bulk T_c. As shown in Eq. (6.10), this is proportional to L^2, not $L^{d/2}$, and so, as discussed in Section 6.3, we expect that the correction to scaling exponent will be ω $(= 1)$ rather than ω' $(= 1/2)$. Quotients of the results are plotted in Fig. 6.10. There are clearly subleading corrections to scaling, so we use a quadratic fit. The result, $y_t = 1.97(1)$, is close to the expected value of 2. We note that the corrections to scaling are quite large, which is not surprising since the values of χ at T_c are small, and thus are more influenced by corrections to scaling than the data at T_L, where χ is larger. Nonetheless, the quadratic fit shows that, although we have not determined the exponent with which χ diverges at T_c with great accuracy, our result is at least *consistent* with the value of 2 expected according to Eq. (6.10). An L^2 divergence in the susceptibility has also been found recently by Lundow and Markström (2014), who were able to study

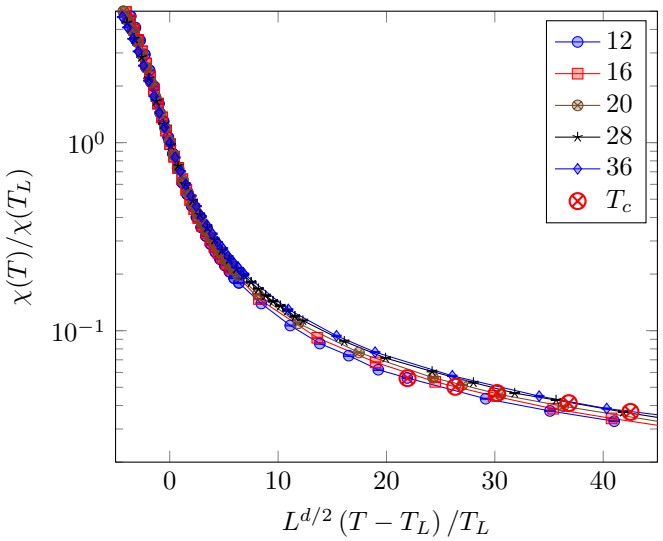

Figure 6.11: Scaling plot of the data for χ for free boundary conditions according to Eq. (6.5a). Also shown are the data at T_c, which are seen to lie on the scaling function (within some small corrections).

larger sizes than those studied here, up to $L = 160$.

Figure 6.11 shows a scaling plot of $\chi(T)/\chi(T_L)$ against $L^{d/2}(T - T_L)/T_L$. We have seen in Fig. 6.9 that there are corrections to the expected $L^{d/2}$ behavior of χ at T_L for the range of sizes studied. Thus we divide $\chi(T)$ by $\chi(T_L)$ rather than by $L^{d/2}$, which appears in Eq. (6.8a), to eliminate the corrections seen in Fig. 6.9. According to Eq. (6.8a), the data in Fig. 6.11 should collapse. There are some corrections to this, which is not surprising since we are probing the scaling function over a large region, but overall the data scale fairly well. Also shown are data at T_c, which appear at different points for different sizes because T_L is, of course, size-dependent. The larger the size, the further to the right is the data point for T_c. This figure supports our claim that the data at T_c are included in the scaling function in Eq. (6.8a).

We have defined the pseudocritical temperatures T_L and the resulting shift exponent λ in Eq. (6.27) by the temperature where the Binder ratio takes the

value 1/2. Suppose we took a different criterion for T_L, such as the temperature at which the Binder ratio has some other value, or where there is a peak in some $\boldsymbol{k} \neq \mathbf{0}$ susceptibility, such as that shown in Fig. 6.3. We note that the finite-size width varies as $1/L^{d/2}$, so temperatures at which the Binder ratio has a value between 0 and 1 would lie in this range, and so they would only give a *subleading* contribution to the shift, the coefficient of $1/L^2$ remaining the same. We expect that the *same* shift amplitude would be obtained no matter what quantity is used to define the shift for the following reason. Suppose we have a shift amplitude A and pseudocritical temperatures T_L determined from where the Binder ratio is 1/2 and a different amplitude A', and correspondingly different temperatures T'_L, determined by some other criteria. Then the Binder ratio has a scaling form in Eq. (6.8b), but if we try to define it in terms of the alternative shift temperatures T'_L, we have

$$g(L,T) = \widetilde{g}\left[L^{d/2}\left(T - T_L\right)\right] \tag{6.40}$$

$$= \widetilde{g}\left[L^{d/2}\left(T - T'_L\right) + \left(A' - A\right)L^{d/2-2}\right]. \tag{6.41}$$

Thus, if different quantities have different shift amplitudes, the argument of the scaling function would be shifted by an *infinite* amount (for $L \to \infty$) if we use the shift obtained from a different quantity, a clear violation of scaling. We therefore postulate that this does not happen and that there is a *unique* shift amplitude for a given system.

Note, however, that we cannot rule out subleading corrections to the shift of order $1/L^{d/2}$. As a result, the value of g at T_L according to Eq. (6.8b) will depend on the precise definition of T_L and therefore will *not* be universal, unlike the situation with periodic boundary conditions; see Eq. (6.5b). Thus one can view the replacement of Eq. (6.5) by Eq. (6.8) as a violoation of the standard finite-size

scaling (Rudnick, Gaspari, and Privman 1985). However, since the behavior of χ, for example, is described by a single function both at T_c and T_L, we view Eq. (6.8) as representing a *modified FSS*, distinct from standard FSS, in that it has different shift and scaling exponents.

6.5.2 $k \neq 0$ fluctuations

With free boundary conditions, the Fourier modes are sine waves given by Eq. (6.26). Modes in which all the integers n_α are odd have a projection onto the uniform magnetization (*i.e.* the $k = 0$ mode) and therefore will acquire a nonzero magnetization in the ordered phase. Such modes will therefore be affected by the dangerous irrelevant variable, and so have the same scaling as fluctuations of the uniform magnetization, given in Eq. (6.8a). We therefore take the smallest wave vector with an even n_α, namely $\boldsymbol{n} = (2, 1, 1, 1, 1)$, since this will not acquire a nonzero magnetization, so we expect it to be governed by the FSS in Eq. (6.12), *i.e.*, with exponent 2 rather than $d/2$ which appears in Eq. (6.8a). We present the data in Fig. 6.12.

According to Eq. (6.12), the height of the peaks in Fig. 6.12 should scale as L^2 and the width should scale as L^{-2}. We define the width to be the difference between the two temperatures where the susceptibility is 3/4 of the maximum. Quotient analyses for the height and width are shown in Fig. 6.13. For the height, the (quadratic) fit gives an extrapolated value of 2.008(10), consistent with the expected value of $y_t = 2$ As discussed in the caption of Fig. 6.13a, a linear fit gave a value 1.950(2), close but slightly different from 2. However, in this case the quality of fit $Q = 0.02$ was unacceptably low, which is why we went to a quadratic fit. For the data of the width in Fig. 6.13b, the amplitudes of the corrections are small and we find an extrapolated value of $-1.97(4)$, consistent with the expected

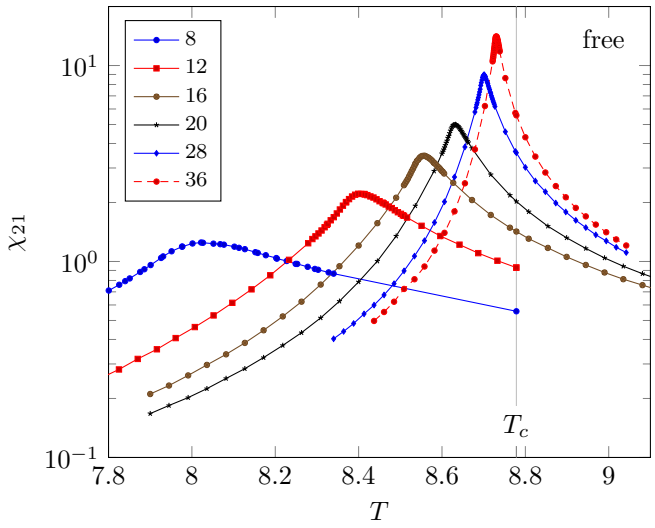

Figure 6.12: Data for $\chi(\boldsymbol{k})$ for $(L+1)\boldsymbol{k}/\pi = (2,1,1,1,1)$ for free boundary conditions.

value of $-y_t$ $(= -2)$.

Thus, we have found strong evidence to suppert our claim that Eq. (6.12) applies to free boundary conditions. Note that since this FSS form uses y_t $(= 2)$ and the deviation of T_L from T_c is proportional to $1/L^2$, asymptotically we can use eigher T_c or T_L in Eq. (6.12).

6.6 Conclusions

Our main conclusions have already been discussed in Section 6.1, so here we summarize our main results:

(i) The *modified* FSS form with exponents $d/2$ rather than 2 only applies to $k = 0$ fluctuations. (For free boundaries it applies to Fourier modes that have a projection onto the uniform magnetization.) For all other wavevectors, standard FSS with an exponent 2 applies. Consequently, the exponent η describing the power-law decay of correlations at T_c is unambiguously $\eta = 0$. (See Figs. 6.4, 6.5

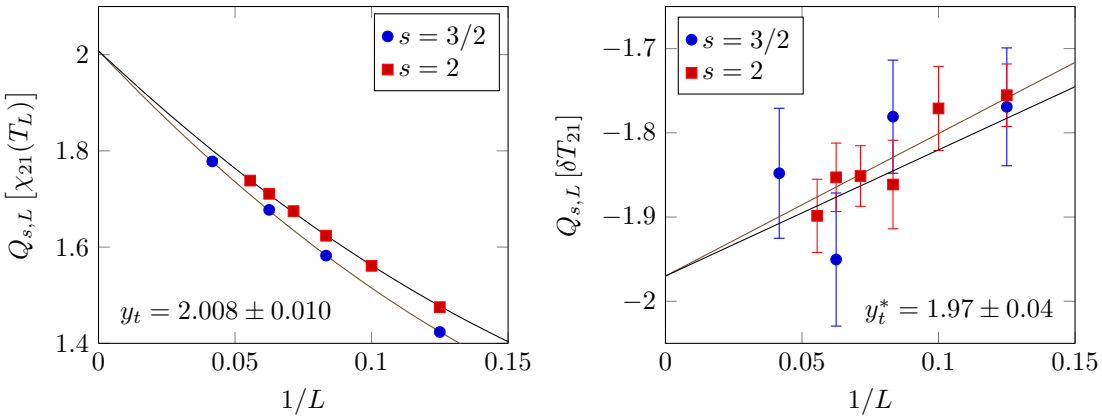

(a) (b)

Figure 6.13: Quotients for the height (a) and width (b) of the peak in $\chi(\boldsymbol{k})$ for $(L+1)\boldsymbol{k}/\pi = (2,1,1,1,1)$ for free boundary conditions. According to Eq. (6.12), the quotients of the peak height should tend to the value y_t $(= 2)$ and the quotients for the width should tend to $-y_t$ $(= -2)$ as $L \to \infty$. The estimates of y_t obtained by extrapolation for both fits are consistent with 2. For both fits we fix the value of the correction exponent to $\omega = 1$. In (a) the correction amplitude is large, but the data are of good quality and a quadratic fit works well, $Q = 0.53$. A linear fit to these data gave an extrapolated value of 1.950(2) but with a poor quality of fit, $Q = 0.02$. In (b), the amplitude of the leading correction is seen to be quite small, and we use a linear fit which works well, $Q = 0.67$.

and 6.13.)

(ii) For free boundary conditions and $k = 0$, the shift, with an exponent 2, is larger than the rounding, which has an exponent $d/2$. Using $T - T_L$, where T_L is the finite-size pseudocritical temperature, rather than $T - T_c$ as a scaling variable, the data have a scalng form that incorporates both the behavior at T_L, where $\chi \propto L^{d/2}$, and at the bulk T_c, where $\chi \propto L^2$. (See Figs. 6.7 to 6.11.)

Bibliography

Aizenman, Michael and Jan Wehr. "Rounding effects of quenched randomness on first-order phase transitions". In: *Communications in mathematical physics* 130.3 (1990), pp. 489–528.

Alvarez Baños, R., L. A. Fernandez, et al. "Correspondence between long-range and short-range spin glasses". In: *Physical Review B* 86.13 (2012), p. 134416.

Alvarez Baños, R. et al. "Nature of the spin-glass phase at experimental length scales". In: *Journal of Statistical Mechanics: Theory and Experiment* 2010.06 (2010), P06026.

— "Static versus Dynamic Heterogeneities in the $D = 3$ Edwards-Anderson-Ising Spin Glass". In: *Phys. Rev. Lett.* 105 (17 Oct. 2010), p. 177202. DOI: 10.1103/PhysRevLett.105.177202.

Anderson, P. W. "Absence of Diffusion in Certain Random Lattices". In: *Phys. Rev.* 109 (5 Mar. 1958), pp. 1492–1505. DOI: 10.1103/PhysRev.109.1492.

Ballesteros, H. G., L. A. Fernandez, et al. "Finite size effects on measures of critical exponents in d= 3 O (N) models". In: *Physics Letters B* 387.1 (1996), pp. 125–131.

Ballesteros, H. G., L. A. Fernández, et al. "Critical exponents of the three-dimensional diluted Ising model". In: *Physical Review B* 58.5 (1998), p. 2740.

Barahona, Francisco. "On the computational complexity of Ising spin glass models". In: *Journal of Physics A: Mathematical and General* 15.10 (1982), p. 3241.

Belletti, F. et al. "An in-depth view of the microscopic dynamics of Ising spin glasses at fixed temperature". In: *Journal of Statistical Physics* 135.5-6 (2009), pp. 1121–1158.

Berche, Bertrand, Ralph Kenna, and J. C. Walter. "Hyperscaling above the upper critical dimension". In: *Nuclear Physics B* 865.1 (2012), pp. 115–132.

Billoire, A., L. A. Fernandez, et al. "Comment on "Evidence of non-mean-field-like low-temperature behavior in the Edwards-Anderson spin-glass model"". In: *Physical review letters* 110.21 (2013), p. 219701.

Billoire, A., A. Maiorano, et al. "Cumulative overlap distribution function in realistic spin glasses". In: *Physical Review B* 90.9 (2014), p. 094201.

Binder, Kurt and Erik Luijten. "Monte Carlo tests of renormalization-group predictions for critical phenomena in Ising models". In: *Physics Reports* 344.4 (2001), pp. 179–253.

Binder, Kurt, M. Nauenberg, et al. "Finite-size tests of hyperscaling". In: *Physical Review B* 31.3 (1985), p. 1498.

Binder, Kurt and A. P. Young. "Spin glasses: Experimental facts, theoretical concepts, and open questions". In: *Reviews of Modern physics* 58.4 (1986), p. 801.

Blöte, Henk W. J. and Erik Luijten. "Universality and the five-dimensional Ising model". In: *EPL (Europhysics Letters)* 38.8 (1997), p. 565.

Brézin, E. "An investigation of finite size scaling". In: *Journal de Physique* 43.1 (1982), pp. 15–22.

Brézin, E. and Jean Zinn-Justin. "Finite size effects in phase transitions". In: *Nuclear Physics B* 257 (1985), pp. 867–893.

Campa, Alessandro, Andrea Giansanti, and Daniele Moroni. "Canonical solution of a system of long-range interacting rotators on a lattice". In: *Physical Review E* 62.1 (2000), p. 303.

Cannas, Sergio A., A. C. N. De Magalhães, and Francisco A. Tamarit. "Evidence of exactness of the mean-field theory in the nonextensive regime of long-range classical spin models". In: *Physical Review B* 61.17 (2000), p. 11521.

Cannas, Sergio A. and Francisco A. Tamarit. "Long-range interactions and nonextensivity in ferromagnetic spin models". In: *Physical Review B* 54.18 (1996), R12661.

Cannella, V. and J. A. Mydosh. "Magnetic ordering in gold-iron alloys". In: *Physical Review B* 6.11 (1972), p. 4220.

Cardy, John. *Scaling and renormalization in statistical physics*. Vol. 5. Cambridge university press, 1996.

de Almeida, J. R. L. and David J. Thouless. "Stability of the Sherrington-Kirkpatrick solution of a spin glass model". In: *Journal of Physics A: Mathematical and General* 11.5 (1978), p. 983.

Dyson, Freeman J. "Existence of a phase-transition in a one-dimensional Ising ferromagnet". In: *Communications in Mathematical Physics* 12.2 (1969), pp. 91–107.

Edwards, Samuel Frederick and P. W. Anderson. "Theory of spin glasses". In: *Journal of Physics F: Metal Physics* 5.5 (1975), p. 965.

Fisher, Daniel S. and David A. Huse. "Absence of many states in realistic spin glasses". In: *Journal of Physics A: Mathematical and General* 20.15 (1987), p. L1005.

— "Equilibrium behavior of the spin-glass ordered phase". In: *Physical Review B* 38.1 (1988), p. 386.

— "Ordered phase of short-range Ising spin-glasses". In: *Physical review letters* 56.15 (1986), p. 1601.

Goldenfeld, Nigel. *Lectures on phase transitions and the renormalization group*. Addison-Wesley, Advanced Book Program, Reading, 1992.

Harris, A. B., T. C. Lubensky, and Jing-Huei Chen. "Critical properties of spin-glasses". In: *Physical Review Letters* 36.8 (1976), p. 415.

Hartmann, Alexander K. and A. P. Young. "Lower critical dimension of Ising spin glasses". In: *Physical Review B* 64.18 (2001), p. 180404.

Hiley, B. J. and G. S. Joyce. "The Ising model with long-range interactions". In: *Proceedings of the Physical Society* 85.3 (1965), p. 493.

Hukushima, Koji and Koji Nemoto. "Exchange Monte Carlo method and application to spin glass simulations". In: *Journal of the Physical Society of Japan* 65.6 (1996), pp. 1604–1608.

Ising, Ernst. "Beitrag zur theorie des ferromagnetismus". In: *Zeitschrift für Physik A Hadrons and Nuclei* 31.1 (1925), pp. 253–258.

Istrail, Sorin. "Statistical mechanics, three-dimensionality and NP-completeness: I. Universality of intracatability for the partition function of the Ising model across non-planar surfaces". In: *Proceedings of the thirty-second annual ACM symposium on Theory of computing*. ACM. 2000, pp. 87–96.

Jones, Jeff L. and A. P. Young. "Finite-size scaling of the correlation length above the upper critical dimension in the five-dimensional Ising model". In: *Physical Review B* 71.17 (2005), p. 174438.

Katzgraber, Helmut G. and Alexander K. Hartmann. "Ultrametricity and clustering of states in spin glasses: A one-dimensional view". In: *Physical review letters* 102.3 (2009), p. 037207.

Katzgraber, Helmut G., Mathias Körner, and A. P. Young. "Universality in three-dimensional Ising spin glasses: A Monte Carlo study". In: *Physical Review B* 73.22 (2006), p. 224432.

Katzgraber, Helmut G., Matteo Palassini, and A. P. Young. "Monte Carlo simulations of spin glasses at low temperatures". In: *Physical Review B* 63.18 (2001), p. 184422.

Katzgraber, Helmut G., Simon Trebst, et al. "Feedback-optimized parallel tempering Monte Carlo". In: *Journal of Statistical Mechanics: Theory and Experiment* 2006.03 (2006), P03018.

Katzgraber, Helmut G. and A. P. Young. "Monte Carlo studies of the one-dimensional Ising spin glass with power-law interactions". In: *Physical Review B* 67.13 (2003), p. 134410.

— "Probing the Almeida-Thouless line away from the mean-field model". In: *Physical Review B* 72.18 (2005), p. 184416.

Kenna, Ralph and Bertrand Berche. "A new critical exponent "qoppa" and its logarithmic counterpart". In: *Condensed Matter Physics* 16 (2013), p. 23601.

— "Fisher's scaling relation above the upper critical dimension". In: *EPL (Europhysics Letters)* 105.2 (2014), p. 26005.

Kirkpatrick, Scott and David Sherrington. "Infinite-ranged models of spin-glasses". In: *Physical Review B* 17.11 (1978), p. 4384.

Kone, Aminata and David A Kofke. "Selection of temperature intervals for parallel-tempering simulations". In: *The Journal of chemical physics* 122.20 (2005), p. 206101.

Kotliar, G., P. W. Anderson, and Daniel L. Stein. "One-dimensional spin-glass model with long-range random interactions". In: *Physical Review B* 27.1 (1983), p. 602.

Larson, Derek et al. "Numerical studies of a one-dimensional three-spin spin-glass model with long-range interactions". In: *Physical Review B* 81.6 (2010), p. 064415.

— "Spin glasses in a field: Three and four dimensions as seen from one space dimension". In: *Physical Review B* 87.2 (2013), p. 024414.

Leuzzi, L. et al. “Dilute one-dimensional spin glasses with power law decaying interactions”. In: *Physical Review Letters* 101.10 (2008), p. 107203.

Luijten, Erik, Kurt Binder, and Henk WJ Blöte. “Finite-size scaling above the upper critical dimension revisited: the case of the five-dimensional Ising model”. In: *The European Physical Journal B-Condensed Matter and Complex Systems* 9.2 (1999), pp. 289–297.

Luijten, Erik and Henk W. J. Blöte. “Finite-size scaling and universality above the upper critical dimensionality”. In: *Physical review letters* 76.10 (1996), p. 1557.

Lundow, P. H. and Klas Markström. “Finite size scaling of the 5D Ising model with free boundary conditions”. In: *Nuclear Physics B* 889 (2014), pp. 249–260.

Manssen, Markus and Alexander K. Hartmann. “Aging at the spin-glass/ferromagnet transition: Monte Carlo simulations using graphics processing units”. In: *Physical Review B* 91.17 (2015), p. 174433.

Manssen, Markus, Alexander K. Hartmann, and A. P. Young. “Nonequilibrium evolution of window overlaps in spin glasses”. In: *Physical Review B* 91.10 (2015), p. 104430.

Marinari, Enzo, Giorgio Parisi, Federico Ricci-Tersenghi, et al. “Replica symmetry breaking in short-range spin glasses: theoretical foundations and numerical evidences”. In: *Journal of Statistical Physics* 98.5-6 (2000), pp. 973–1074.

Marinari, Enzo, Giorgio Parisi, Juan J. Ruiz-Lorenzo, et al. “Numerical evidence for spontaneously broken replica symmetry in 3D spin glasses”. In: *Physical review letters* 76.5 (1996), p. 843.

Martın-Herrero, J. “Hybrid cluster identification”. In: *J Phys A: Math Gen* 761 (2004), p. 37.

McMillan, W. L. “Scaling theory of Ising spin glasses”. In: *Journal of Physics C: Solid State Physics* 17.18 (1984), p. 3179.

Metropolis, Nicholas et al. “Equation of state calculations by fast computing machines”. In: *The Journal of Chemical Physics* 21.6 (1953), pp. 1087–1092.

Mézard, Marc et al. “Nature of the spin-glass phase”. In: *Physical review letters* 52.13 (1984), p. 1156.

Middleton, A. Alan. “Extracting thermodynamic behavior of spin glasses from the overlap function”. In: *Physical Review B* 87.22 (2013), p. 220201.

Monthus, Cécile and Thomas Garel. "Typical versus averaged overlap distribution in spin glasses: Evidence for droplet scaling theory". In: *Physical Review B* 88.13 (2013), p. 134204.

Moore, M. A., Hemant Bokil, and Barbara Drossel. "Evidence for the droplet picture of spin glasses". In: *Physical review letters* 81.19 (1998), p. 4252.

Moore, M. A. and Allan J. Bray. "Disappearance of the de Almeida-Thouless line in six dimensions". In: *Physical Review B* 83.22 (2011), p. 224408.

Mori, Takashi. "Instability of the mean-field states and generalization of phase separation in long-range interacting systems". In: *Physical Review E* 84.3 (2011), p. 031128.

Narayan, Onuttom and A. P. Young. "Convergence of Monte Carlo simulations to equilibrium". In: *Physical Review E* 64.2 (2001), p. 021104.

Newman, Charles M. and Daniel L. Stein. "Metastate approach to thermodynamic chaos". In: *Physical Review E* 55.5 (1997), p. 5194.

— "Multiple states and thermodynamic limits in short-ranged Ising spin-glass models". In: *Physical Review B* 46.2 (1992), p. 973.

— "Non-mean-field behavior of realistic spin glasses". In: *Physical review letters* 76.3 (1996), p. 515.

— "Ordering and broken symmetry in short-ranged spin glasses". In: *Journal of Physics: Condensed Matter* 15.32 (2003), R1319.

— "Simplicity of state and overlap structure in finite-volume realistic spin glasses". In: *Physical Review E* 57.2 (1998), p. 1356.

Newman, E. J. and G. T. Barkema. *Monte Carlo Methods in Statistical Physics*. Clarendon Press, 1999. ISBN: 9780198517979.

Nightingale, Mp P. "Scaling theory and finite systems". In: *Physica A: Statistical Mechanics and its Applications* 83.3 (1976), pp. 561–572.

Onsager, Lars. "Crystal statistics. I. A two-dimensional model with an order-disorder transition". In: *Physical Review* 65.3-4 (1944), p. 117.

Parisi, Giorgio. "Infinite number of order parameters for spin-glasses". In: *Physical Review Letters* 43.23 (1979), p. 1754.

— "Magnetic properties of spin glasses in a new mean field theory". In: *Journal of Physics A: Mathematical and General* 13.5 (1980), p. 1887.

Parisi, Giorgio. "Order parameter for spin-glasses". In: *Physical Review Letters* 50.24 (1983), p. 1946.

— "The order parameter for spin glasses: A function on the interval 0-1". In: *Journal of Physics A: Mathematical and General* 13.3 (1980), p. 1101.

Parisi, Giorgio, Federico Ricci-Tersenghi, and Juan J. Ruiz-Lorenzo. "Equilibrium and off-equilibrium simulations of the Gaussian spin glass". In: *Journal of Physics A: Mathematical and General* 29.24 (1996), p. 7943.

Parisi, Giorgio and Juan J. Ruiz-Lorenzo. "Scaling above the upper critical dimension in Ising models". In: *Physical Review B* 54.6 (1996), R3698.

Peierls, Rudolph. "On Ising's model of ferromagnetism". In: *Mathematical Proceedings of the Cambridge Philosophical Society* 32 (03 Oct. 1936), pp. 477–481. ISSN: 1469-8064. DOI: 10.1017/S0305004100019174.

Press, William H. *Numerical Recipes 3rd Edition: The Art of Scientific Computing*. Cambridge University Press, 2007.

Privman, Vladimir and Michael E. Fisher. "Finite-size effects at first-order transitions". In: *Journal of Statistical Physics* 33.2 (1983), pp. 385–417.

Rathore, Nitin, Manan Chopra, and Juan J de Pablo. "Optimal allocation of replicas in parallel tempering simulations". In: *The Journal of chemical physics* 122.2 (2005), p. 024111.

Read, N. "Short-range Ising spin glasses: The metastate interpretation of replica symmetry breaking". In: *Physical Review E* 90.3 (2014), p. 032142.

Reger, J. D., R. N. Bhatt, and A. P. Young. "Monte Carlo study of the order-parameter distribution in the four-dimensional Ising spin glass". In: *Physical review letters* 64.16 (1990), p. 1859.

Rieger, Heiko. "Nonequilibrium dynamics and aging in the three-dimensional Ising spin-glass model". In: *Journal of Physics A: Mathematical and General* 26.15 (1993), p. L615.

Rudnick, Joseph, George Gaspari, and Vladimir Privman. "Effect of boundary conditions on the critical behavior of a fi-nite high-dimensional Ising model". In: *Physical Review B* 32.11 (1985), p. 7594.

Shapiro, Jonathan and Joseph Rudnick. "The fully finite spherical model". In: *Journal of statistical physics* 43.1-2 (1986), pp. 51–83.

Sherrington, David and Scott Kirkpatrick. "Solvable model of a spin-glass". In: *Physical review letters* 35.26 (1975), p. 1792.

Stein, Daniel L. and Charles M. Newman. *Spin Glasses and Complexity*. Princeton University Press, 2013.

Swendsen, Robert H. and Jian-Sheng Wang. "Nonuniversal critical dynamics in Monte Carlo simulations". In: *Phys. Rev. Lett.* 58 (2 Jan. 1987), pp. 86–88. DOI: 10.1103/PhysRevLett.58.86.

Talagrand, Michel. *Spin glasses: a challenge for mathematicians: cavity and mean field models*. Vol. 46. Springer Science & Business Media, 2003.

Viana, L and Allan J. Bray. "Phase diagrams for dilute spin glasses". In: *Journal of Physics C: Solid State Physics* 18.15 (1985), p. 3037.

Weigel, Martin and Wolfhard Janke. "Cross correlations in scaling analyses of phase transitions". In: *Physical review letters* 102.10 (2009), p. 100601.

White, Olivia L and Daniel S. Fisher. "Scenario for spin-glass phase with infinitely many states". In: *Physical review letters* 96.13 (2006), p. 137204.

Wittmann, Matthew and A. P. Young. "Finite-size scaling above the upper critical dimension". In: *Phys. Rev. E* 90 (6 Dec. 2014), p. 062137. DOI: 10.1103/PhysRevE.90.062137.

— "Spin glasses in the nonextensive regime". In: *Phys. Rev. E* 85 (4 Apr. 2012), p. 041104. DOI: 10.1103/PhysRevE.85.041104.

— "The connection between statics and dynamics of spin glasses". Submitted. July 9, 2015.

Wittmann, Matthew, Burcu Yucesoy, et al. "Low-temperature behavior of the statistics of the overlap distribution in Ising spin-glass models". In: *Phys. Rev. B* 90 (13 Oct. 2014), p. 134419. DOI: 10.1103/PhysRevB.90.134419.

Wolff, Ulli. "Collective Monte Carlo Updating for Spin Systems". In: *Phys. Rev. Lett.* 62 (4 Jan. 1989), pp. 361–364. DOI: 10.1103/PhysRevLett.62.361.

Yoshino, Hajime, Koji Hukushima, and Hajime Takayama. "Extended droplet theory for aging in short-range spin glasses and a numerical examination". In: *Physical Review B* 66.6 (2002), p. 064431.

Young, Peter. *Everything You Wanted to Know About Data Analysis and Fitting but Were Afraid to Ask*. Springer International Publishing, 2015.

Yucesoy, Burcu, Helmut G. Katzgraber, and Jonathan Machta. "Evidence of non-mean-field-like low-temperature behavior in the Edwards-Anderson spin-glass model". In: *Physical review letters* 109.17 (2012), p. 177204.

Yucesoy, Burcu, Helmut G. Katzgraber, and Jonathan Machta. "Yucesoy, Katzgraber, and Machta Reply". In: *Physical review letters* 110.21 (2013), p. 219702.

Yucesoy, Burcu, Jonathan Machta, and Helmut G. Katzgraber. "Correlations between the dynamics of parallel tempering and the free-energy landscape in spin glasses". In: *Physical Review E* 87.1 (2013), p. 012104.

Zippelius, Annette. "Critical dynamics of spin-glasses". In: *Physical Review B* 29.5 (1984), p. 2717.